Numerical Simulation of Enhanced Mixing in Scramjet Combustor Using Ramp, Tabs and Suction Collar

Seung-Jae Hwang

2011

Numerical Simulation of Enhanced Mixing in Scramjet Combustor Using Ramp, Tabs and Suction Collar

By
Seung-Jae Hwang

B.S., Aerospace Engineering, University of Kansas, 2000
M.S., Aerospace Engineering, University of Kansas, 2002

Submitted to the graduate degree program in Aerospace Engineering and the Graduate Faculty of the University of Kansas School of Engineering in partial fulfillment of the requirements for the degree of Doctor of Philosophy.

Thesis Committee

_____
Dr. Saeed Farokhi, Faculty Advisor

_____
Dr. Ray Taghavi, Committee Member

_____
Dr. Ron Barrett-Gonzalez, Committee Member

_____
Dr. Shahriar Keshmiri, Committee Member

_____
Dr. Weizhang Huang, Committee Member

_____
Date Defended

The Dissertation Committee for Seung-Jae Hwang certifies that this is the approved version of the following dissertation:

Numerical Simulation of Enhanced Mixing in Scramjet Combustor Using Ramp, Tabs and Suction Collar

_____

Chairperson: Dr. Saeed Farokhi

Date approved: May 18, 2011

Abstract

Numerical simulations of the scramjet combustor by using the commercial CFD code Fluent with the coupled implicit method with second-order accurate discretization have been obtained for the reacting flows with the parallel fuel injection (ramp injection) and normal fuel injection (wall injection) schemes. Incorporated in the scramjet combustors are delta tabs and suction collars of two types as means of mixing enhancement. The main mechanism of the tabs and suction collars for mixing enhancement is the generation of streamwise vorticity and providing outstanding flame-holding capability along with the induced global instability of the shear layer. The idea has been previously recommended for mixing enhancement of the scramjet combustor, but no experimental or computational data on the combustor performance has been reported, yet. The finite rate reaction model is used for the species transport model that only considers four species, H_2, O_2, H_2O and N_2. Vitiated air (mass fraction of O_2, H_2O, and N_2 being 0.198, 0.139, and 0.663, respectively) enters the combustor at Mach number of 2.5 at a stagnation temperature and pressure of 1500 K and 101,325 Pa, respectively. The equivalence ratio is fixed at 0.45 in the present study. An optimization study of the combinations of the tabs and suction collars has been performed. Uninstalled thrust force for the optimal combination which was composed of the relieved ramp, 4 delta tabs, suction collar type I and 4 delta tabs in the fuel inlet scheme produced an additional 73% increase in thrust with only an additional 3.37% loss of the total pressure compared to the ramp injection alone, i.e., the baseline case. The numerical results clearly indicate that the fuel injection schemes investigated in the present study are more efficient than a strut or multi-staged strut and wall injection scheme.

Acknowledgment

The author, Seung-Jae Hwang, would like to express an appreciation and his sincere gratitude toward his advisor, Dr. Saeed Farokhi first about his great support and consistent guidance. Without his kindness and great knowledge, the present work would not be accomplished. Also, the author would like to thank all of his committee members, Professor Ray Taghavi, Professor Ron Barrett-Gonzalez, Professor Shahriar Keshmiri and Professor Weizhang Huang, to keep a faith in him. Finally, the author would like to thank his lovely wife, Kyung-Ya Hwang, his children, Sung-Ho, In-Ae, Myung-Ho and Jun-Ho and his mother, Young-Suk Park, who have consistently been the greatest support, encouragement and source of prayers to the author.

Table of Content Page

Nomenclature

Symbols/Abbreviation	Definition	Units
A	Cross-sectional area of the combustor	m^2
b	Inlet Fuel Jet Dimension	m
c	Speed of sound	m/sec
CFD	Computational Fluid Dynamics	-
C_A	Concentration of air	$lbmolA/ft^3$
C_δ	Shear layer growth rate	-
$(C_\delta)_0$	Incompressible growth rate	-
D	Diameter	m
D_{FA}	Molecular diffusivity	-
F	Un-installed thrust	N
f	Fuel to air ratio	-
f_{st}	Stoichiometric fuel to air ratio	-
j_A	Net molar diffusive flux of air	$lbmolA/ft^2$
H, h	Height	m
H_2	Hydrogen	-
H_2O	Water	-
L_m	Distance of mixing layer	m
lbmol	Pound mole	lbs
M	Mach number	-
M_c	Convective Mach number	-
$\dot{m}_f$	Mass flow rate of fuel	kg/sec
$\dot{m}_o$	Entry air mass flow rate	kg/sec

Symbols/Abbreviation	Definition	Units
N_2	Nitrogen	-
O_2	Oxygen	-
P	Pressure	Pascal
P_s	Static Pressure	Pascal
P_0	Stagnation pressure	Pascal
Pa	Pascal	-
-R	Negative velocity and trailing vorticies	-
RNG	Re-Normalization Group	-
T	Temperature	K
T_s	Static Temperature	K
T_0	Stagnation temperature	K
U	Streamwise velocity	m/sec
U_c	Convective velocity	m/sec
V	Velocity	m/sec
W	Width	m
x, y, z	Cartesian coordinates	-
y^+	Distance from the wall to the first grid point	-

Greek Symbols	Definition	Units
γ	Specific heat ratio	-
δ	Shear layer thickness	m
δ_m	Mixing layer thickness	m

Greek Symbols	Definition	Units
η	Mixing parameter	-
ρ	Density	kg/m^3
Φ	Equivalence ratio	-

List of Figures Page

List of Tables Page

1 Introduction

In the recent years, many countries including the United States of America and Japan have been developing and testing the supersonic combustion scramjet engines. Scramjet engines are believed to be one of the most efficient and economical propulsion system in the hypersonic flight regime. Since scramjets are air-breathing engines, they have several advantages over rocket propulsion systems: They take oxygen from the atmosphere and rely on aerodynamic forces instead of purely on rocket thrust. In the past several years, the X-51A scramjet engine that is the world's first hypersonic hydrocarbon-fueled and hydrocarbon–cooled engine targeting at Mach 4.5-6.0+, a collaborative effort of the joint Air Force Research Laboratory (AFRL), Defense Advanced Research Projects Agency (DARPA), NASA, Pratt & Whitney Rocketdyne (PWR), and Boeing X-51A Scramjet Engine Demonstrator-WaveRider (SED) vehicle, has been developed and started to test in a series of 4 flight test beginning in August 2009.

Developing scramjet engines presents many challenges. One of these difficulties is supersonic combustion. High-speed ramjets are limited to about Mach 6 because of inefficiency. When the free-stream airflow is decelerated to subsonic speeds by the ramjets, both the relative velocity and kinetic energy decrease. The reduction of kinetic energy will reappear as internal energy (via conservation of energy). Consequently, the pressure, density and temperature of the flow entering the combustion chamber are considerably higher than in the free-stream. However, this effect becomes so pronounced over Mach 6 that there are no more advantages to decelerating the flow to subsonic speeds. The pressure and temperature also become too high to combust any fuel in the combustion chamber due to the normal shock wave system. To obtain higher speeds the air flow has to remain supersonic, avoiding the normal shock wave system, to prevent dramatic temperature rise ahead of the combustion chamber. As a result, fuel is injected in the supersonic airflow, where it has to mix and burn typically within few milliseconds, i.e., the residence time in the combustor. Ensuring flame-holding

capability and preventing the engine unstart within such a short fuel residence time is very hard to achieve. Thus, enhancing combustion efficiency is one of the major areas of research in the past several decades, but a clear solution has not yet been found.

In the past decades, extensive research on exhaust jet mixing enhancement and noise suppression have been made and many methods have been recommended such as solid/fluid tabs, serrated nozzles, acoustic excitation, lobed mixers and counterflow concept, ect. Two of these already proven concepts, solid/fluid tabs and counterflow, along with or without relieved ramp will be adapted to the present Computational Fluid Dynamic (CFD) study to enhance mixing efficiency of the scramjet combustion. Delta tabs are well known method in subsonic conditions, but in the present study they will be adapted to the supersonic flow field. Delta tabs will be mounted on the top of the ramp and inside engine walls to generate counter-rotating streamwise vortices along the mixing layer and hydrogen fuel will be injected in the vortex stream. The size, angle, locations and numbers of the delta tabs will be investigated with the present CFD study to maximize combustion efficiency and to minimize aerodynamic loss, i.e., total pressure drop. After finishing the CFD study of the delta tabs concept, the counterflow concept will be investigated. The counterflow concept is already demonstrated to contribute to mixing efficiency by Strykowski et al[1,2] for the exhausting jets and Seiner et al[3] also recommends that it would provide outstanding flame-holding capability if applied to scramjet combustion. The idea of the counterflow has been previously described, but no experimental or computational data on the combustor performances has been reported. Only a few percent of the primary flow needs to be sucked to achieve the dramatic effect on mixing, but the amount of the suction backflow and location of the suction collar will be decided with the present CFD analysis. Also, the CFD study of the combined two concepts, delta tabs and counterflow, will be carried out. The efficiency of the combustion and aerodynamic loss will be compared to each other.

2 Literature Review

2.1 Fuel-Air Mixing

The mixing rate for nonreacting turbulent free shear layers of two different gas species has been theoretically,[4,5] numerically[6,7] and experimentally[8-11] studied in the past. The past studies have clearly shown a rapid decrease in mixing efficiency as Mach number is increased into the supersonic regime.

2.1.1 Fuel-Air Mixing in Parallel Streams

When the two velocities differ in parallel flows, a shear layer is generated at the interface between the two streams that vorticity, momentum, thermal and mechanical energy and mass (molecules) may be transported laterally. As shown in Figure 1, when the two streams have different molecular identities (e.g., air and fuel), the shear layer is also a mixing layer and the mixing layer thickness δ_m is defined as the region within that the mole fractions of the two streams differ by one or more percent from their respective values in the unmixed streams. Even though the two velocities (air and fuel) are equal and there is no lateral transport of either vorticity or momentum because of no shear stress between the two streams (zero-shear mixing layer), there is still lateral transport due to molecular diffusion at the fuel-air interface. The local rate of molecular diffusion (Fick's law[12]), the time rate of molecular transport of fuel into air, is proportional to the product of the interfacial area and the local concentration gradient. Fick's law may be written:

$$j_A = -D_{FA} \cdot \frac{\delta C_A}{\delta y} \tag{2.1}$$

Where j_A is the net molar diffusive flux of air (lbmolA/ft^2) in the y direction, D_{FA} is molecular diffusivity, C_A is the concentration of air (lbmolA/ft^3), and $\delta C_A/\delta y$ is the lateral concentration gradient. The mixing layer thickness is approximated as:

$$\delta_m \approx 8\sqrt{\frac{D_{FA}x}{U_c}} \tag{2.2}$$

Where u_c is a convective velocity.

The total distance L_m required for the mixing layer boundary to reach the walls may be estimated from Eq. (2), by setting $\delta_m = 2b$ (where b is inlet fuel jet dimension) and solving for $x = L_m$:

$$L_m = \frac{U_c b^2}{16 D_{FA}} \tag{2.3}$$

The maximum permitted mixing aspect ratio $(L_m/b)_{max}$ is limited to about 20 due to internal skin friction and shock wave drag leading to an unacceptable decrease in overall cycle efficiency. However, the estimated value of L_m/b to achieve complete micromixing in a zero-shear mixing layer is much higher than 20 (For example, let L_m = 6 ft, flight Mach = 10 and at the burner entry static T = 1556 K, then L_m/b is about 1440 to achieve complete micromixing). Thus, molecular diffusion alone clearly cannot meet the requirement of rapid lateral mixing in a supersonic flow. The obvious way is to develop a shear layer between the two streams to enhance the growth rate of the mixing layer. Also, effects of upstream entropy and shear layer thickness in the supersonic boundary layer combustion has been recently studied by Kirchhartz, R. M., et al.[36]

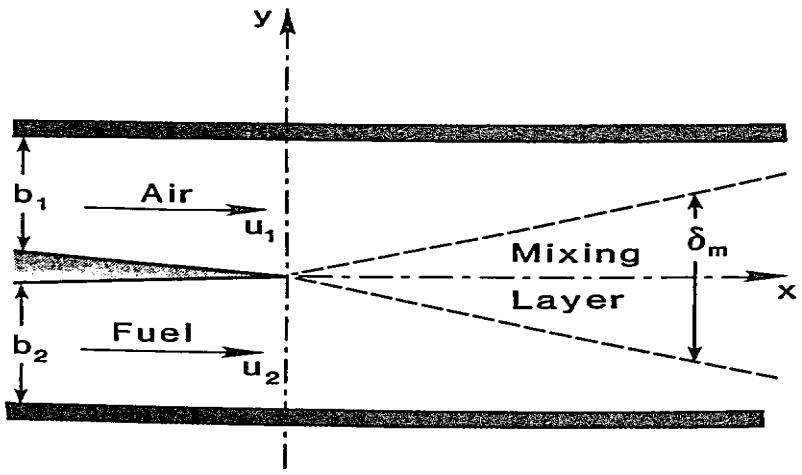

Fig. 1 Mixing of parallel streams of air and gaseous fuel in a constant-area duct (from Ref. 13)

2.1.2 Turbulent Mixing (Shear) Layer

As the velocity difference between the two streams (fuel-air) is further increased, the flow eventually undergoes transition from laminar to turbulent flow. When the mixing layer becomes turbulent, the time-steady shear layer becomes unstable and large vortices are periodically formed between the two streams. This phenomenon is schematically shown in Figure 2. Brown and Roshko[9] attempted to explain the effect of density on decreased mixing efficiency with Mach number in terms of a vorticity thickness (with low subsonic parallel streams). Their results showed little influence of density ratio on decreased mixing efficiency, but their studies obviously demonstrated the existence of large-scale turbulence structure in the mixing layer that could be connected to linear stability theory. Papamouschou and Roshko[10] extended their research to supersonic pressure balanced parallel streams (with stream Mach number from 0.2 to 3.4). Their study utilized Gropengiesser[14] application of linear stability theory to relate the decreased mixing efficiency to convective Mach number. Their study showed that the convective Mach number, M_C could be expressed by

$$M_C = \frac{U_1}{c_1}\left\{\frac{\left[1+(U_2/U_1)\sqrt{\rho_2/\rho_1}\right]}{\left(1+\sqrt{\rho_2/\rho_2}\right)}\right\} = 2\,\frac{(U_1-U_2)}{(c_1+c_2)} \qquad (2.4)$$

where c_1 and c_2 are the speeds of sound, U_1 and U_2 are the streamwise velocity, and ρ_1 and ρ_2 are the density in each stream.

Then, their study explicitly related reduced shear layer growth at compressible speed to incompressible shear layer growth according to:

$$\frac{C_\delta}{(C_\delta)_0} = \frac{C_\delta c_1 M_C}{const(U_1-U_2)} \qquad (2.5)$$

where $C_\delta = d\delta/dx$ and $(C_\delta)_0$ are the measured shear layer growth rate and incompressible growth rate at the same velocity and density ratios, respectively. The constant, in equation 2.5, is 0.17 based on the measurement by flow visualization and

0.14 based on the measurement by Pitot tube. Figure 3 is a composite graph, which includes Papamouschou and Roshko[10], NASA Langley Research Center experimental curve from Birch and Eggers[8] and others clearly shows the effect compressibility has on mixing efficiency.

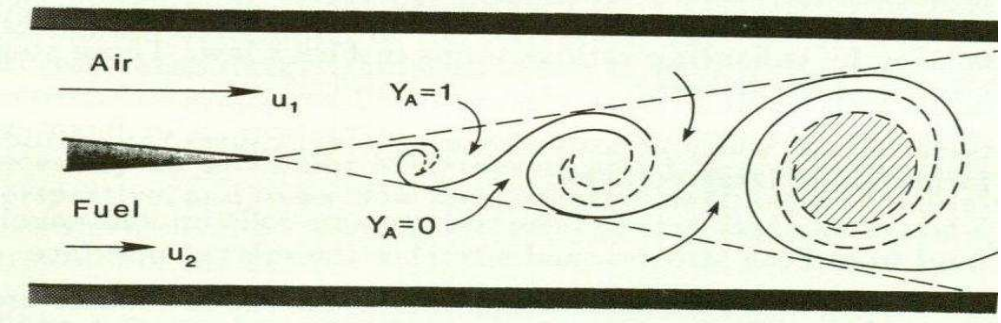

Fig. 2 Formation of vortex structures in a transitional shear layer, for $u_1 > u_2$. Dashed curves at mixant boundaries indicate molecular diffusion. Crosshatched area represents fully micromixed region (from Ref. 13).

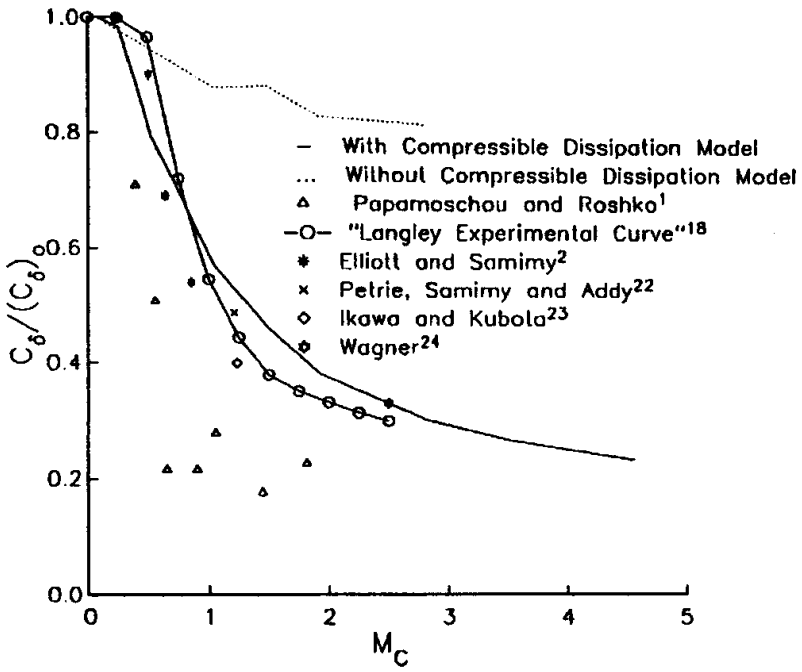

Fig. 3 Normalized shear layer growth with convective Mach number (from Sarkar and Balarkrishnan[15])

2.2 Concepts from the Reduction of Supersonic Jet Noise

Previously proven technical concepts of the reduction of supersonic jet noise, enhancing the exhaust jet mixing technology, can be successfully applied to improving the efficiency of the scramjet's supersonic combustion.

2.2.1 Solid and Fluid Tabs

For several decades extensive research on exhaust jet mixing enhancement and noise suppression have been studied and many devices both passive and active have been suggested such as solid/fluid tabs, counterflow, serrated (Chevron) nozzles, lobed mixers, and acoustic excitation, etc. Seiner, J. M., et al.[3] have provided a summary of these devices. Throughout the years, solid tab has received most attention out of all devices due to its simplicity and effectiveness. The most effective tab shape found is the delta-tab, which is of triangular shape, and the most effective angle is at 45^o with respect to exhaust jet stream. The orientation of the tab angle is more important than the precise tab shape. Solid tabs are usually placed at the jet nozzle exit and produce counter-rotating streamwise vortices, which entrain ambient fluid into the jet core. The tabs emerge to be a practical device to enhance the exhaust jet mixing in the first 10 jet diameters from nozzle exit. Two distinctly different concepts with the use of tabs have been studied to reduce supersonic jet noise through enhanced mixing: The first concept explicitly attempts to generate a streamwise vorticity to increase a contact area between low and high speed streams. The second concept explicitly attempts to generate a streamwise vorticity to stimulate large scale shear layer instabilities through injection of additional shear layer velocity inflection profiles. The first concept has been experimentally and numerically investigated in a round axisymmetric nozzle by Seiner and Grosch[16]. The tabs with the total projected blockage area of 3% of the nozzle exit area are mounted away from the nozzle lip at a ramp angle of 45 deg. The study shows that the supersonic flow over these tabs clearly leads to flow separation and the generation of counter-rotating vorticity. Some of the results are shown in Figure 4. The second concept also has been investigated with a tab design based on the Rayleigh

equation, $\ddot{x} + F(\dot{x}) + x = 0,\ \dot{x} = \frac{dx}{dt}, where\ uf(u) < 0\ for\ small\ |u|\ or\ uF(u) > 0\ for\ large\ |u|,$ and mounted on the ducted supersonic slot jet with heated flow and subsonic co-flow by Grosch et al.[17] The Schematic drawing of the channel and coordinate system and some of their results are presented in Figure 5 and 6. Since the scramjet combustion has a limited area to mix and burn the fuel-air mixture in a short residence time, the tabs would provide significant advantages when applied to scramjet combustion. Besides, the required tab geometry shrinks with increasing Mach number. More precise experimental and computational studies can be found in reference 16 to 20.

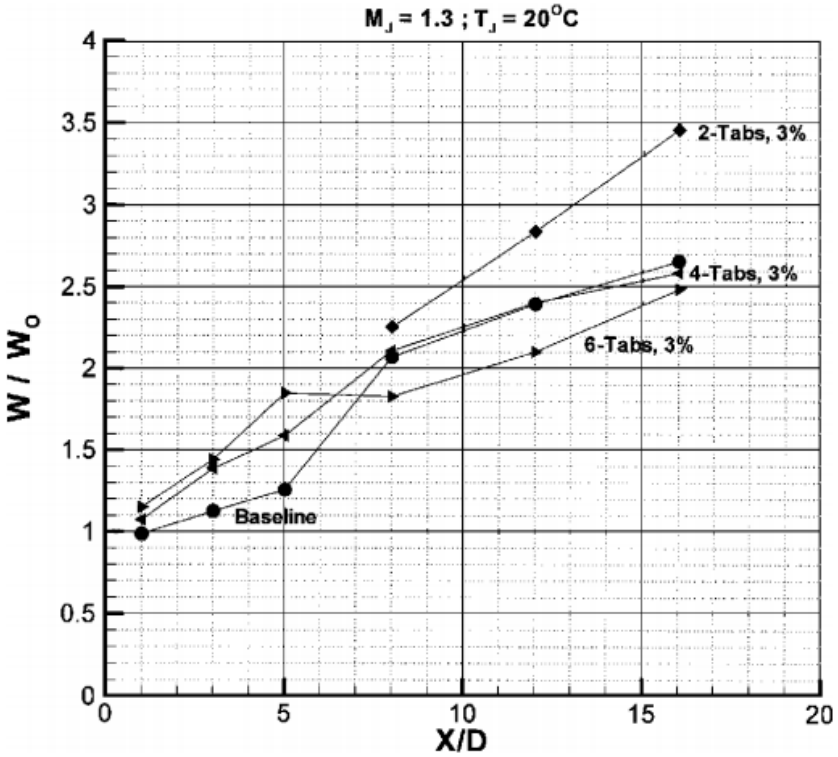

a) Mass flow ratio, relative to nozzle mass flow

Fig. 4a Measured mass entrainment of various tabbed nozzles (from Ref. 16)

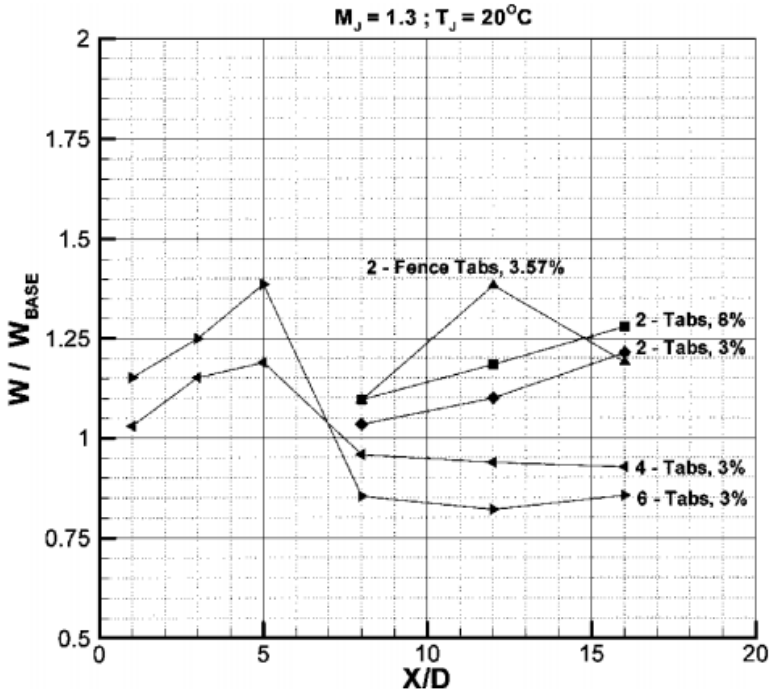

b) Mass flow ratio, relative to baseline nozzle mass flow

Fig. 4b Measured mass entrainment of various tabbed nozzles (from Ref. 16)

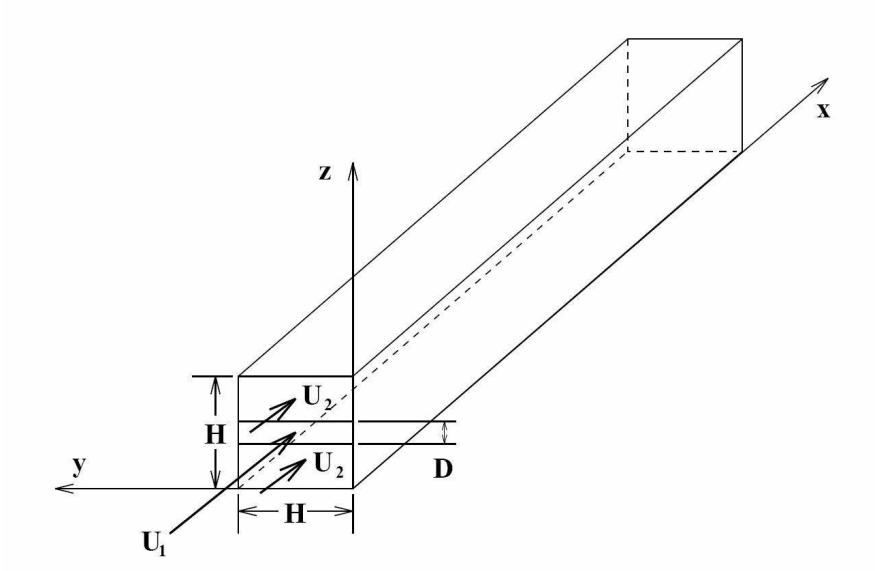

Fig. 5 Schematic drawing of the channel and coordinate system (from Ref. 17)

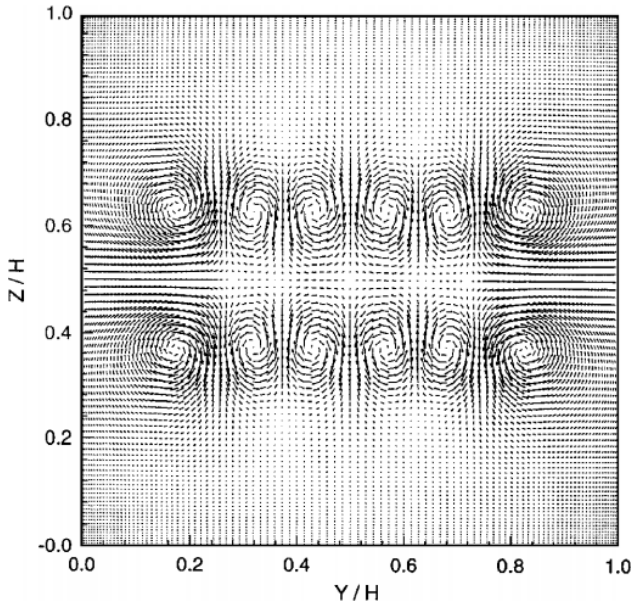

a) numerical simulation of tab array and coflow
(vector plot of the velocity field)

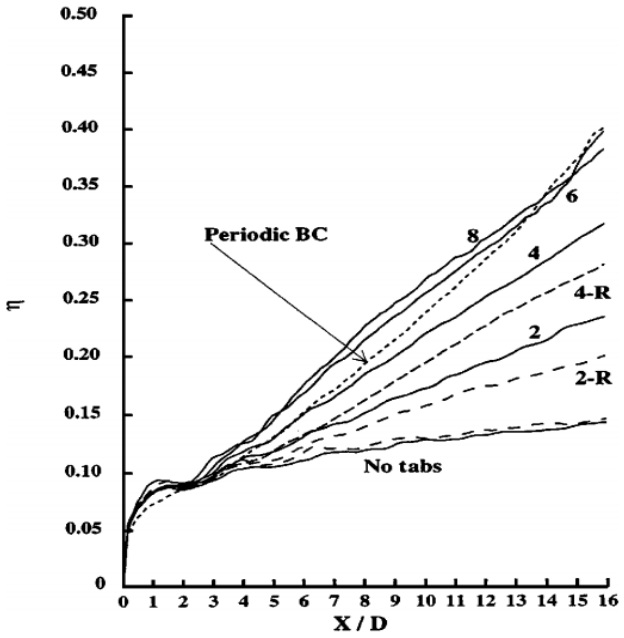

b) comparison of mixing effectiveness, η≡mixing parameter
(-R ≡ negative V_0 and trailing vortices)

Fig. 6 Mixing effectiveness for various tab arrays from a slot nozzle (from Ref. 17)

Recently a fluid tab concept is computationally and experimentally investigated by Parviz Behrouzi and James J. McGuirk[21]. The streamwise vorticity fields generated by fluid and solid tabs are almost identical in size and strength, although slightly different in shape and location. Also, the vortex formation of the fluid tabs depends on the fluid tab jet penetration. Required flow rate of the fluid tabs is about 1% of the core nozzle flow and fluid tabs can be switched on and off. Therefore, associated drag/thrust loss penalties with installing solid tabs can be minimized through the application of fluid tabs. The experimental setups and results are shown in Figure 7 and 8.

a) solid tabs (2) b) fluid tabs (2)

(a tab height/width = 20%/6% of the nozzle diameter, a 1.3% area blockage per tab)

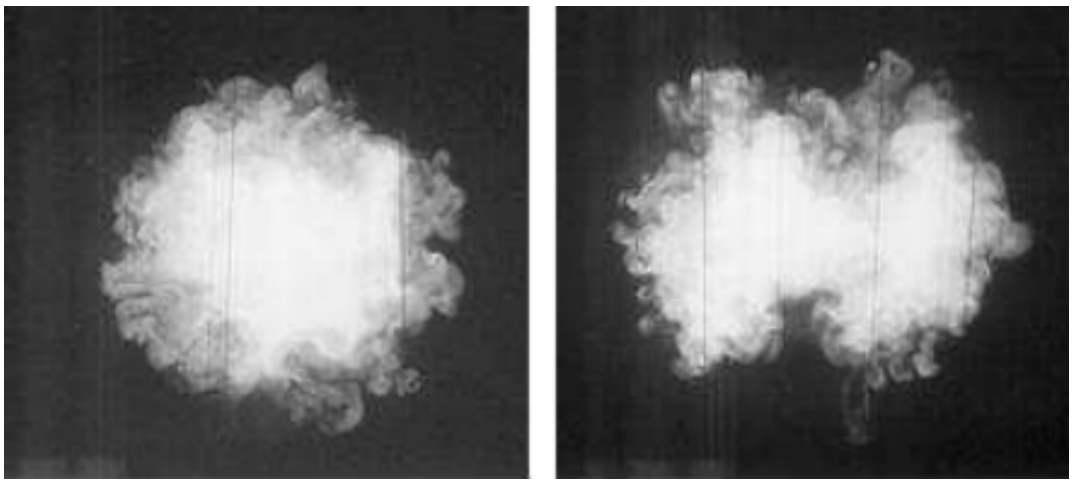

c) plain circular jet d) tabbed jet

Fig. 7 Experimental setups of solid and fluid tabs and laser induced fluorescence (instantaneous) images of jet cross-section at $x/D_n = 5$ (from Ref. 21)

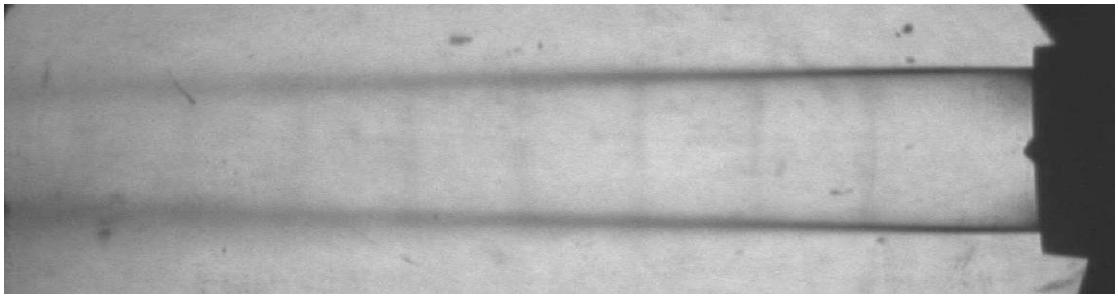

a) plain jet

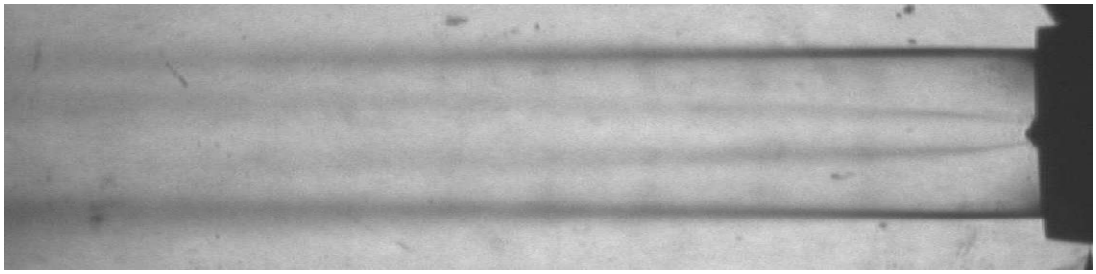

b) fluid tabs

Fig. 8 Schlieren images of jet plume in a plain jet and the jet with fluid tabs (from Ref 21.)

2.2.2 Counterflow

The counterflow concept utilizes the instability theory of Huerre and Monkewitz[22] for self-excited resonance caused by acoustic feedback, which is based on the absolute or temporal instabilities associated with the solution of the Rayleigh equation. This concept, i.e., the absolute instabilities of mixing layers, is demonstrated by Strykowski et al.[1] and Strykowski and Niccum[2]. With suction backflow with only a few percent of the primary exhaust jet flow, a massive increase of the mixing enhancement could be achieved. For an ideally expanded Mach 2 axisymmetric jet, it was shown by Strykowski et al.[1] that the exhaust jet mixing is enhanced by as much as 60% when counterflow is applied to the jet periphery. Schematic of the concept and experimental results are shown in figure 9. The results show that counterflow significantly enhances shear-layer mixing and reduces the jet potential core length due to the global instability of the flowfield. Also, both the shock-cell strength and their spacing are drastically reduced. The counterflow technique is particularly an effective approach to mixing control in a high speed heated jet because the jet becomes more controllable at higher temperature ratio; as less counterflow is required to attain equivalent levels of mixing. The results are shown in figure 10. The similar experimental results of the shear layer growth and reduction of the potential core length by applying the counterflow to a supersonic jet were found by Shih et al.[23] The experimental results are shown in figure 11. Their studies also indicate that the counterflow results in minor thrust penalties caused by the vacuum pressure establish in the suction collar region. The thrust loss is mostly dependent on the geometry and shape of the suction collar.

The counterflow concept along with the tabs would be an extremely effective combination if applied to scramjet combustion, especially the fluid tabs. The fluid tabs can be generated by the suction backflow brought to upstream of the incoming flow before the fuel is injected as the flow tab jet penetration can be controlled by the amount of the suction backflow, to produce counter-rotating streamwise vortices. Outstanding flame-holding capability, increased fuel residence time that is provided by

the counterflow along with the counter-rotating vortices created by the tabs could be the most effective fuel mixing enhancement mechanism if applied to a scramjet combustor.

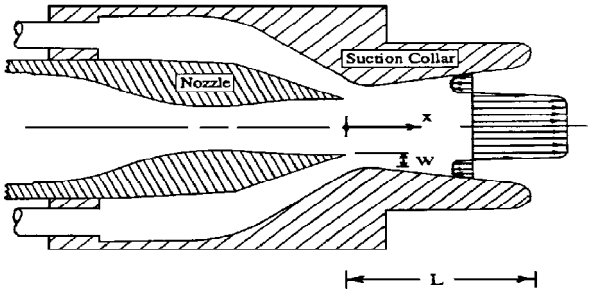

a) schematic of counterflow

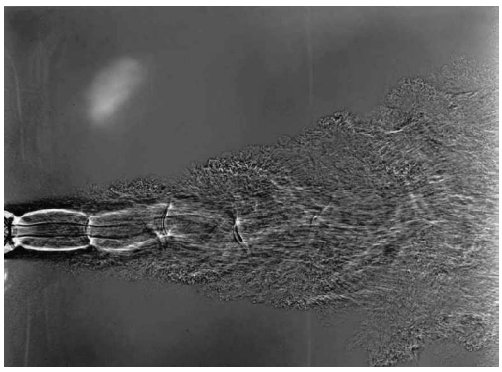

b) Counterflow off

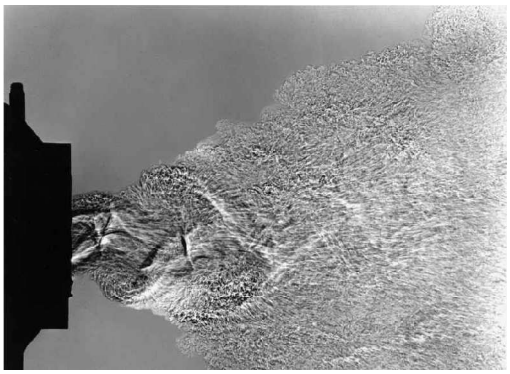

c) Counterflow on

Fig. 9 Exhaust jet mixing enhancement with counterflow at M = 1.45 (from Ref. 1)

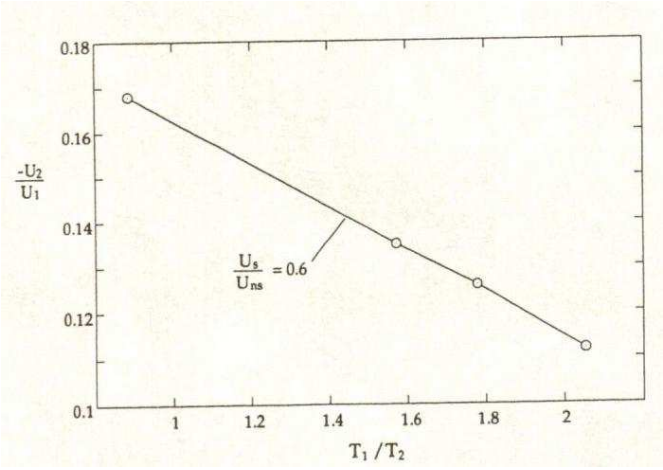

Fig. 10 Relationship between velocity and temperature ratio at M_1=0.8 (from Ref.1)

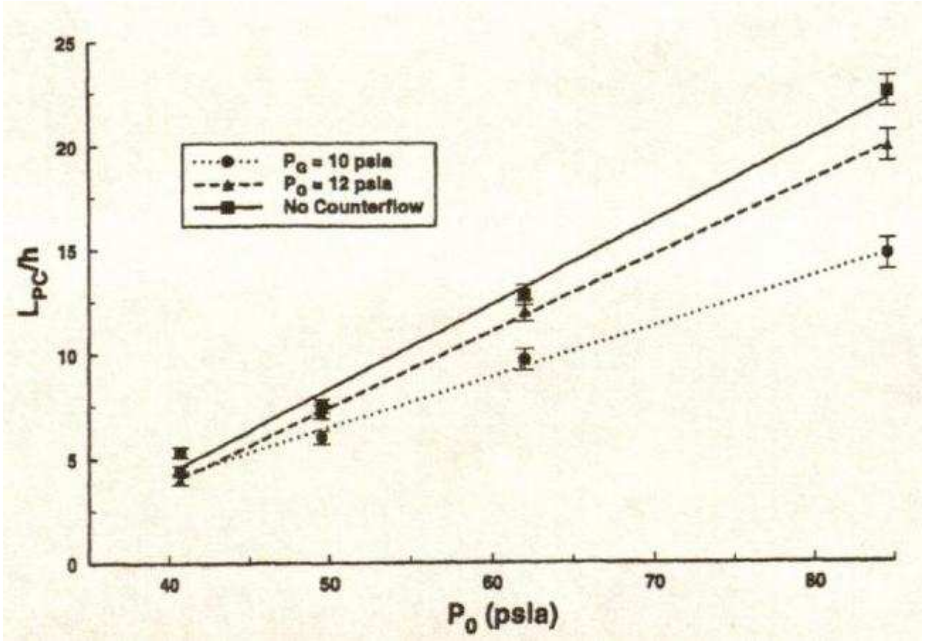

a) potential core length

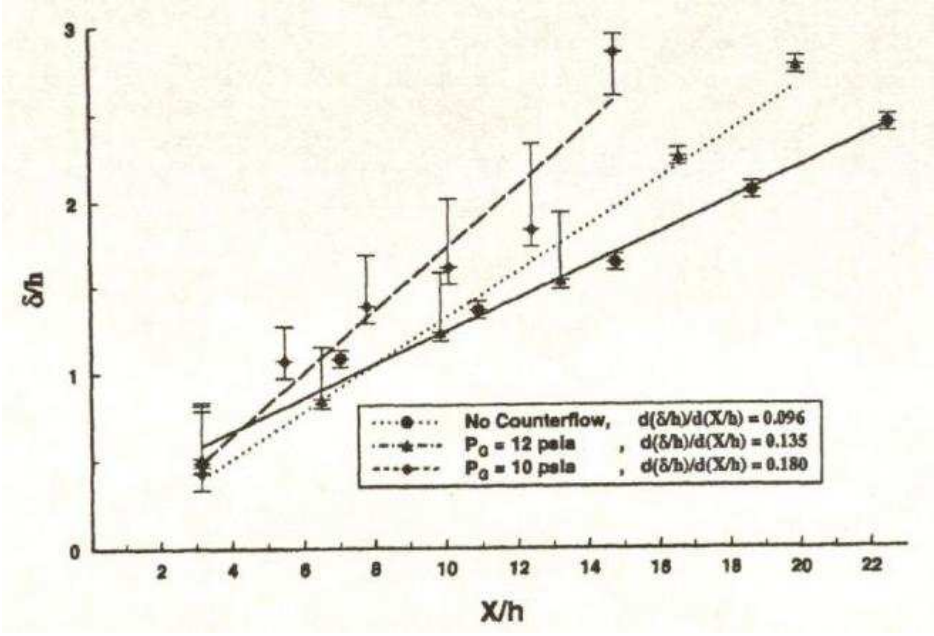

b) shear layer growth for P_0= 84.5 Psia

Fig. 11 Experimental data of effects of the counterflow on the potential core length and shear layer (from Ref. 23)

2.3 Fuel Injection Mechanism for the Scramjet

An initial scramjet combustor was designed with the normal fuel injection into the supersonic free stream as shown in figure 12. Even though combustion can be achieved in very short distances from the injection because the separation zone caused by a detached normal shock upstream of the jet acts as a flame holder, significant losses in total pressure and scramjet cycle efficiency are the major problems with the wall mounted normal fuel injection. Therefore, a parallel fuel injection mechanism is an obvious choice for the scramjet to minimize performance losses, but the parallel mixing has extremely low combustion efficiency due to poor mixing rate at a supersonic speed. This problem could however be solved if assisted with generation of axial vorticity, which was concluded by Dimotakis[25] study. The most popular parallel fuel injection mechanisms that have numerically and experimentally been investigated are ramps[26,27,30] and struts[28,29]. These methods are proven to be more effective than wall injection. Also, a strut with fuel injectors is a more efficient method than ramps, but it causes higher aerodynamic loss, i.e., drag and total pressure drop. Since the strut with fuel injectors is usually located along the centerline of the scramjet combustor, it produces stronger shocks and complicated structural problems. The effect of ramp was investigated numerically by Drummond et al.[26] and experimentally by Donohue et al.[27] Their results, which are presented in Figure 13, are clearly shown that the ramp generates the axial vorticity that is needed to enhance the mixing. As shown in a numerical study of Abdel-Salam et al[30], the purpose of the wall mounted ramps is to generate a pair of counter-rotating vortices to hold the injected fuel and increase the mixing rate by converting a part of the flow energy into tangential kinetic energy, i.e., a vortex. The study shows that the unswept relieved ramp gives better mixing rate than the unswept raised ramp. Also, the swept ramp gives higher mixing rate than unswept ramps. Some of the results are presented in figure 14 and 15. However, all of the previously studied fuel injecting mechanisms are not sufficient to overcome the overall decrease in combustion efficiency and thrust with increasing combustor Mach number since the degree of fuel-air mixing, which can be achieved by the natural convective

and diffusive processes, is reduced. The present CFD study is aimed to explore mixing enhancement opportunities in a scramjet combustor to produce maximum combustion efficiency and minimum aerodynamic penalties and thrust loss.

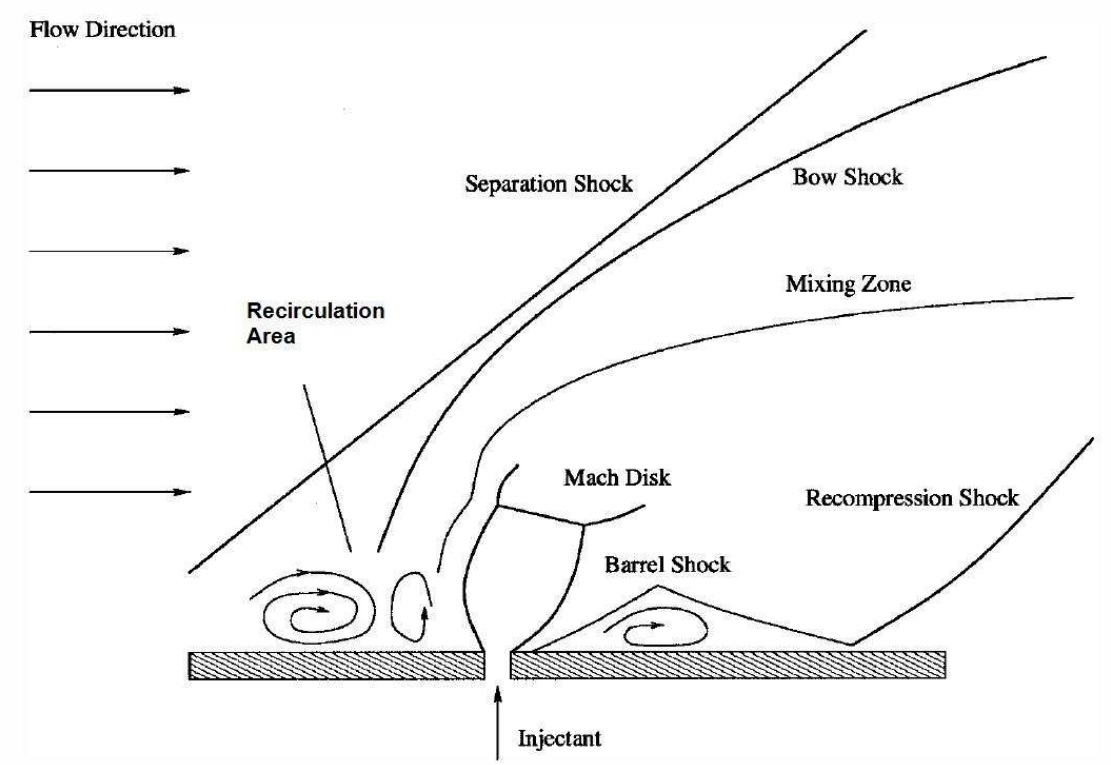

Fig. 12 Normal fuel injection mechanism for the scramjet (from Ref. 24)

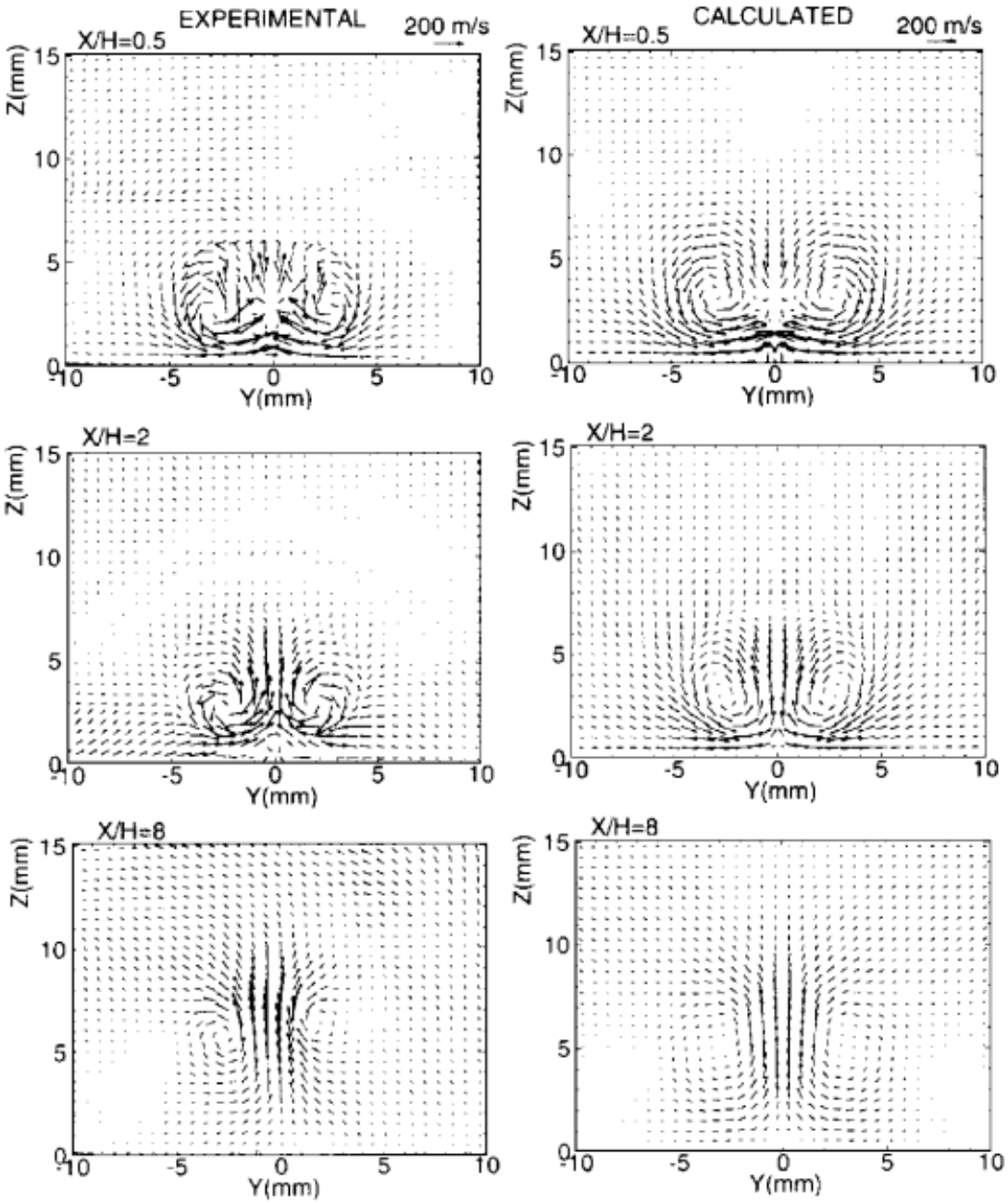

Fig. 13 Measured and predicted crossflow velocities with ramp (from Ref. 27) (Velocity vector plot)

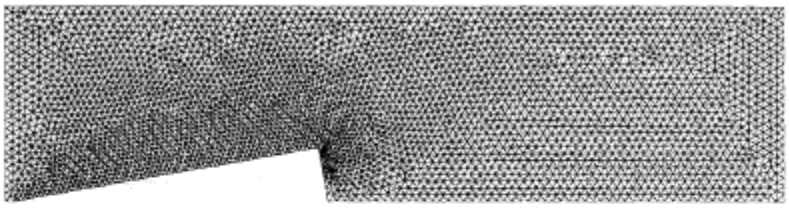

Raised ramp.

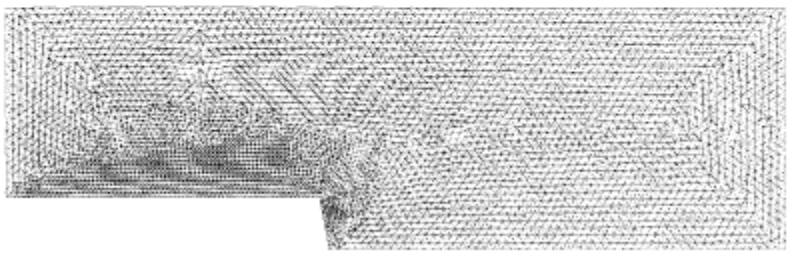

Relieved ramp.

a) generated grids

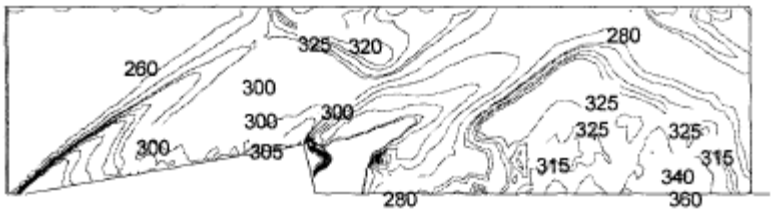

Unswept raised ramp

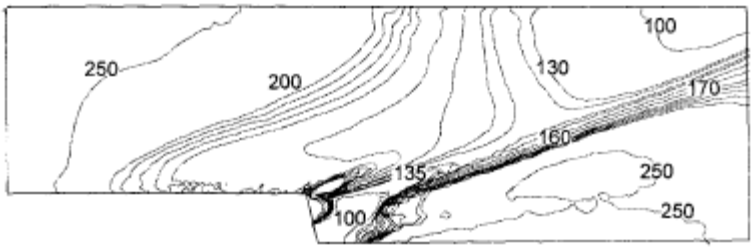

Unswept relieved ramp

b) static pressure contours in the plane of symmetry

Fig. 14 Numerical study of mixing efficiency for the scramjet (from Ref. 30)

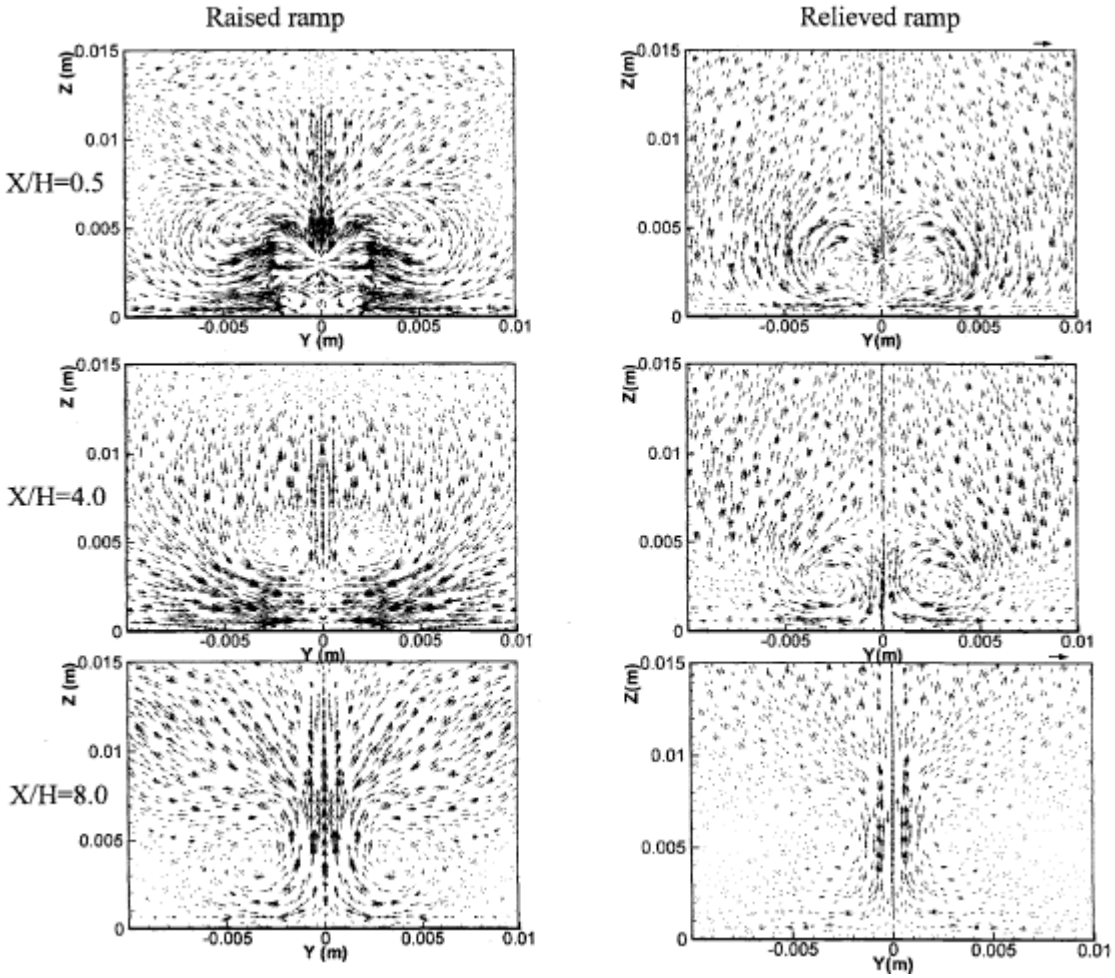

Fig. 15 Cross-stream velocity vectors for 5 degrees swept ramps at different axial locations (from Ref. 30)

3 Numerical Method

In the present study, three-dimensional numerical simulations are carried out using the commercial CFD code FLUENT[35]. The coupled implicit method with explicit time stepping is used with second–order accurate discretization. RNG k-ε model[35] that includes additional term in its ε equation, which significantly improves the accuracy, is used and the effect of swirl turbulence is also included in the model. The finite rate reaction model is used for the species transport model that only considers four species, H_2, O_2, H_2O and N_2. A comparison of numerical predictions of supersonic combustion of hydrogen using different chemistry models can be found in Ref. 37. Vitiated air (mass fraction of O_2, H_2O, and N_2 being 0.198, 0.139, and 0.663, respectively) enters the combustor at a Mach number of 2.5 and a stagnation temperature and pressure of 1500 K and 1 MPa, respectively. The inlet conditions of the hydrogen fuel injection ports are adjusted to achieve sonic injection with the desired fuel mass flow rate.

For boundary conditions, a fully developed turbulent flow for the incoming air and fuel jet is assumed. Also, the conventional no-slip condition along the combustor solid walls is used. All of the wall surfaces are assumed to be adiabatic along with the standard wall functions. At the air inlet, pressure inlet conditions are used and a stagnation pressure, stagnation temperature, static pressure and species mass fraction are specified. At the hydrogen fuel inlet, mass-flow inlet conditions are used and mass-flow rate of hydrogen, static pressure, total temperature and species mass fraction are specified. For turbulent calculations, wall y+ values less than 100 are generally acceptable[31], but the use of standard wall functions in the simulations requires that the wall y+ values less than 30 to achieve an accurate result. However, in flows with shocks, especially at the points of impingement and reflection of shocks, it is not always feasible to get the wall y+ value below 30. Therefore, the area-average wall y+ is used as a companion metric for the flows. Further details of the numerical modeling of the scramjet combustor can be found in reference 31 to 33 and the Fluent user's guide[35].

The geometry of the scramjet combustor for the present CFD study is intentionally selected to be identical to Tomioka et al.[29] to be able to compare with their experimental results. The schematic diagram of the combustor and part of the facility are shown in figure 16.

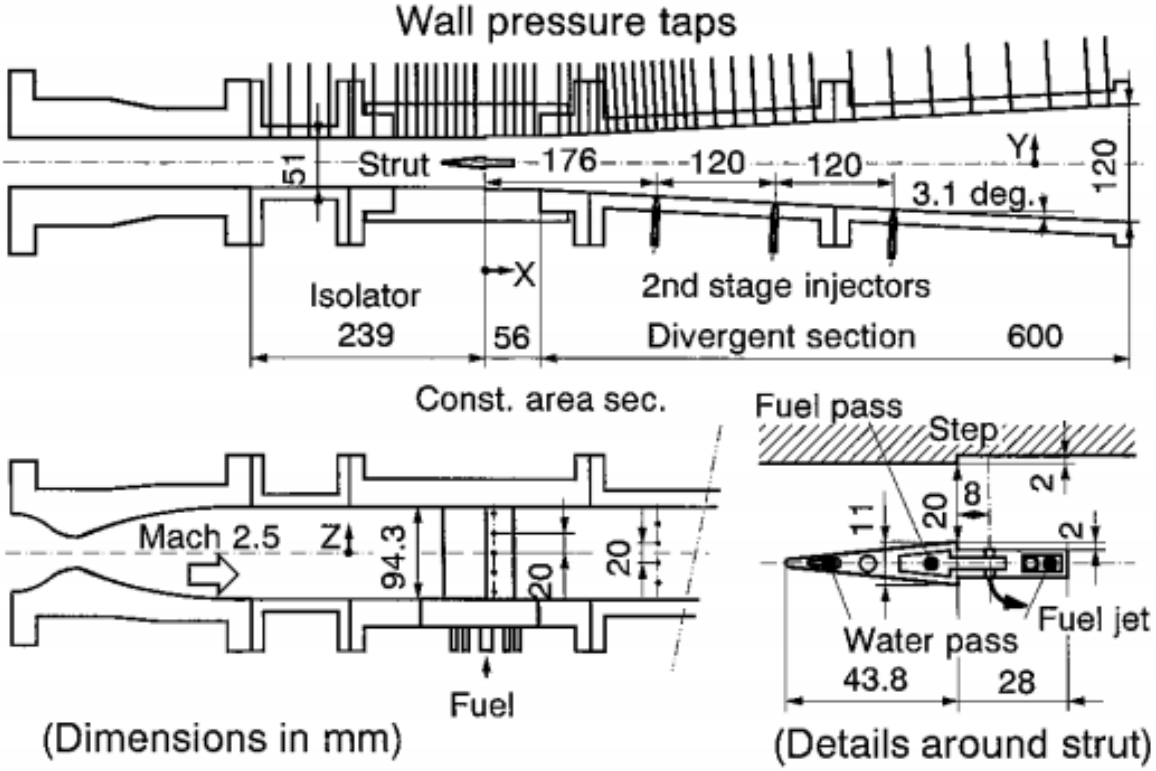

Fig. 16 Schematic drawing of the supersonic combustor (from Ref. 29)

4 Initial Numerical Studies

Initial numerical studies have been carried out without H_2 injection. For the parallel fuel injection schemes, relieved ramp is used. For the normal fuel injection schemes, wall injection is used. The coupled solver available in the commercial software FLUENT has been used with explicit time stepping and second-order accurate discretization.

4.1 Grid Generation

Structured (hexahedral) grids have been generated for the numerical models without tabs. With the delta tabs (2 or 4 tabs), structured and un-structured (tetrahedral/hybrid) grids have been generated. The flow field is assumed to have a plane of symmetry along the central plane (center of the x and y plane). Thus, one half of the scramjet combustor is generated to save on computational time. An initial hexahedral grid with the relieved ramp with 877,912 grid nodes was obtained. Based on the convergence rate (history of residual), the grid nodes are increased to 1,129,344 due to refinement near all of the no-slip surfaces, to achieve wall y^+ values as low as possible. The initial grid point studies and results are shown in figure 17. For the initial grid point studies, standard k-ε model with the standard wall functions are used at a Mach number of 2.5 and a stagnation temperature and pressure of 660 K and 1 MPa, respectably.

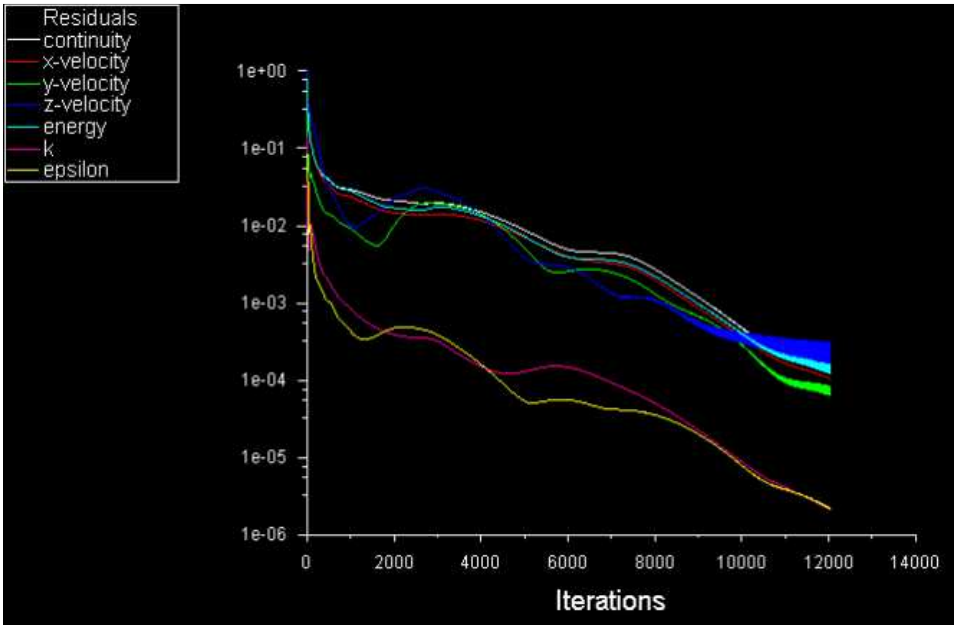

a) 877,912 grid nodes, 1000 iterations/4 hours CPU time (PC)

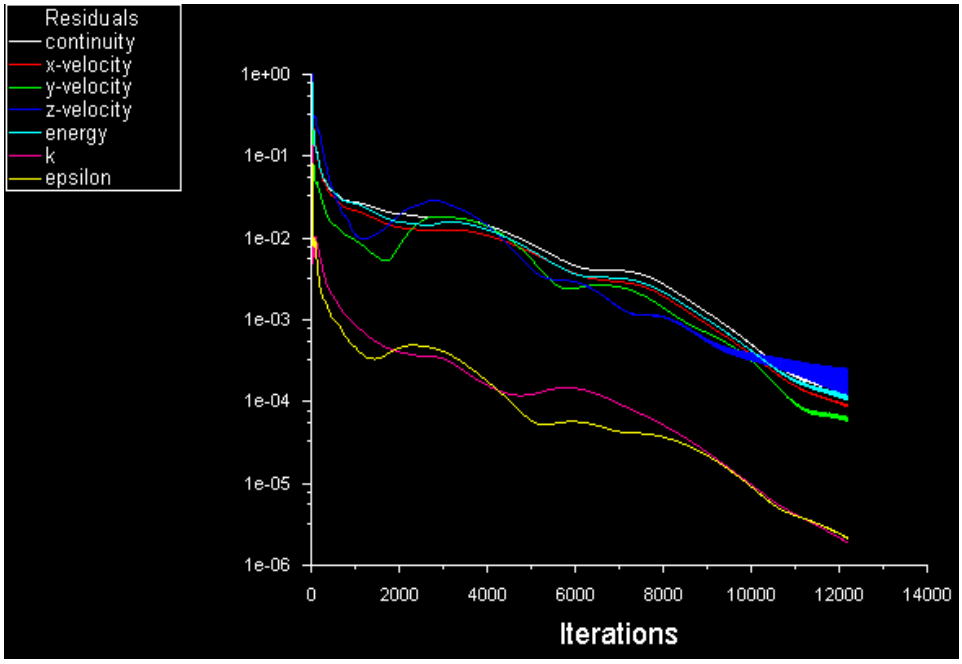

b) 1,042,032 grid nodes, 1000 iterations/7 hours CPU time (PC)

Fig. 17a Convergence rate (residual) study of the different grid nodes with ramp at M= 2.5 and T = 660 K

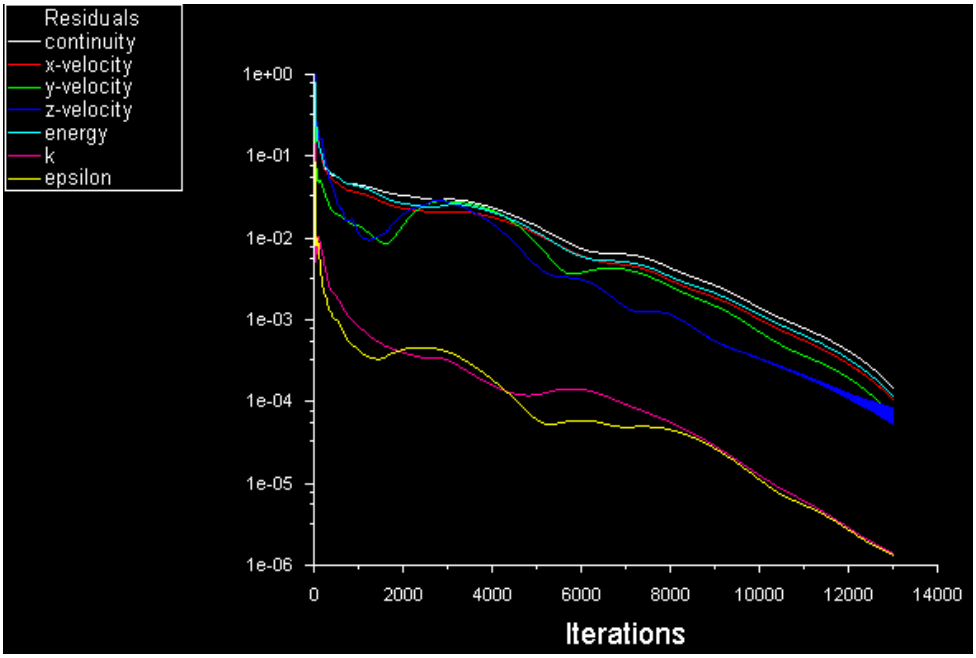

c) 1,129,344 grid nodes, 1000 iterations/8 hours CPU time (PC)

Fig. 17b Convergence rate (residual) study of the different grid nodes with ramp at M= 2.5 and T = 660 K

4.2 Turbulence Model Study

The turbulence model used for the present study is the RNG k-ε model (2 equations) with swirl dominated flow. Default values for the model constants (C_{μ}=0.0845, $C_{1\varepsilon}$=1.42, $C_{2\varepsilon}$=1.68, Swirl factor =0.07) are used with standard wall functions for the near-wall treatment. However, the Spalart-Allmaras model with default values for the model constants (C_{b1}=0.1355, C_{b2}=0.622, C_{w1}=7.1, C_{w2}=0.3, C_{w3}=2, Prandtl number=0.667) has also been investigated for turbulence modeling. The Spalart-Allmaras is a relatively simple one equation viscous model that solves a transport equation for the kinematic eddy, turbulent, viscosity. In general, especially for three dimensional flows, the use of a one equation model over a two equations model usually results in considerable savings of the computational effort. Even though the k-ε model takes more computational time and requires more iterations than the Spalart-Allmaras model, the convergence rate (residual) is much more stable and the shocks are captured more accurately. The flow conditions used for the numerical studies are: Mach number of 2.5 and a stagnation temperature and pressure of 660 K and 1 MPa, respectively. The results are presented in figure 18 through 21.

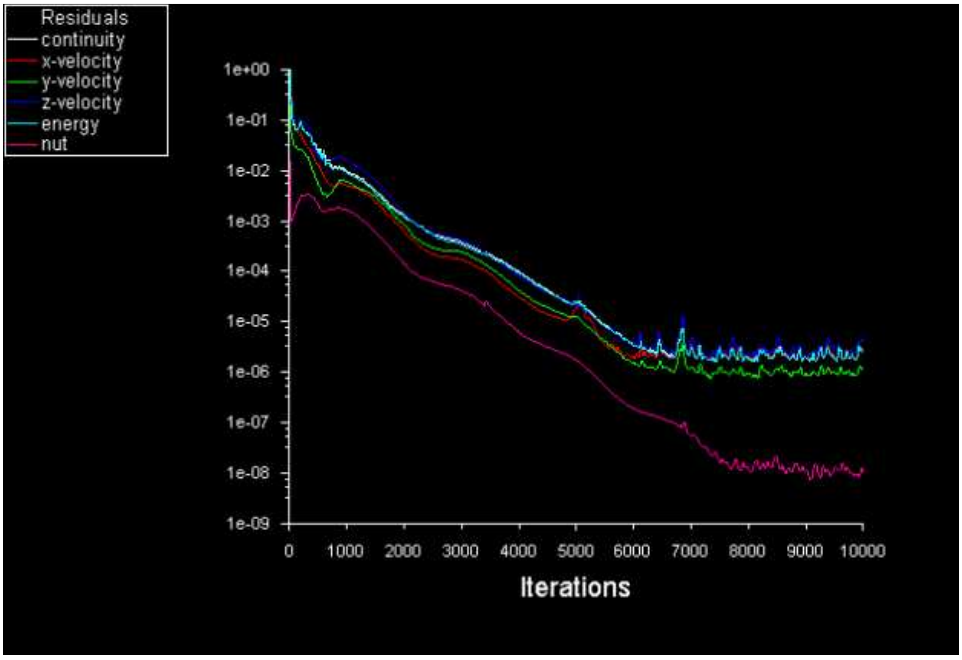

a) Spalart-Allmaras (1 equation)

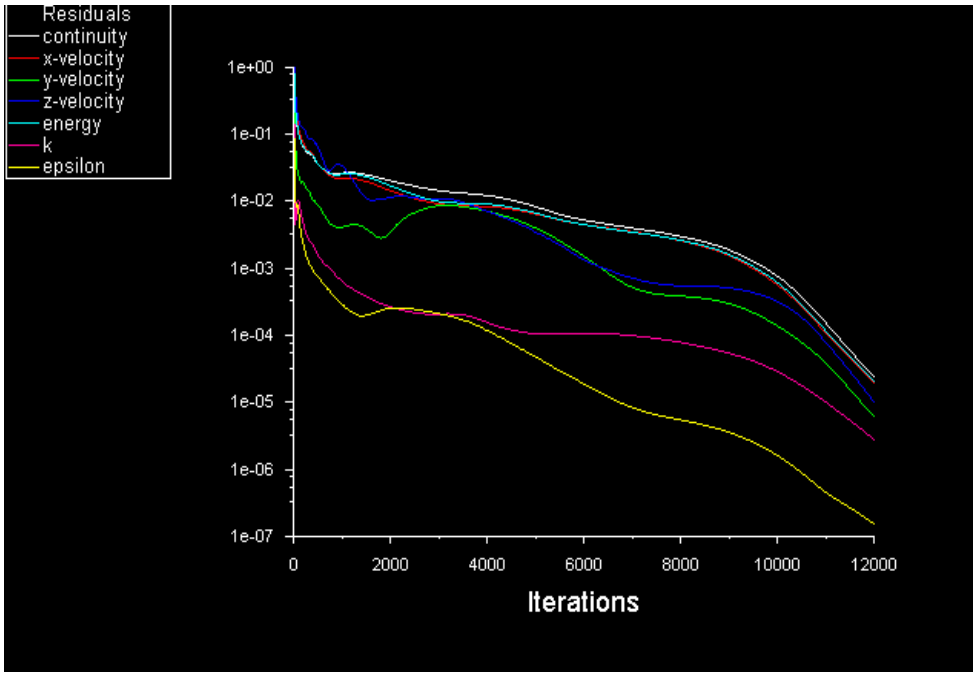

b) K-epsilon (2 equations)

Fig. 18 Study of the convergence rates (residuals) for cold air (660 K) at M = 2.5

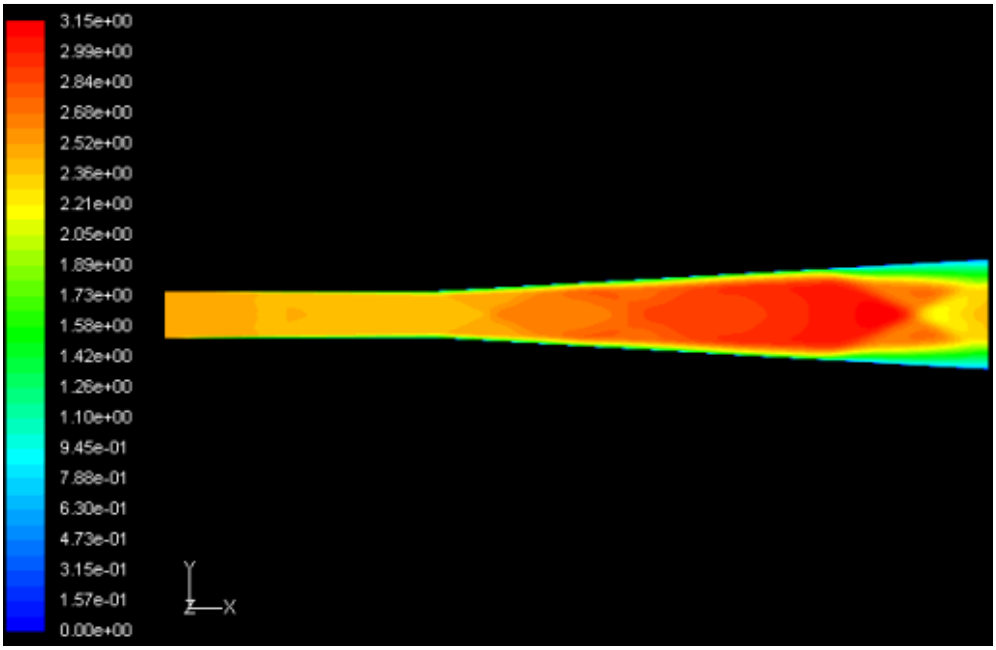

a) Spalart-Allmaras (1 equation)

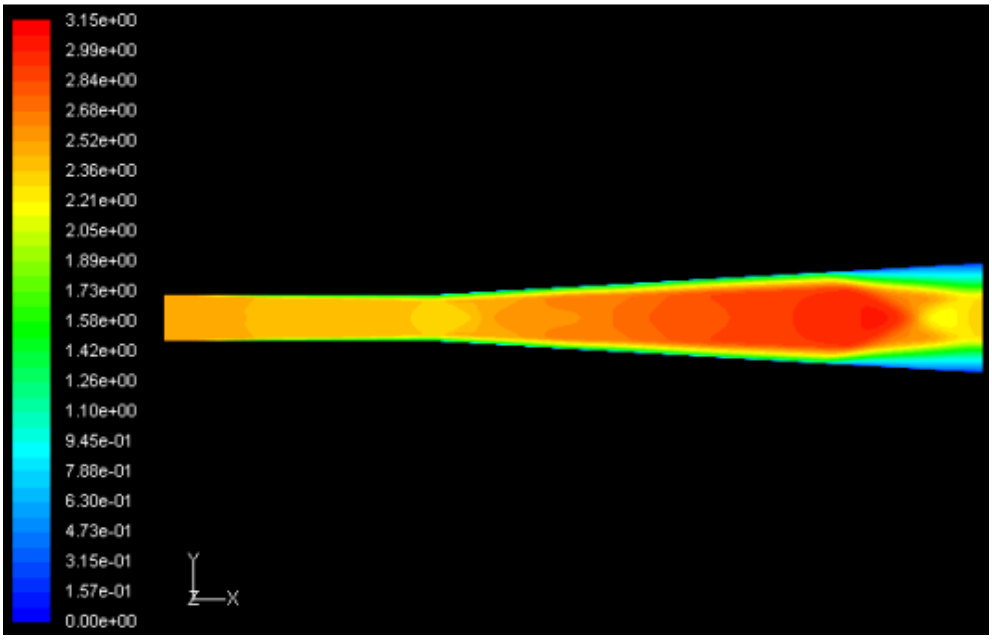

b) K-epsilon (2 equations)

Fig. 19 Mach number contours for cold air (660 K) using different turbulence models

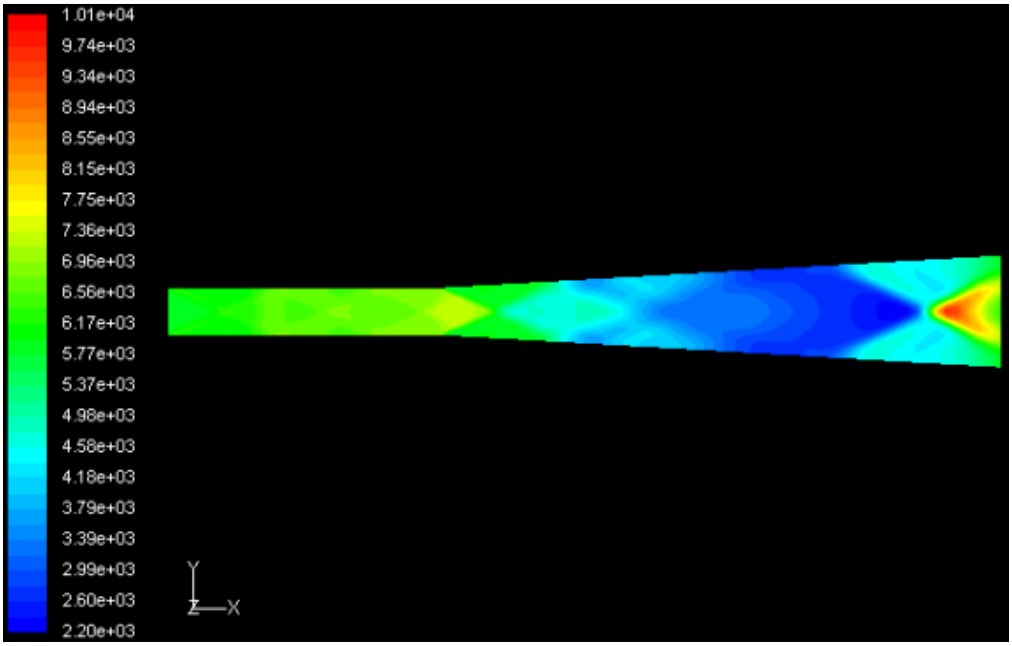

a) Spalart-Allmaras (1 equation)

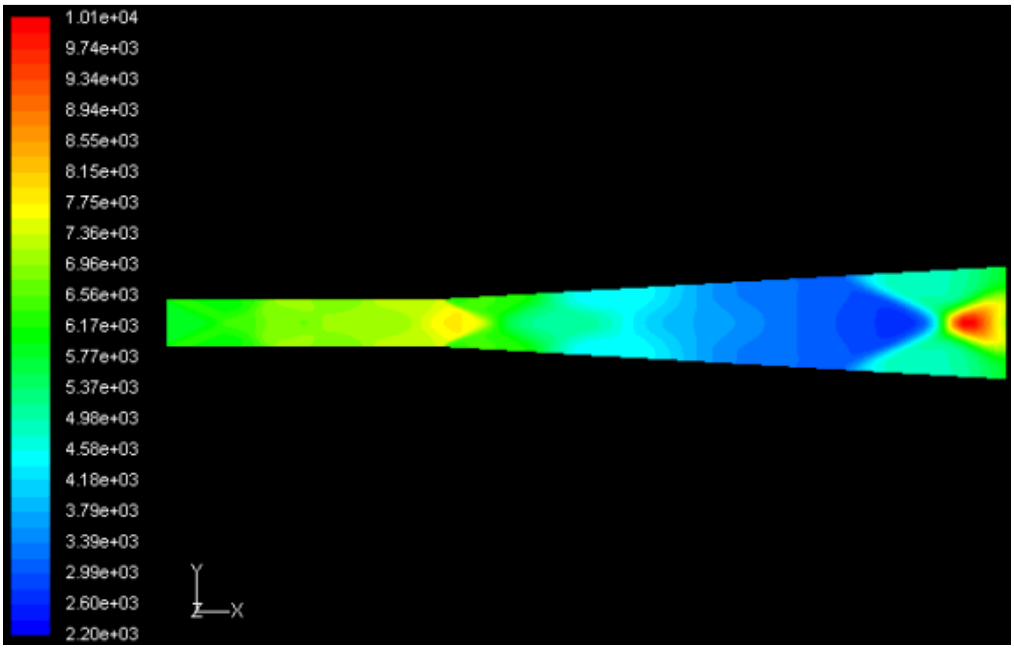

b) K-epsilon (2 equations)

Fig. 20 Static pressure (Pascal) contours for cold air (660 K) at M = 2.5 using different turbulence models

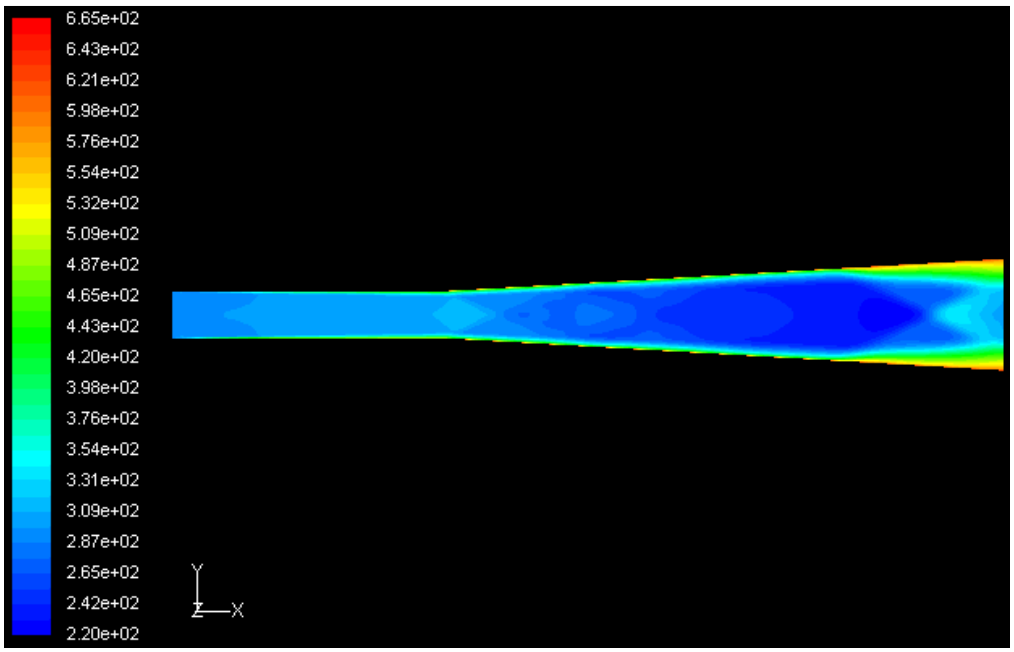

a) Spalart-Allmaras (1 equation)

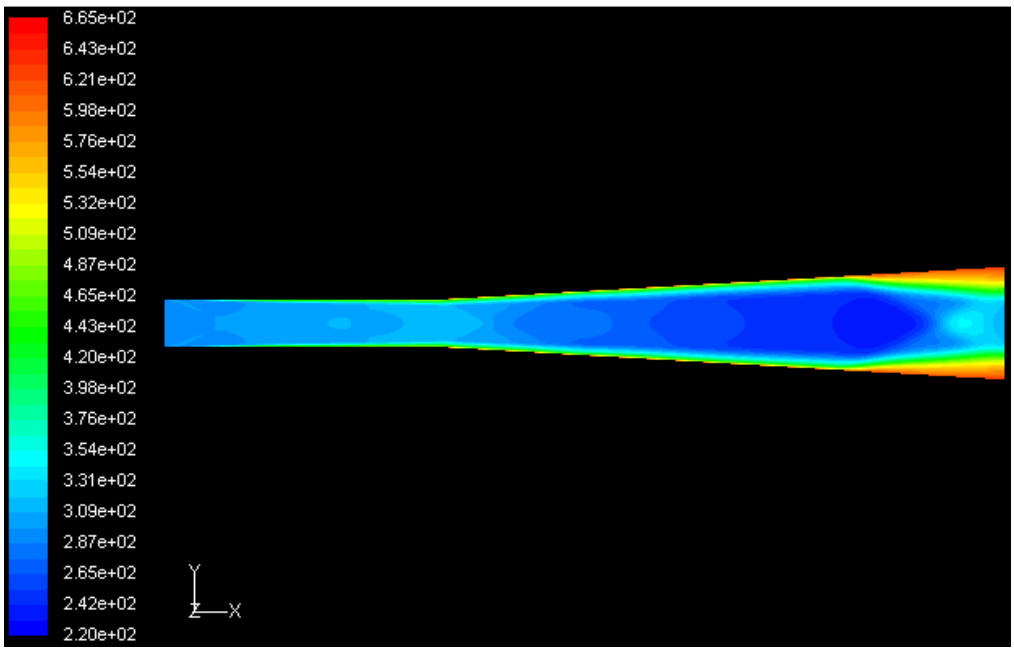

b) K-epsilon (2 equations)

Fig. 21 Static temperature (K) contours at M = 2.5 using different turbulence model

4.3 Basic Scramjet Model Studies with Ramps and Tabs

Structured (hexahedral) grids with about 1.12 million grid points have been generated for the scramjet with and without the relieved ramp. Flow conditions for the initial numerical studies are a Mach number of 1.25 and a stagnation temperature and pressure of 1500 K (hot/heated air) and 1 MPa, respectively without fuel (H_2) injection, clean air cases. The basic scramjet without the ramp is used as the baseline numerical study for the normal fuel injection. In the later CFD studies, hydrogen fuel is injected in the normal to the incoming air (increased up to M=2.5) from the lower wall of the scramjet at the sonic speed. The numerical model with the relieved ramp is used as the baseline study for the parallel fuel injection case. H_2 is injected parallel to the incoming air at the end of the ramp. The location and amount of the injected fuel for the two cases is deliberately kept the same to make a meaningful comparison of the two cases. Size of the relieved ramp is $1/10^{th}$ of the height of the scramjet inlet (51 mm). The generated hexahedral grids are shown in Figure 22. As expected oblique shocks that cause asymmetric flow are generated at the end of the ramp and the flow is turning downward. Also, the region of the flow separation is growing toward the outlet of the scramjet that causes significant losses in total pressure and scramjet cycle efficiency. The effect can be minimized with tabs and counterflow that create shear layer instabilities through injection of additional shear layer velocity inflection profiles to control the shear flow. The computational results are presented in figure 23 through 26.

Mixture of the structured and un-structured (tetrahedral/hybrid) grids with about 1.12 million grid points have been generated for the scramjet with 2 or 4 delta tabs. The dimension of the tabs is 5.66 mm (baseline) and 2.83mm (height) and the tabs are initially located at the end of the uniform inlet section and 45 degree toward the incoming flow. The generated grids are shown in figure 27. The tabs are generating counter-rotating vortices that increase shear layer (mixing layer) about 10 % and make more rapid mixing. As Mach number is increased, the required tabs size is getting smaller to generate the similar effects and the flow is became more controllable. Thus,

the tabs size shrinks with a Mach number of 2.5 for the further studies to minimize total pressure losses and scramjet efficiency. The results are present in figure 28 to 31.

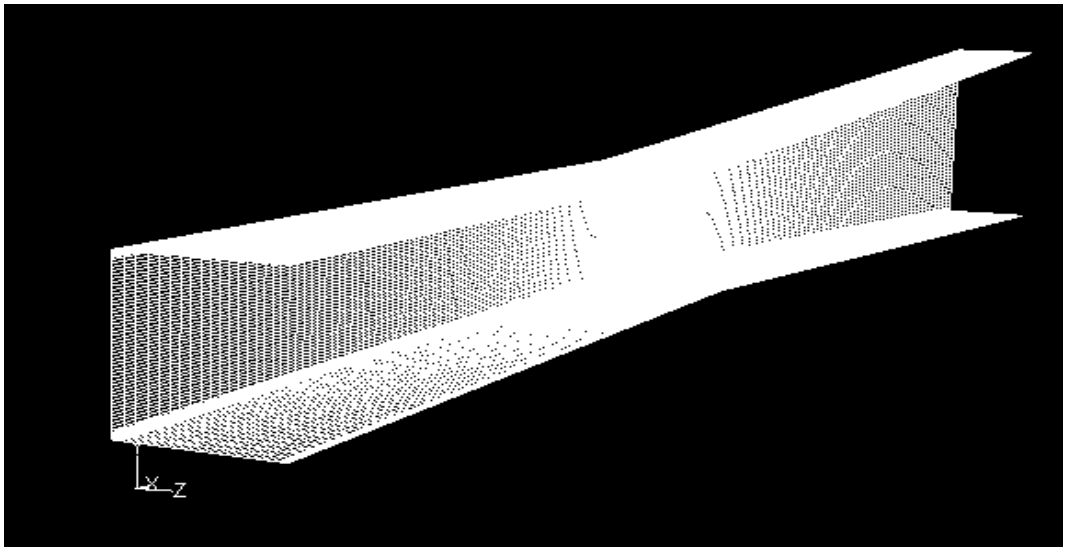

a) Grid in the Scramjet

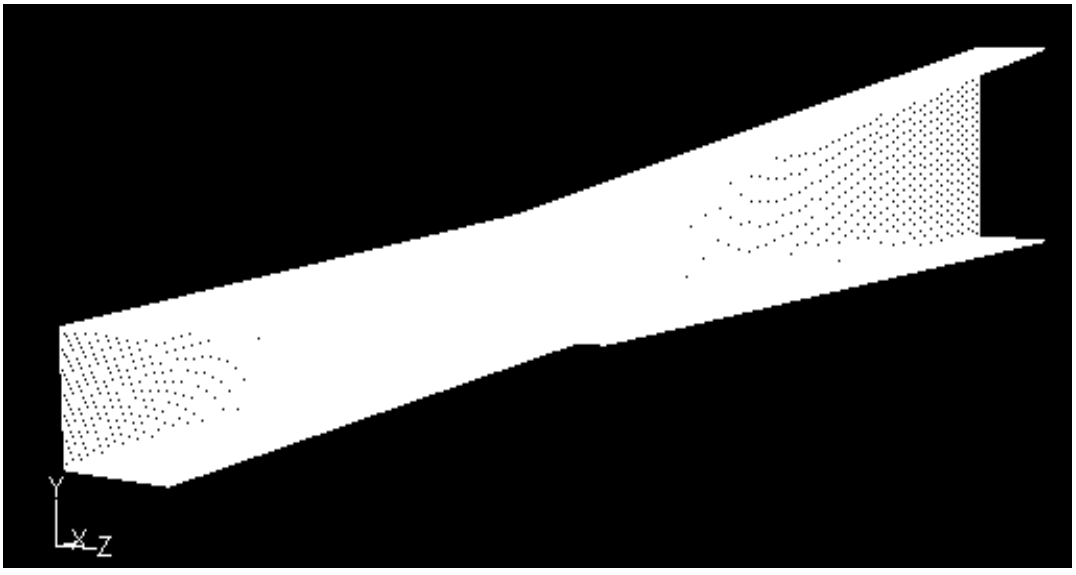

b) Grid in the Scramjet with Ramp

Fig. 22a Geometry of the Scramjet (Ramp Size is 1/10th of the Height of the Scramjet Inlet)

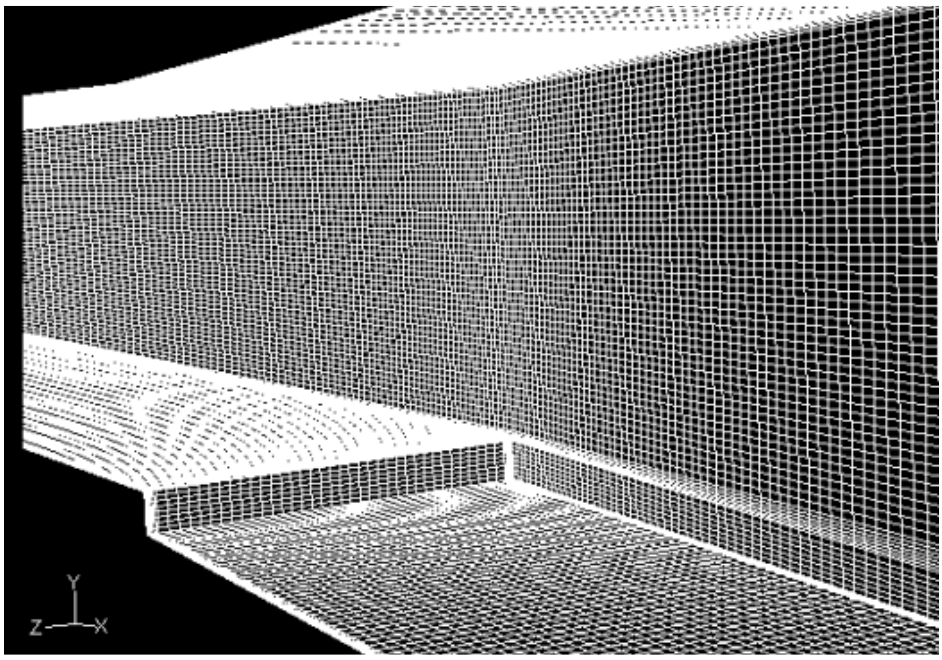

c) Detailed View of the Ramp

Fig. 22b Geometry of the Scramjet (Ramp Size is 1/10th of the Height of the Scramjet Inlet)

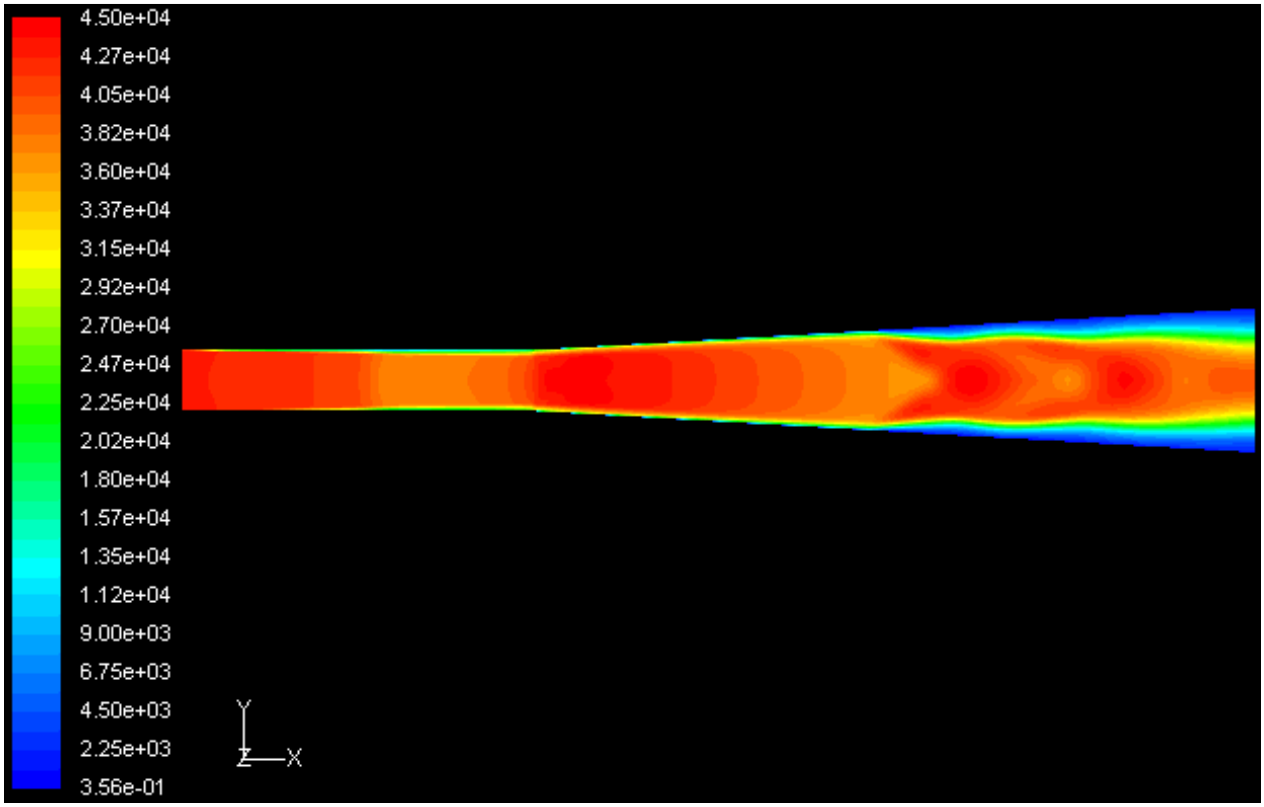

a) at the Plane of symmetry without ramp

Fig. 23a Dynamic Pressure (Pascal) Contours in the Scramjet with and without Ramp at M = 1.25 and T = 1500 K

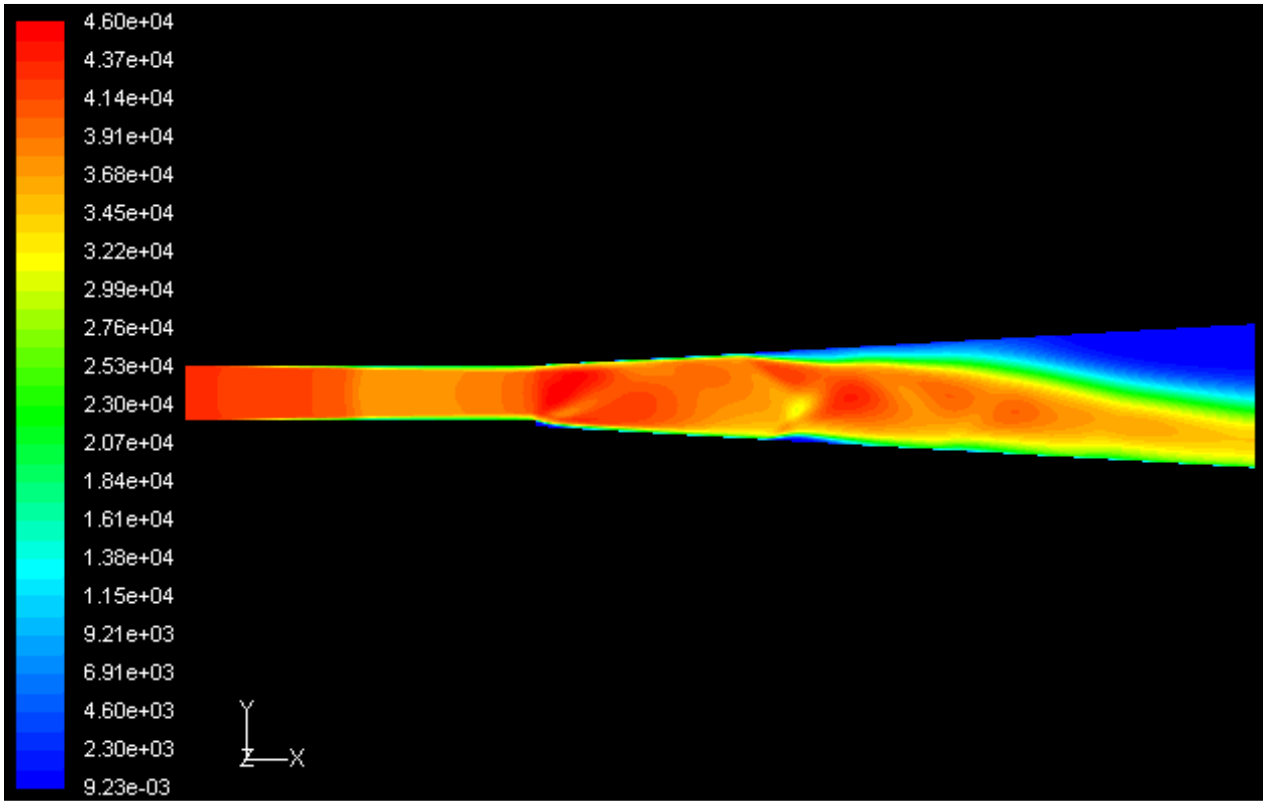

b) at the Plane of symmetry with Ramp

Fig. 23b Dynamic Pressure (Pascal) Contours in the Scramjet with and without Ramp at M = 1.25 and T = 1500 K

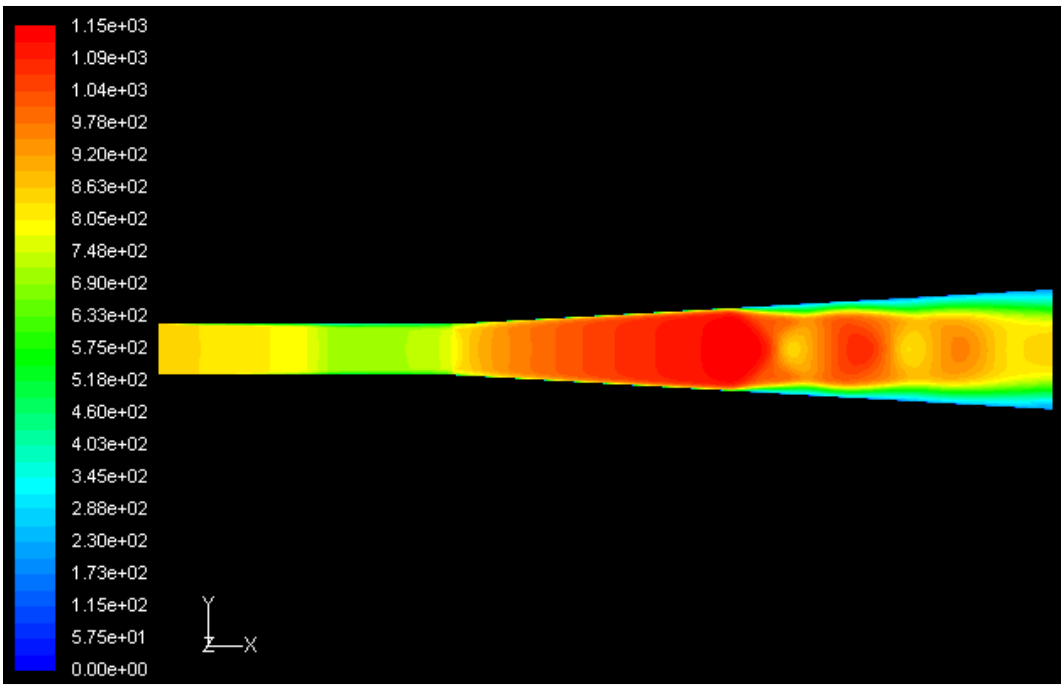

a) at the Plane of symmetry without ramp

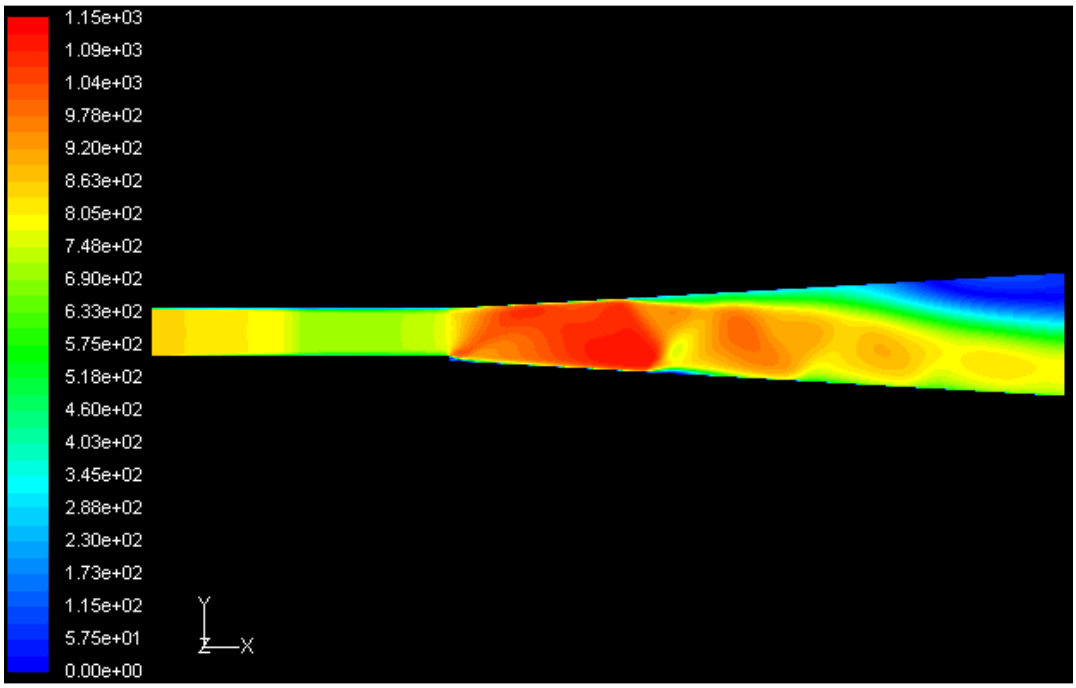

b) at the Plane of symmetry with Ramp

Fig. 24a Velocity (m/s) Contours in the Scramjet with and without Ramp at M = 1.25 and T = 1500 K

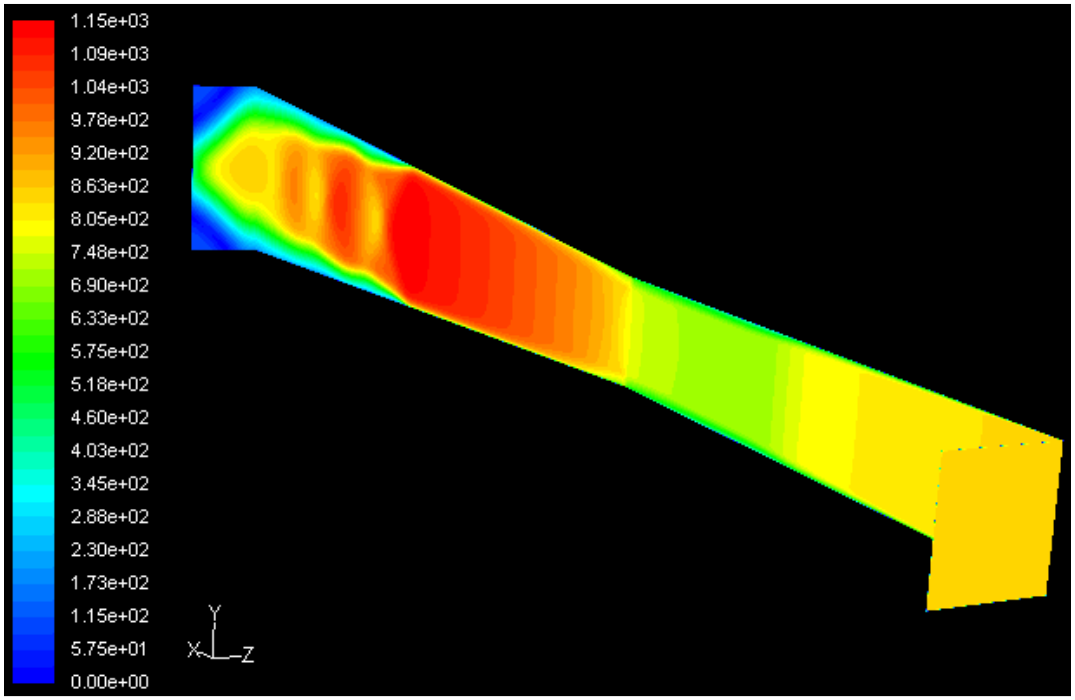

c) at the Symmetric Plane, Inlet and Outlet without ramp

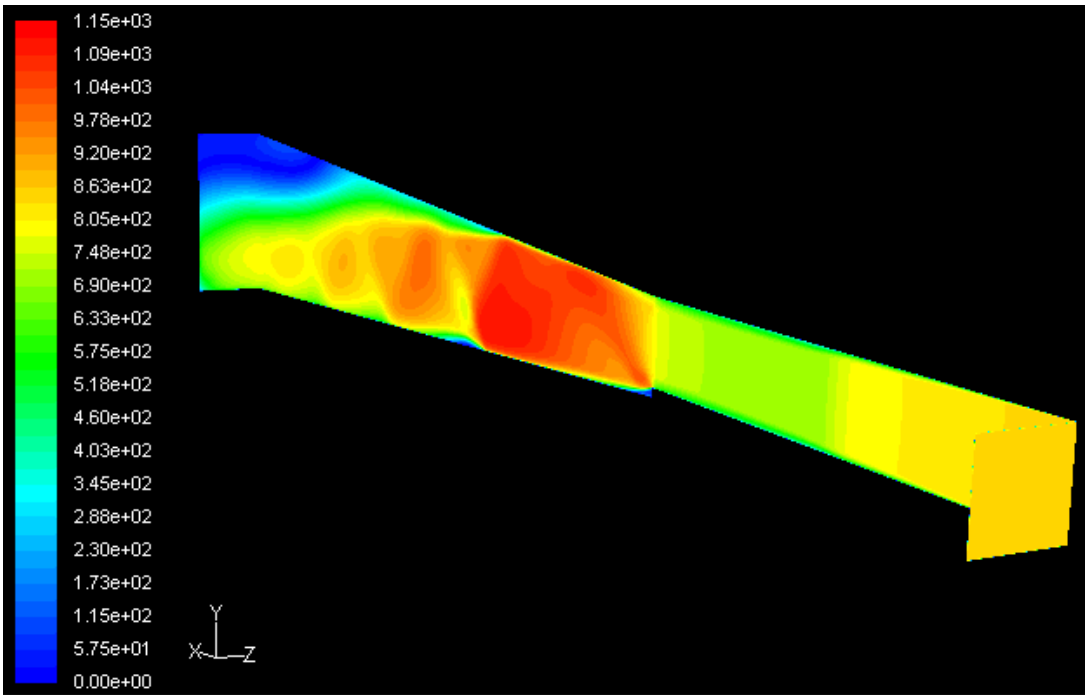

d) at the Symmetric Plane, Inlet and Outlet with Ramp

Fig. 24b Velocity (m/s) Contours in the Scramjet with and without Ramp at M = 1.25 and T = 1500

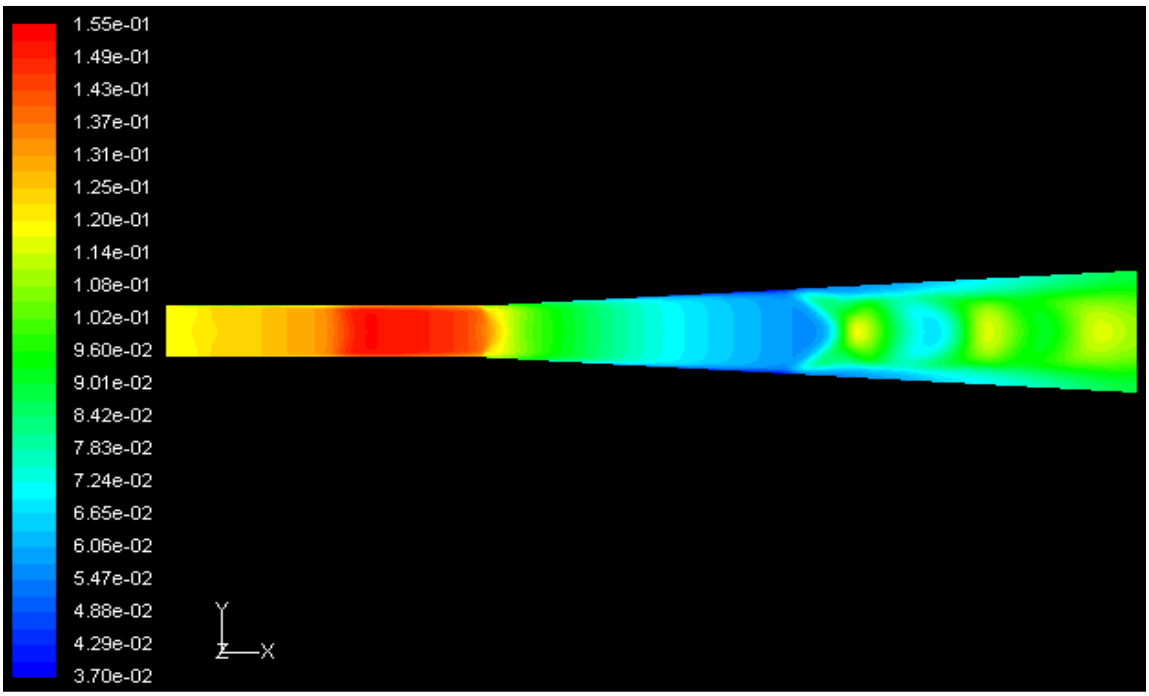

a) at the Plane of symmetry without ramp

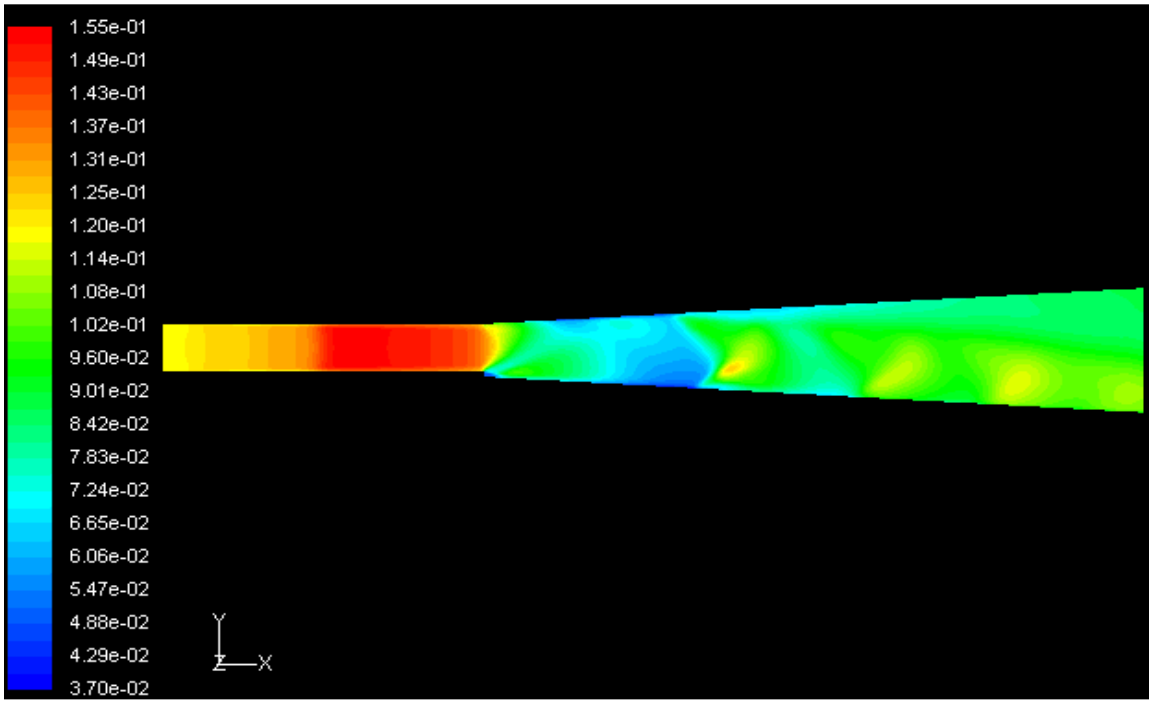

b) at the Plane of symmetry with Ramp

Fig. 25 Density (kg/m^3) Contours in the Scramjet with and without Ramp at M = 1.25 and T = 1500 K

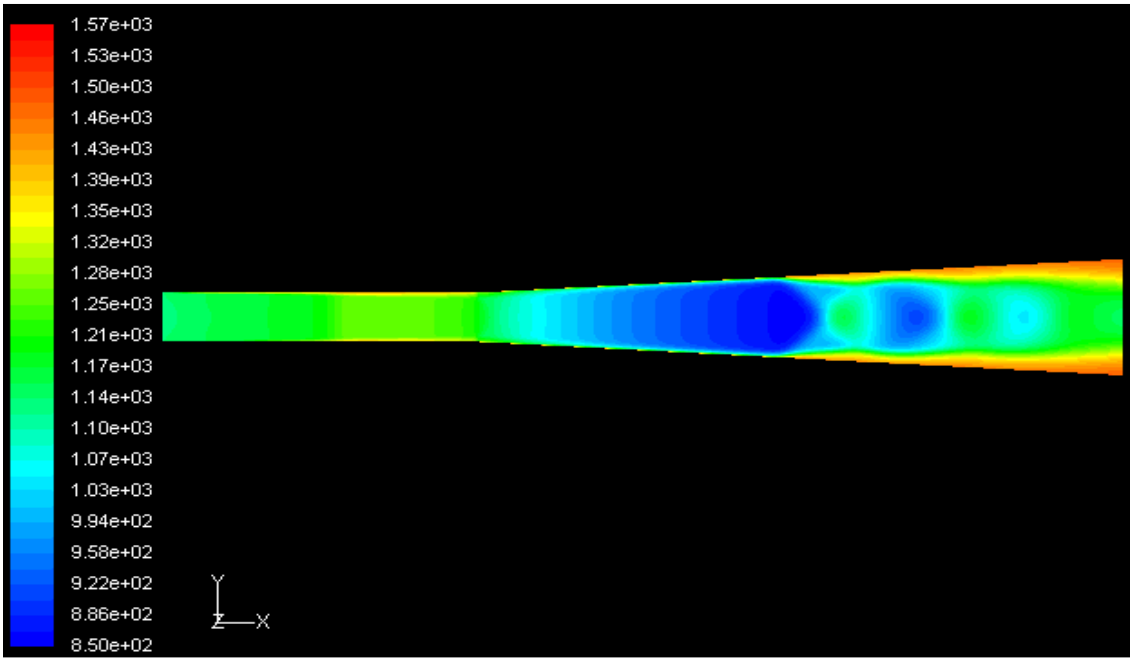

a) at the Symmetric Plane

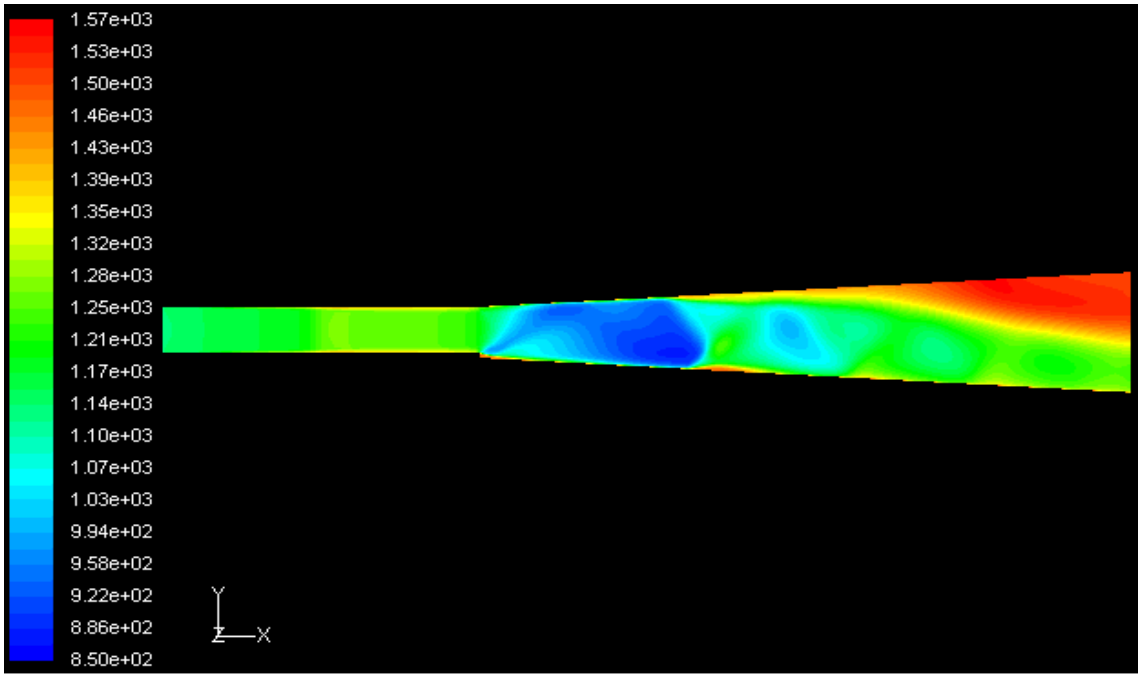

b) at the Symmetric Plane with Ramp

Fig. 26 Static Temperature (k) Contours in the Scramjet with and without Ramp at M = 1.25 and T = 1500 K

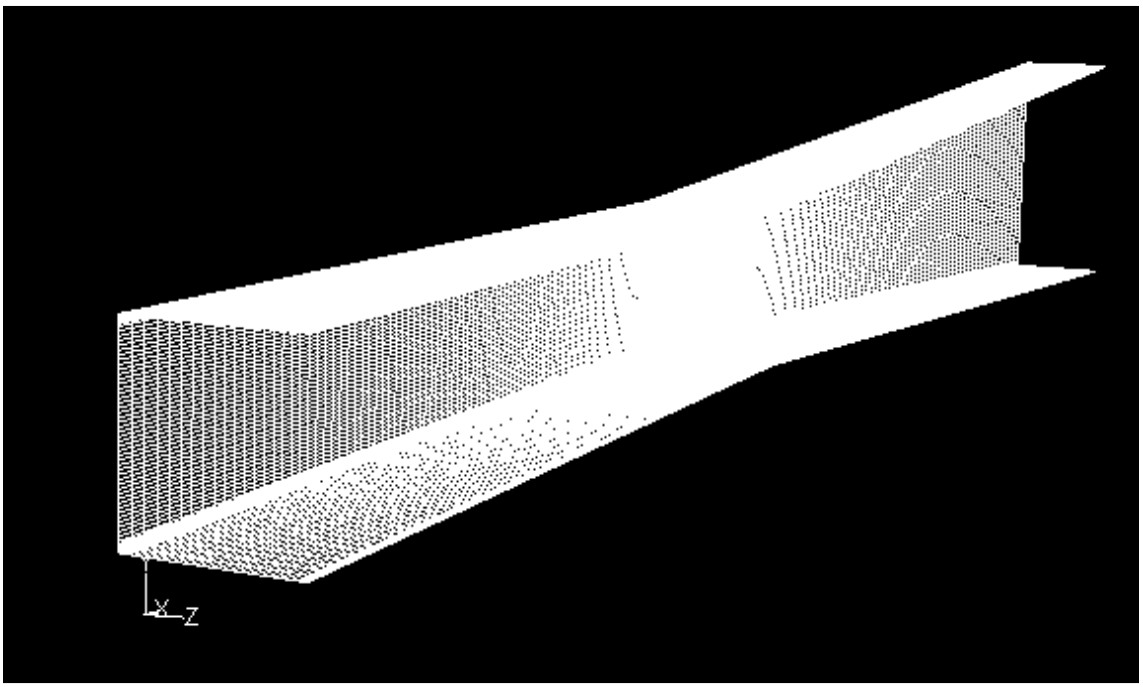

a) grid in the Scramjet (no tabs)

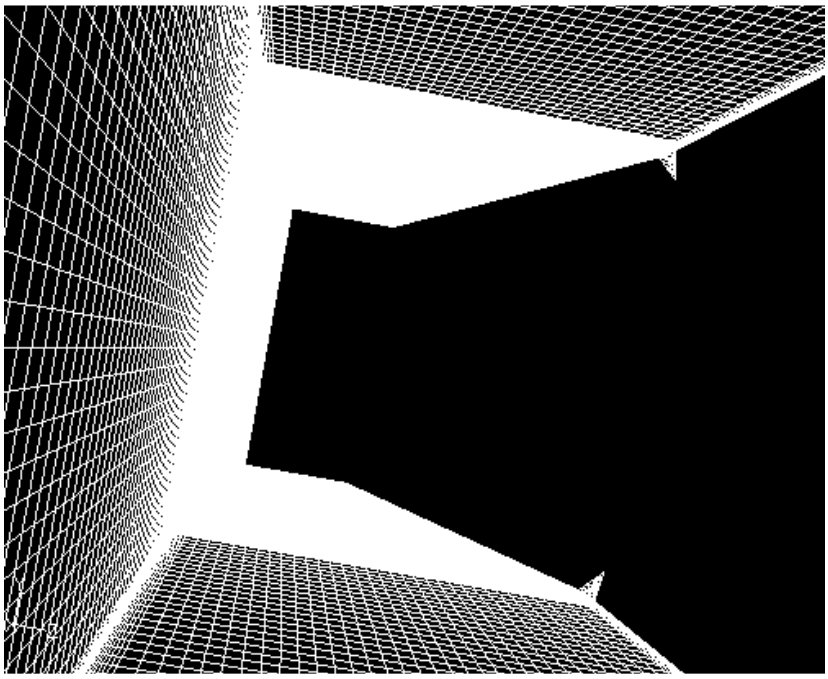

b) detailed View of 2 Tabs

Fig. 27a Geometries of the Scramjet without Tabs and with 2 and 4 Tabs

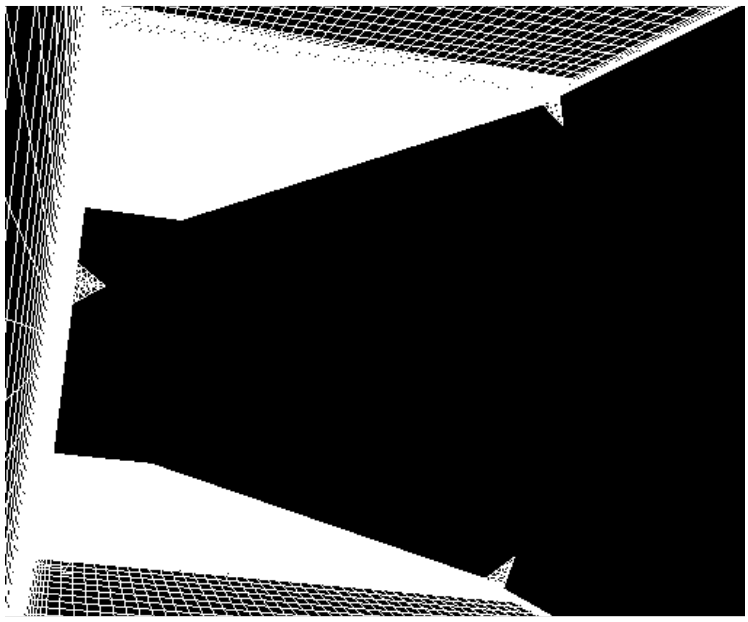

c) detailed View of 4 Tabs

Fig. 27b Geometries of the Scramjet without Tabs and with 2 and 4 Tabs

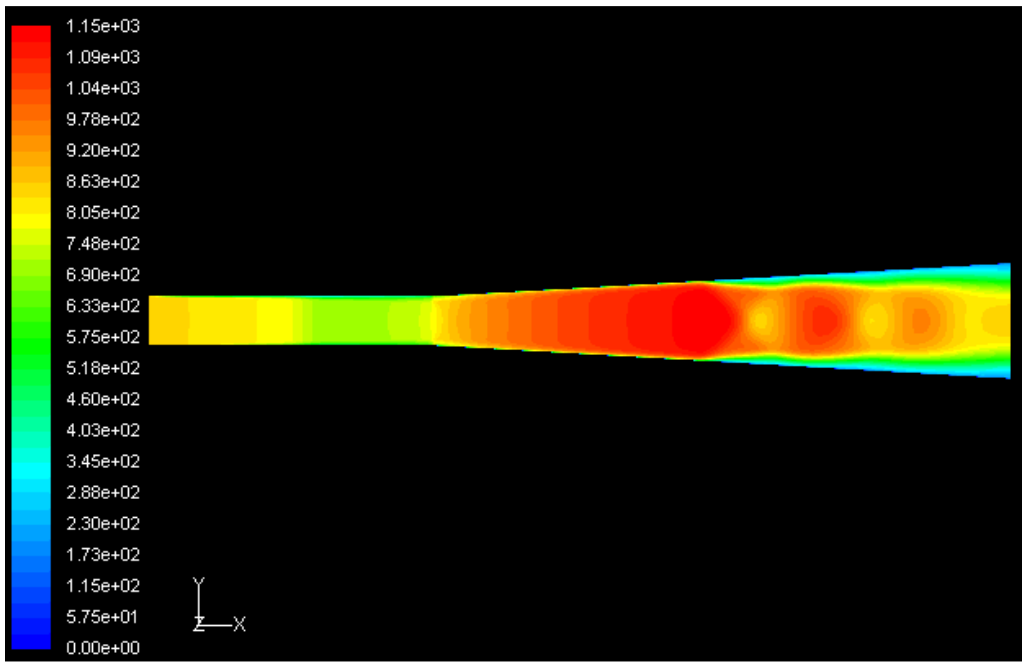

a) basic Scramjet (no tabs)

Fig. 28a Velocity (m/sec) Contours in the Scramjet at M = 1.25 and T = 1500 K including the effect of tabs

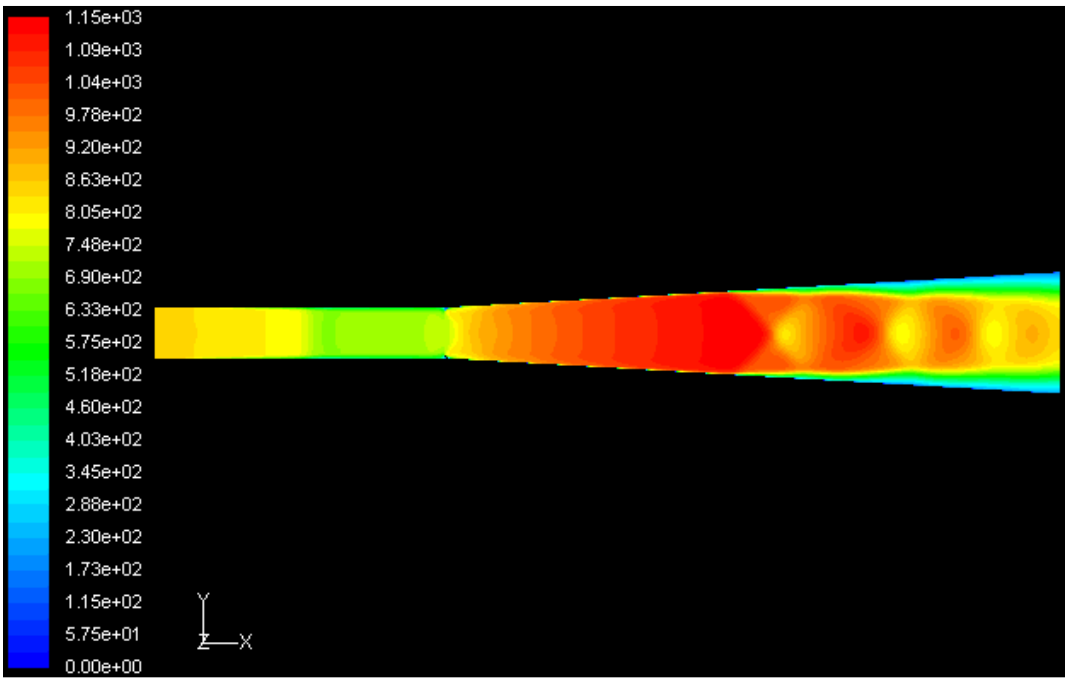

b) with 2 Tabs

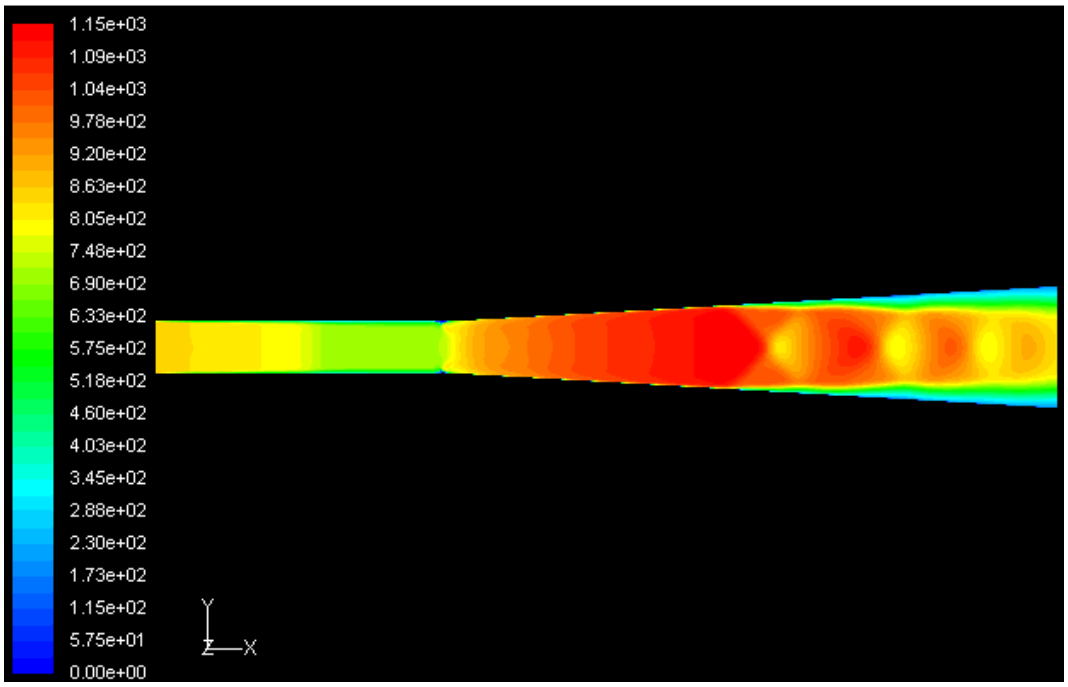

c) with 4 Tabs

Fig. 28b Velocity (m/sec) Contours in the Scramjet at M = 1.25 and T = 1500 K including the effect of tabs

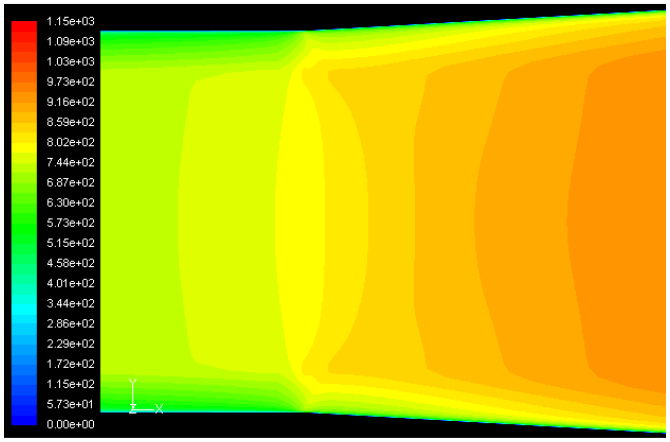

a) basic Scramjet (no tabs)

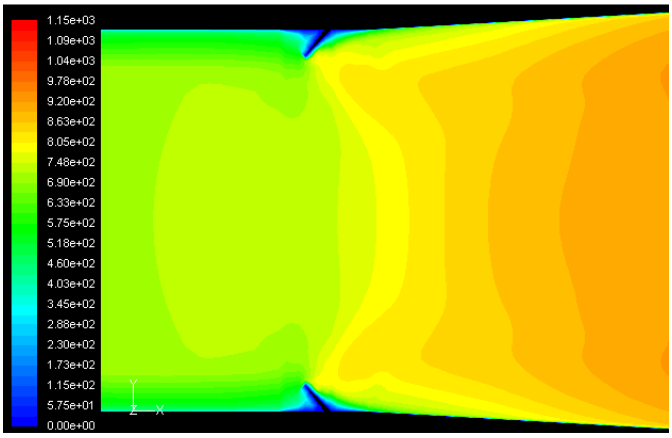

b) with 2 Tabs

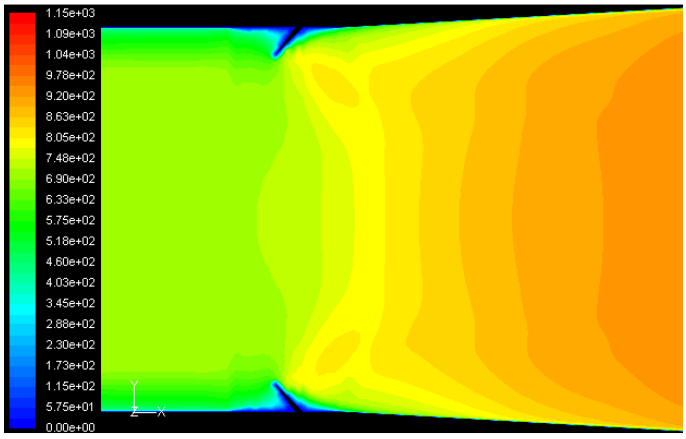

c) with 4 Tabs

Fig. 29a Detailed Velocity (m/sec) Contours in the Scramjet at M = 1.25 and T = 1500 K including the effect of tabs

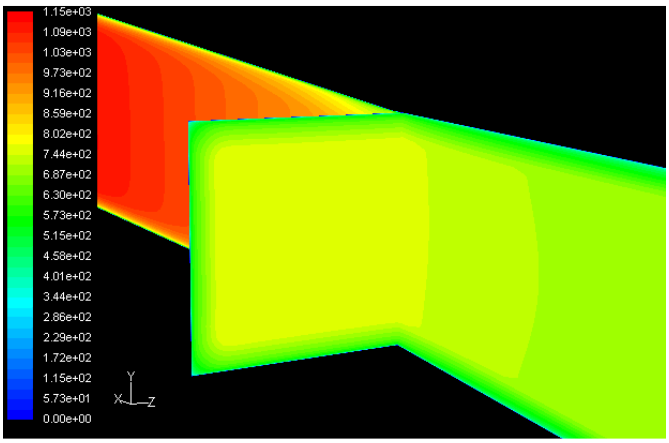

d) basic Scramjet (no tabs)

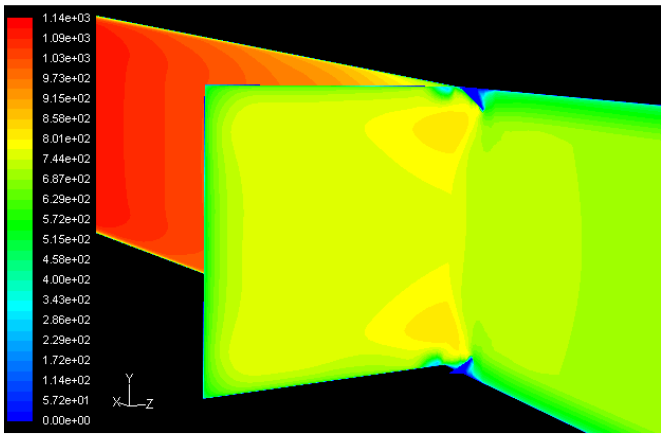

e) with 2 Tabs

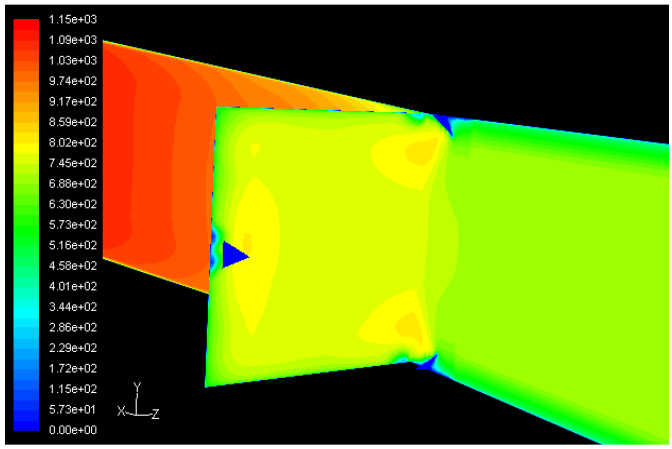

f) with 4 Tabs

Fig. 29b Detailed Velocity (m/sec) Contours in the Scramjet at M = 1.25 and T = 1500 K including the effect of tabs

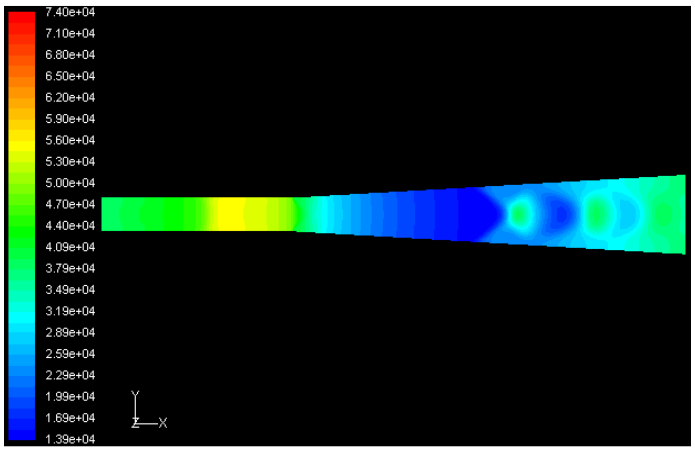

a) basic Scramjet (no tabs)

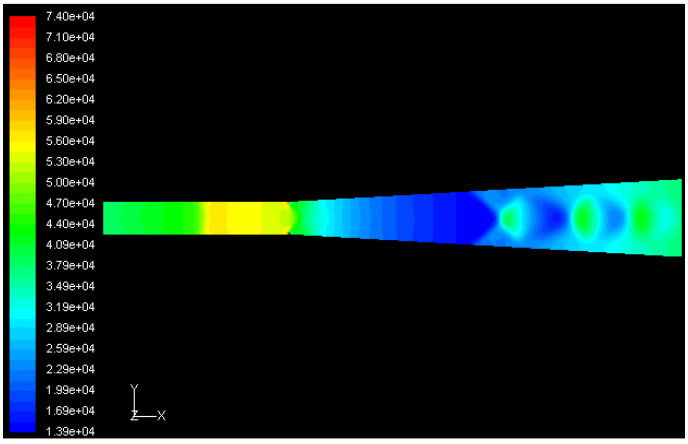

b) with 2 Tabs

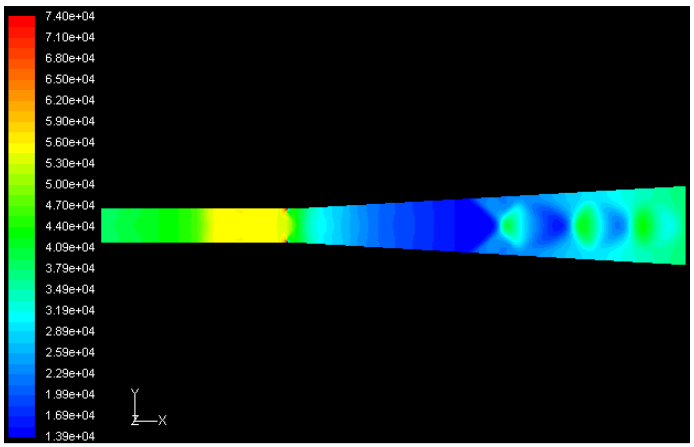

c) with 4 Tabs

Fig. 30a Static Pressure (Pascal) Contours in the Scramjet at M = 1.25 and T = 1500 K including the effect of tabs

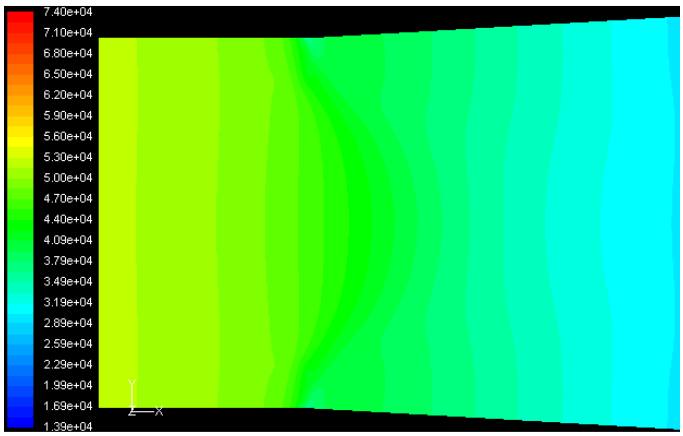

d) basic Scramjet (no tabs)

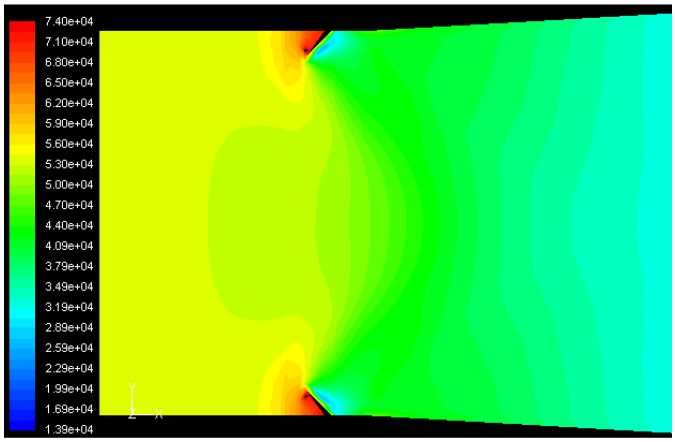

e) with 2 Tabs

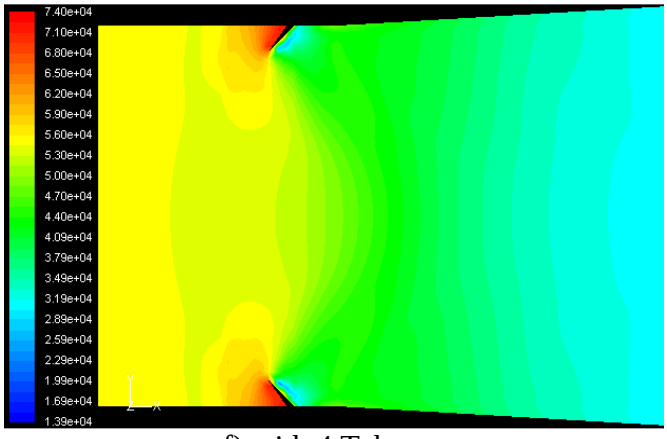

f) with 4 Tabs

Fig. 30b Static Pressure (Pascal) Contours in the Scramjet at M = 1.25 and T = 1500 K including the effect of tabs

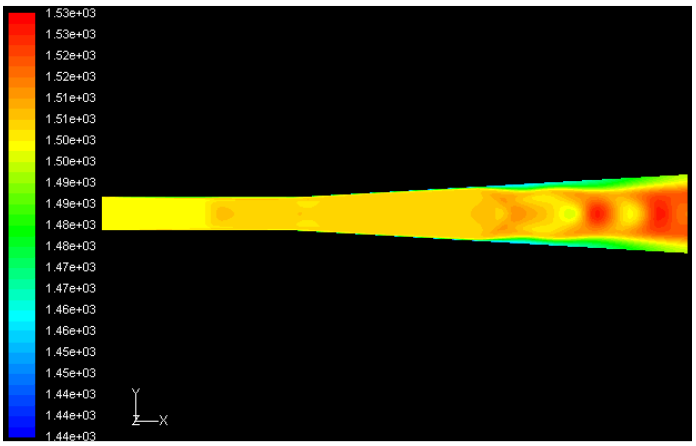

a) basic Scramjet (no tabs)

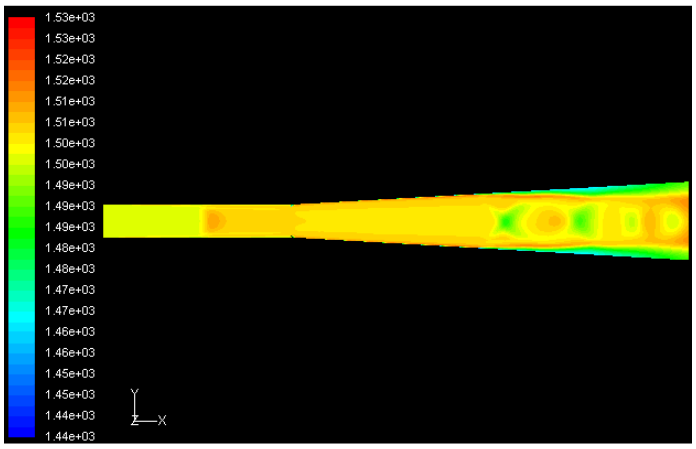

b) with 2 Tabs

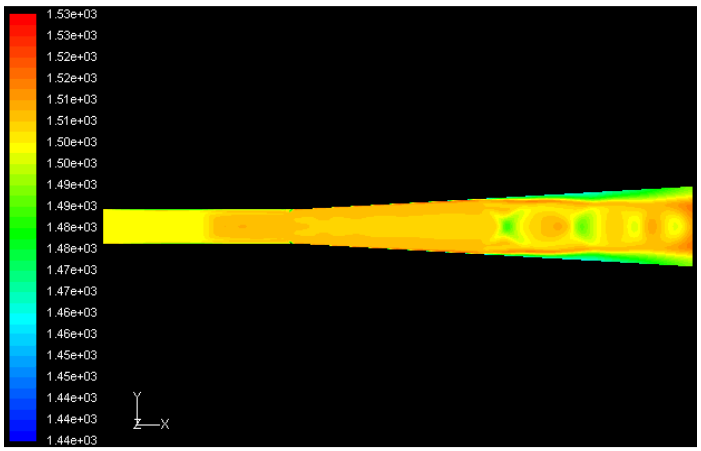

c) with 4 Tabs

Fig. 31a Total Temperature (K) Contours in the Scramjet at M = 1.25 and T = 1500 K including the effect of tabs

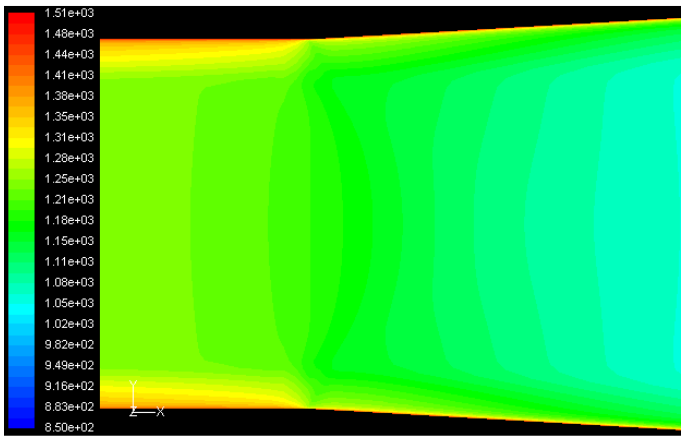

d) basic Scramjet (no tabs)

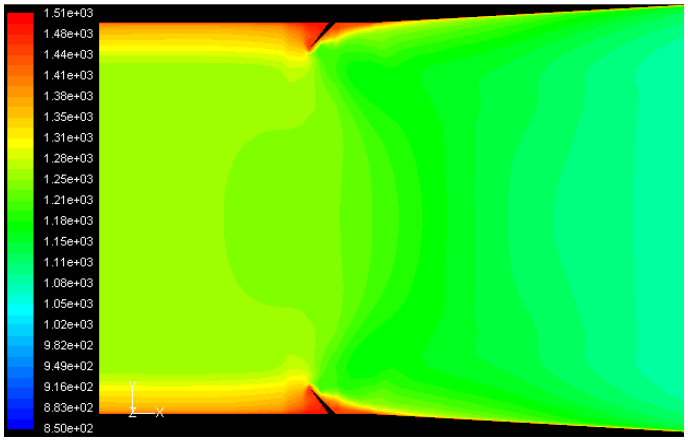

e) with 2 Tabs

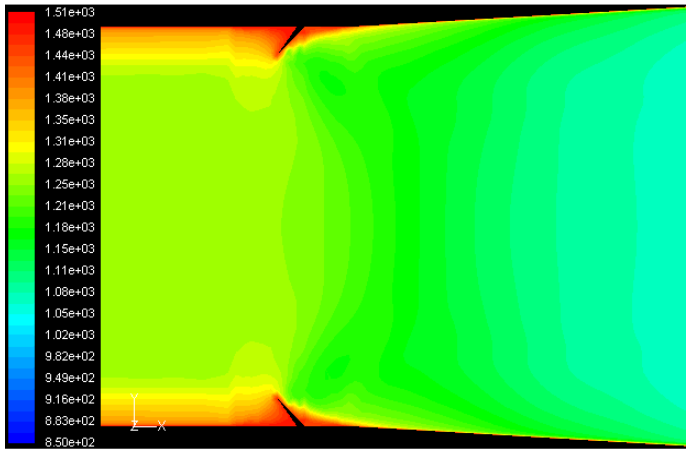

f) with 4 Tabs

Fig. 31b Total Temperature (K) Contours in the Scramjet at M = 1.25 and T = 1500 K including the effect of tabs

5 Scramjet Simulation with Fuel Injection & Flow Control

Numerical solutions have been obtained for the reacting flows with five different flow control schemes-ramp, ramp + tabs, ramp + suction collar, ramp + tabs + suction collar and 4 delta tabs at the hydrogen fuel injection inlet. Also, numerical solutions without the ramp, normal fuel injection, have been obtained. The finite rate reaction model with four species, H_2, O_2, H_2O and N_2 (mass fraction of O_2, H_2O, and N_2 being 0.198, 0.139, and 0.663, respectively) is used as the vitiated air enters the combustor at a Mach number of 2.5 and a stagnation temperature and pressure of 1500 K and 101,325 Pa, respectively. The inlet conditions of the hydrogen fuel injection port are adjusted to achieve sonic injection with the desired fuel mass flow rate. In order to save computational effort, all of the results presented correspond to the right half of the geometry shown in Fig. 15. The maximum value of wall y^+ on the generated grids is 57, while the area-averaged value is kept below 20. The generated grids cells are between 2.2 and 4.5 millions depending on the flowfield. All of the numerical results used for the present study have the difference in mass flow rate between inlets (air inlet and fuel injection inlet) and outlet is about 10^{-6} kg/sec. CPU time to achieve the convergence rate below 10^{-6} is between 70-120 hours in the advanced personal computer.

5.1 Results and Discussion of the Parallel Fuel Injection (Relieved Ramp)

The relieved ramp, $1/10^{th}$ high of the inlet (51 mm) is generated at the bottom of the constant area section of the scramjet combustor (shown in Fig. 22). At the center of the relieved ramp, gaseous hydrogen fuel is injected parallel to the incoming air. Comparison of hydrogen and hydrocarbon fueled scramjet engines and hydrogen and ethylene combustion can be found in Ref. 38 and 39, respectively. Entry air mass flow rate, $\dot{m}_o$, is 0.0804713 kg/sec and fuel mass flow rate, $\dot{m}_{f,}$ is 0.0010478 kg/sec . The

fuel/air ratio, f, is thus 0.013. The general expression for the stoichiometric fuel/air ratio for a hydrocarbon fuel of C_xH_y formula is

$$f_{st} = \frac{36x+3y}{103(4x+y)} \tag{5.1}$$

for hydrogen fuel, i.e., H_2, x = 0 and y = 2, and Eq. (5-1) shows that $f_{st} = 0.0291$.
Then, equivalence ratio, ϕ, is

$$\phi = \frac{f}{f_{st}} \tag{5.2}$$

for which f = 0.013 and $f_{st} = 0.0291$, and Eq. (5.2) shows that $\phi = 0.45$.
For the present CFD studies, the equivalence ratio of ϕ = 0.45 is used for all of the numerical computations. Mass-averaged values of pressure, static temperature (non-dimensionalized with the inlet stagnation conditions, T_{0i} = 1500 K, P_{0i} = 101,325 Pa), Mach number, and ratio of specific heats, γ, at the exit plane for all numerical configurations are calculated and compared to Table 1 (Tomioka et al.[29] measured pitot pressure and gas composition at the exit plane & Rajasekaran et al.[33] produced CFD data at the exit plane). Thrust force un-installed is obtained as the difference in the integrated value of the impulse function at the inlet and outlet, that is

$$F = \left(\int pdA + \int \rho u^2 dA\right)_{inlet}^{outlet} \tag{5.3}$$

The thrust developed for the ramp injection is predicted to be 70.28 N and mass-averaged exit Mach number is 1.97. Total pressure loss and γ are 40.92 % and 1.374, respectively. According to Pellett, G, L. et al.[34] study, the presence of the additional water vapor at the exit caused by combustion lowers the molecular weight of the mixture and γ. The value of γ decreases from 1.399 to 1.374 with combustion.

Nondimensionalized static pressure, total pressure and static temperature at the exit plane are 0.0571, 0.591 and 0.576, respectively. The thrust developed for the strut

injection case[33] is 96.7 N with the exit Mach number 1.77. Compare with the strut injection in experimental[29] and numerical[33] data, it clearly shows that the strut injection gives higher mixing rate and produces more thrust than the ramp injection, but total pressure loss for the strut injection is about 30 % higher than the ramp injection. Based on the Tomioka's experimental data[29], the presence of the strut in the flow causes the total pressure loss as high as 56 % even in the absence of combustion. The flow properties of the ramp injection on the symmetric plane are shown in Fig. 32 to 34.

Table 1 Mass-averaged values for properties at the exit plane (from Ref. 33)

Source	Mach number	Pressure*		Static Temp*	γ
		Static	Total		
		Baseline (no fuel)			
CFD	2.275	0.03	0.4473	0.556	1.331
		Strut injection, ϕ= 0.34			
CFD	1.77	0.0533	0.322	1	1.28
Expt	1.83	0.05	0.29	0.99	1.28
		Strut, ϕ= 0.44, + wall, ϕ= 0.61, injection			
CFD	1.386	0.085	0.273	1.333	1.25
Expt	1.31	0.092	0.24	1.39	1.25
		Wall injection, ϕ= 0.94			
CFD	1.36	0.087	0.271	1.186	1.265
Expt	1.21	0.094	0.22	1.43	1.25

(*non-dimensionalized with T_{0i} = 1500 K and P_{0i} = 101,325 Pa)

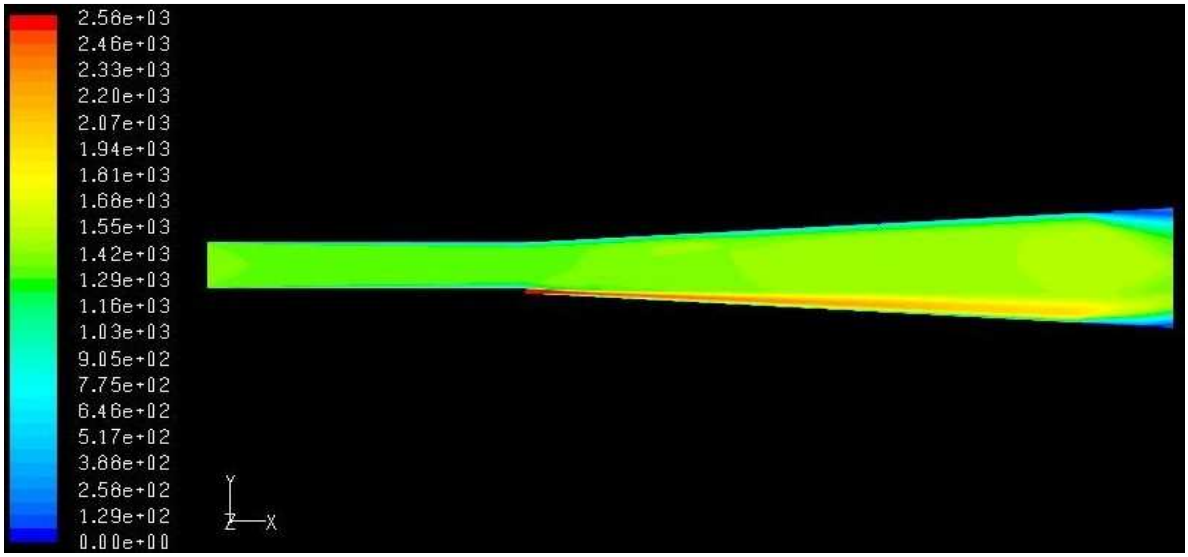

a) velocity contours at the plane of symmetry

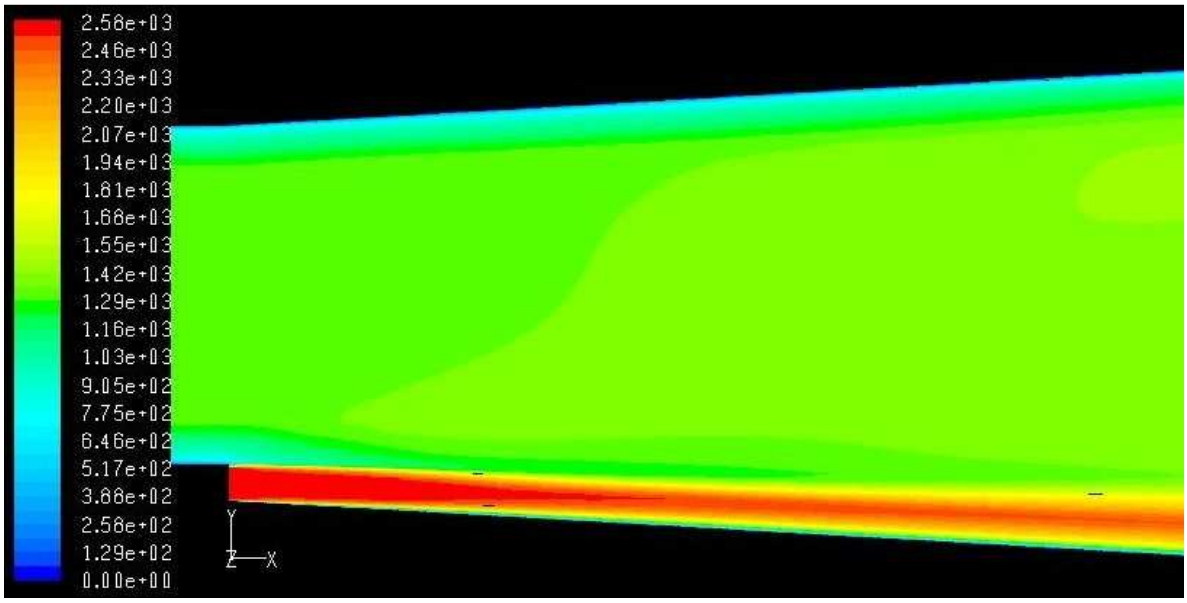

b) detailed velocity contours around the ramp

Fig. 32 Velocity (m/sec) Contours in the Scramjet with Ramp injection with Convective Mach number, M_c = 2.5, T_{oi} = 1500 K and ϕ = 0.45

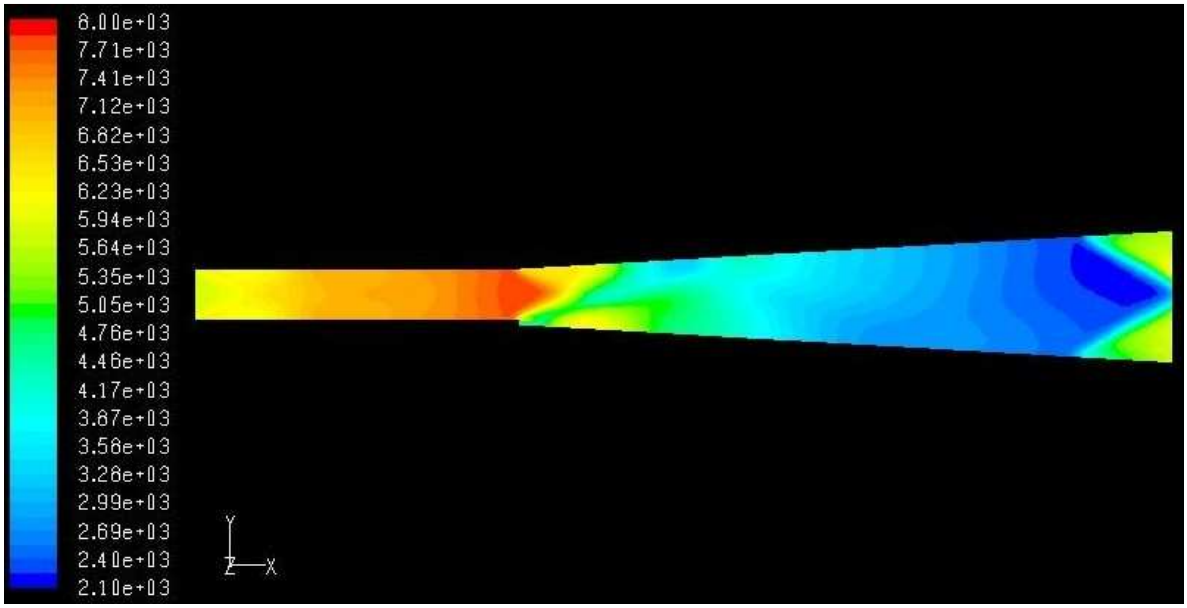

a) static pressure contours at the plane of symmetry

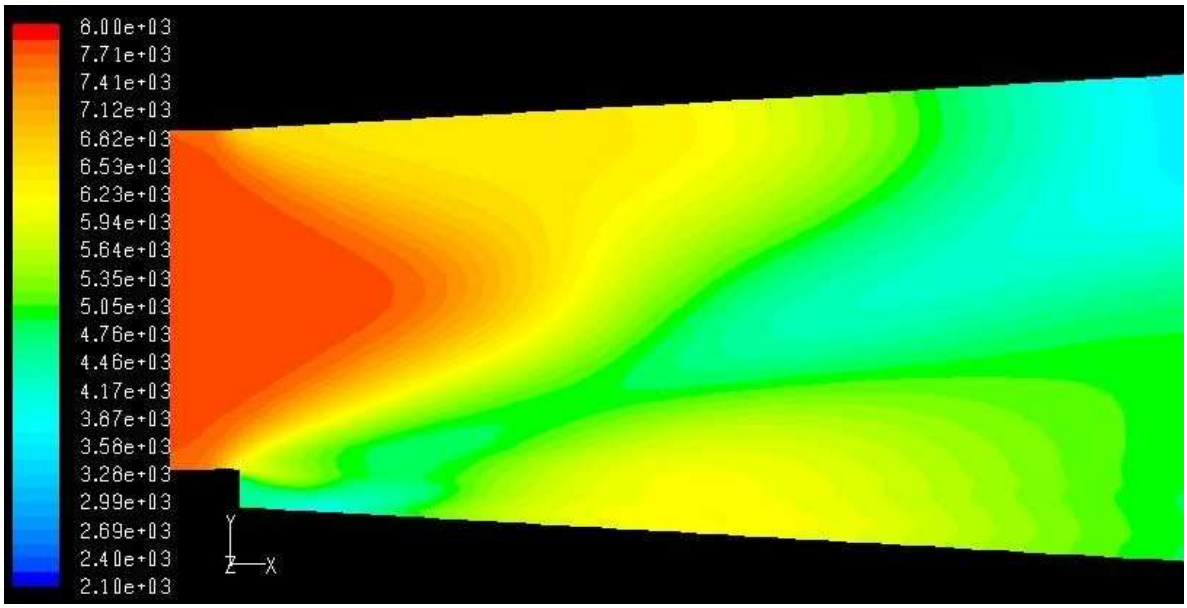

b) detailed static pressure contours around the ramp

Fig. 33 Static Pressure (Pa) Contours in the Scramjet with Ramp injection with Convective Mach number, M_c = 2.5, T_{oi} = 1500 K and ϕ = 0.45

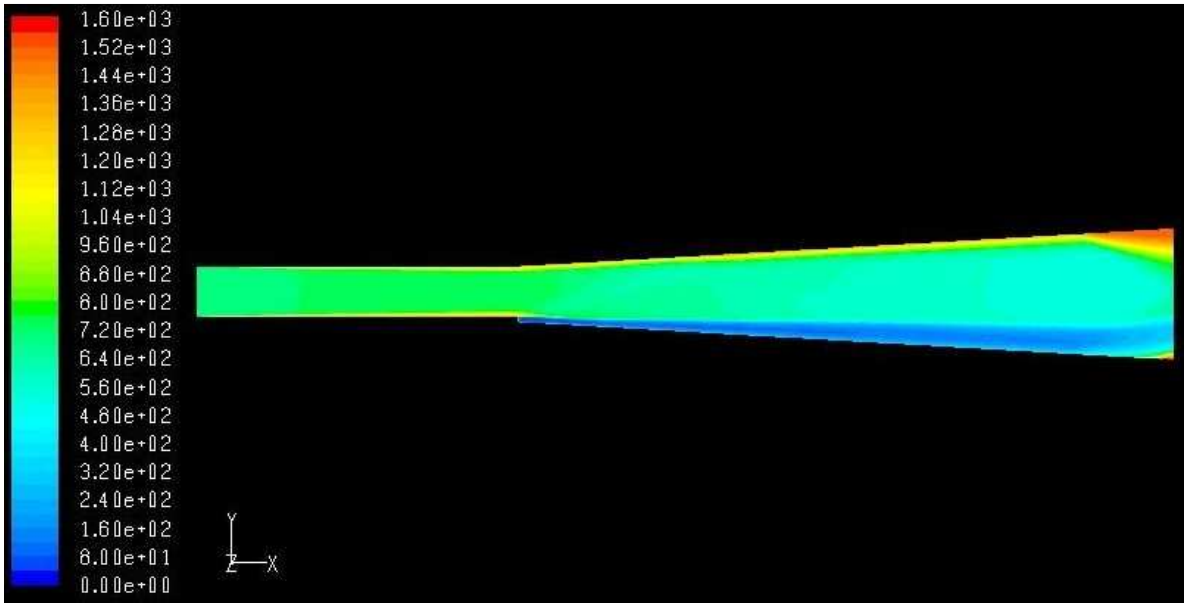

Fig. 34 Static Temperature (K) Contours in the Scramjet with Ramp injection with Convective Mach number, M_c = 2.5, T_{oi} = 1500 K and ϕ = 0.45

5.2 Results and Discussions of the Scramjet with Relieved Ramp and Delta Tabs

Three different sets of the delta tab configurations are numerically tested in the present study. The tabs are located along the centerlines of the x-y and y-z plane at the constant area section of the combustor a 45 degree angle toward the incoming air flow. Total projected blockage area is 0.33 % of the scramjet inlet area for the 2 tabs and 0.67 % for the 4 and 8 tabs configurations of the y-z plane on the inlet. The outline drawings of scramjet combustor with tabs are shown in Fig. 35. The un-installed thrust developed for the cases of 2, 4 and 8 tabs comes out to be 90.73, 105.42 and 99.09 N, respectively. The total pressure loss of the 2, 4 and 8 tabs is 43.72, 41.25 and 42.60 %, respectively. The 4 delta tabs configuration produces the best aerodynamic properties. Compare to the ramp injection data without the tabs, there is an additional 50.6 % increase of the thrust, but there is only an additional 0.33 % loss of total pressure caused by the presence of the 4 tabs in the flowfield with a 3 % additional increase of the static temperature at the exit plane. Numerical results and the computed aerodynamic properties are presented in Table 2 and Fig. 36 to 40. Compare to the experimental[29] and numerical[33] data of the strut injection (Table 1), the thrust developed for the ramp+4 delta tabs and strut injection is almost even with the exit Mach numbers equal to 1.815 and 1.77. The ramp+4 delta tabs scheme generates an additional 9 % of thrust, but more fuel is injected to. Equivalence ratio is 0.45 for the ramp+4 tabs and 0.34 for the strut injection. However, the total pressure loss of the ramp+4 tabs is about 30 % less than the strut injection. This is a clear indication that the ramp+4 tabs injection system is more efficient method than the strut injection for the scramjet combustor.

Table 2 Mass-averaged values for the flow properties at the exit plane (tabs, ϕ = 0.45)

Number of tabs	Mach number	Pressure*		Static Temp*	γ	Thrust increment (%)
		Static	Total			
2	1.815	0.069	0.563	0.606	1.374	29.1
4	1.815	0.073	0.588	0.602	1.374	50.6
8	1.819	0.071	0.574	0.603	1.374	40.9

(*non-dimensionalized with T_{0i} = 1500 K and P_{0i} = 101,325 Pa)

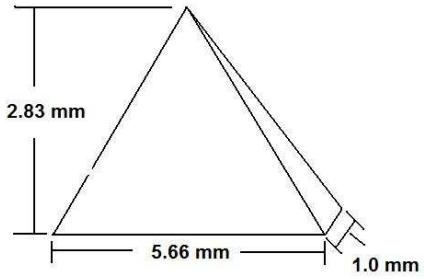

a) dimensions of delta tab

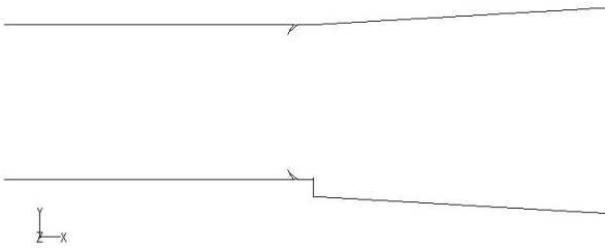

b) scramjet combustor with 2 delta tabs

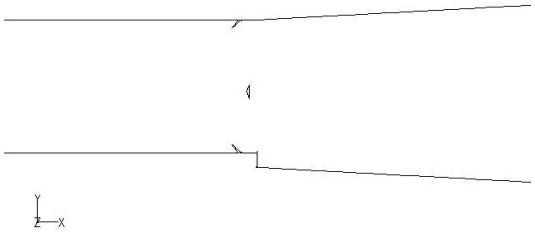

c) scramjet combustor with 4 delta tabs

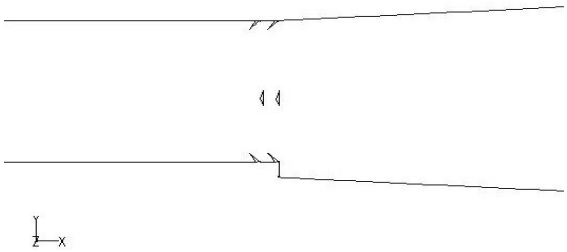

d) scramjet combustor with 8 delta tabs

Fig. 35 Outline Drawing of the Scramjet Combustor with Tabs

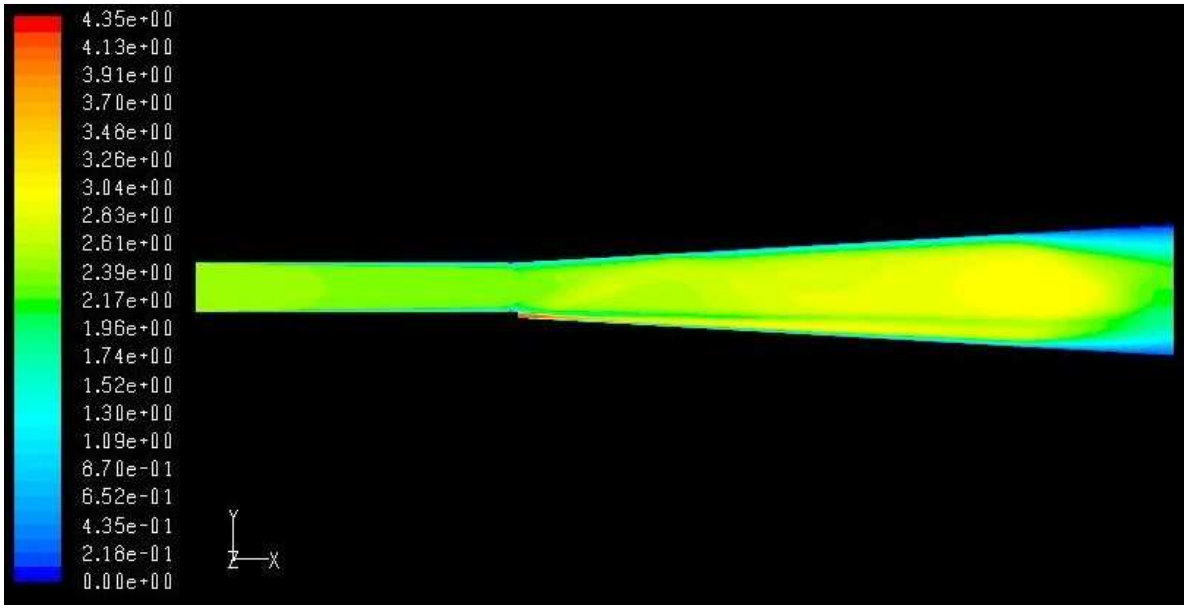

a) scramjet combustor with 2 delta tabs

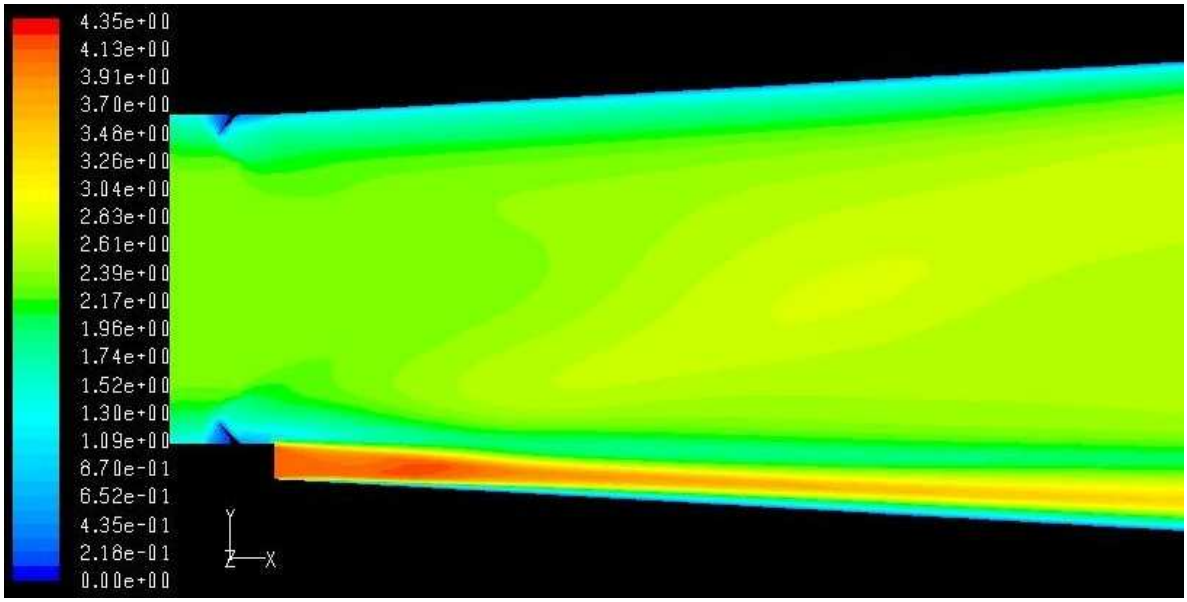

b) detailed Mach number contours around the ramp with 2 delta tabs

Fig. 36 Mach Number Contours in the Scramjet with 2 Tabs in the Plane of Symmetry with Convective Mach Number, M_c = 2.5, T_{oi} = 1500 K and ϕ = 0.45

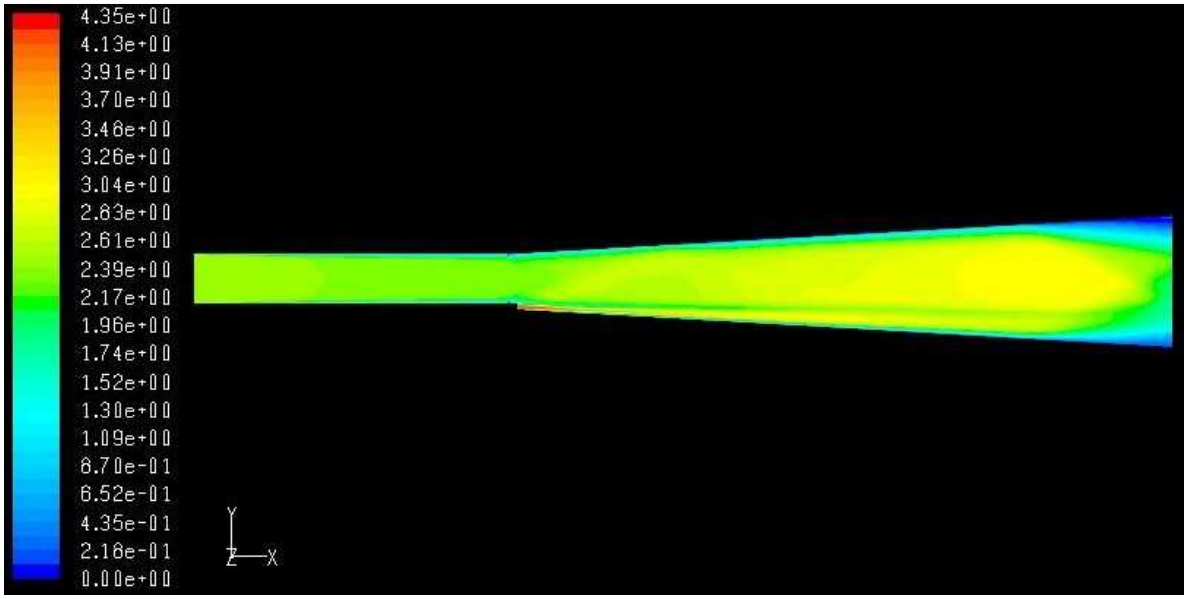

a) scramjet combustor with 4 delta tabs

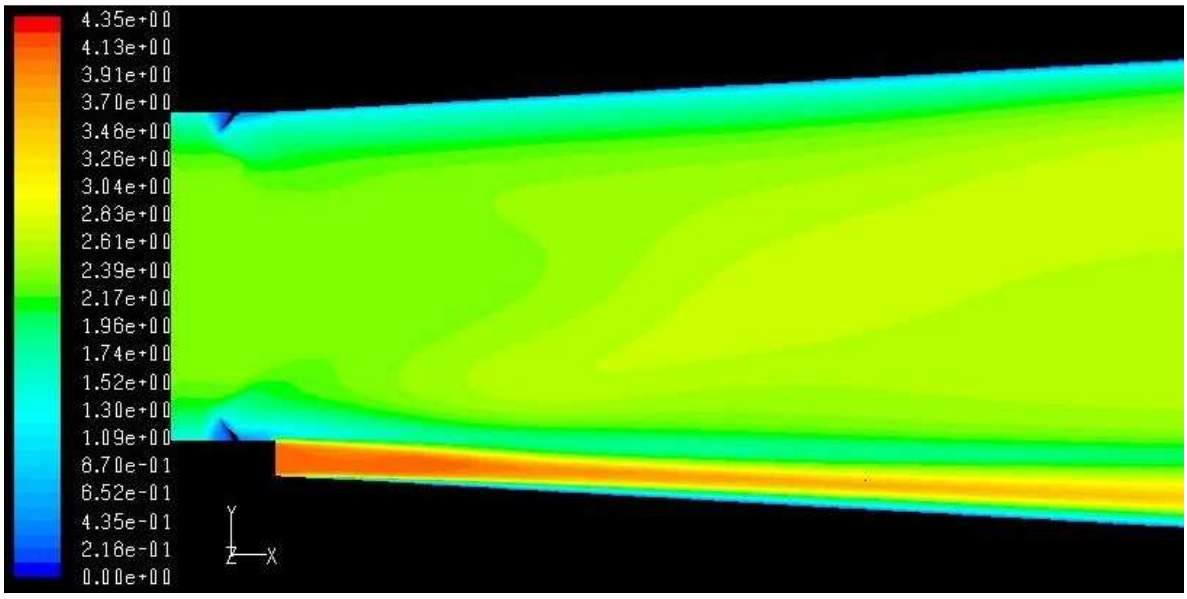

b) detailed Mach number contours around the ramp with 4 delta tabs

Fig. 37 Mach Number Contours in the Scramjet with 4 Tabs in the Plane of Symmetry with Convective Mach Number, M_c = 2.5, T_{oi} = 1500 K and ϕ = 0.45

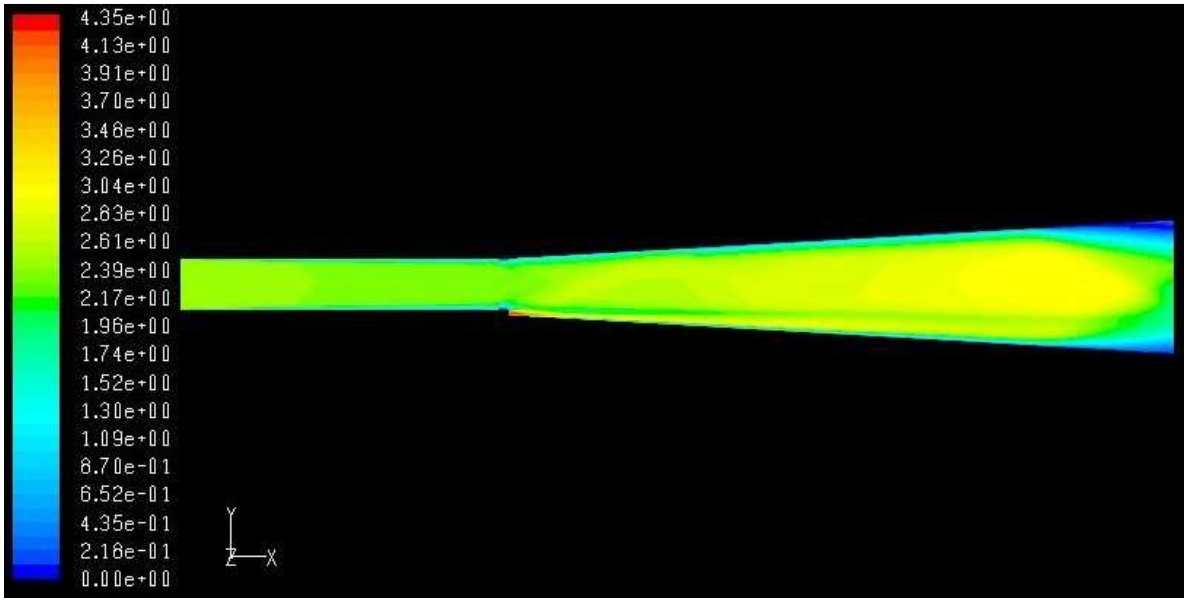

a) scramjet combustor with 8 delta tabs

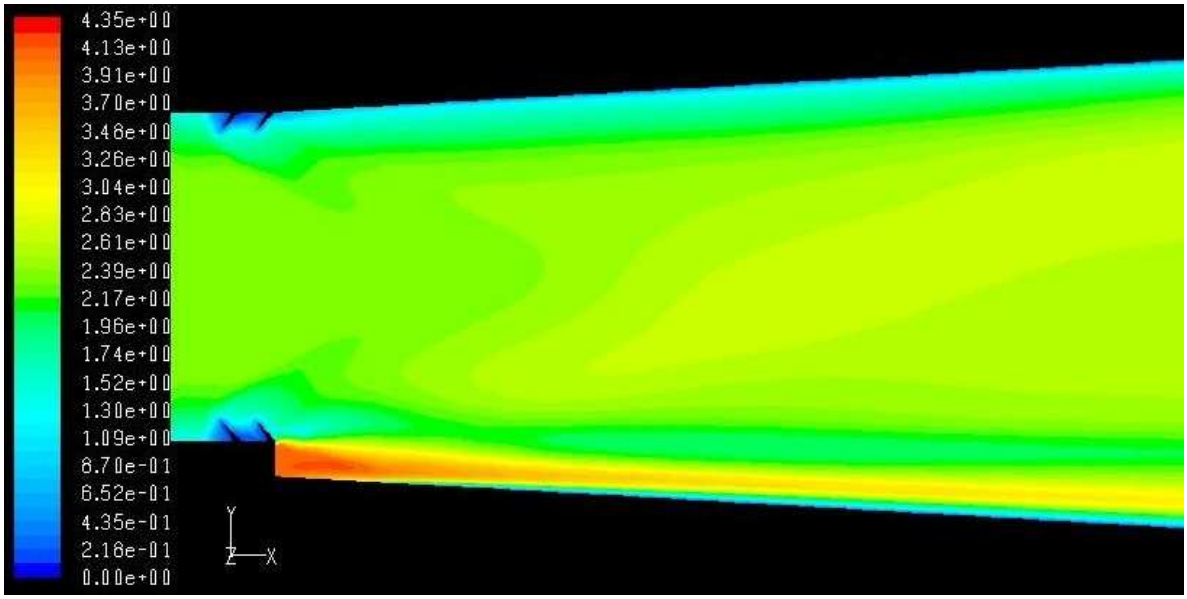

b) detailed Mach number contours around the ramp with 8 delta tabs

Fig. 38 Mach Number Contours in the Scramjet with 8 Tabs in the Plane of Symmetry with Convective Mach Number, M_c = 2.5, T_{oi} = 1500 K and ϕ = 0.45

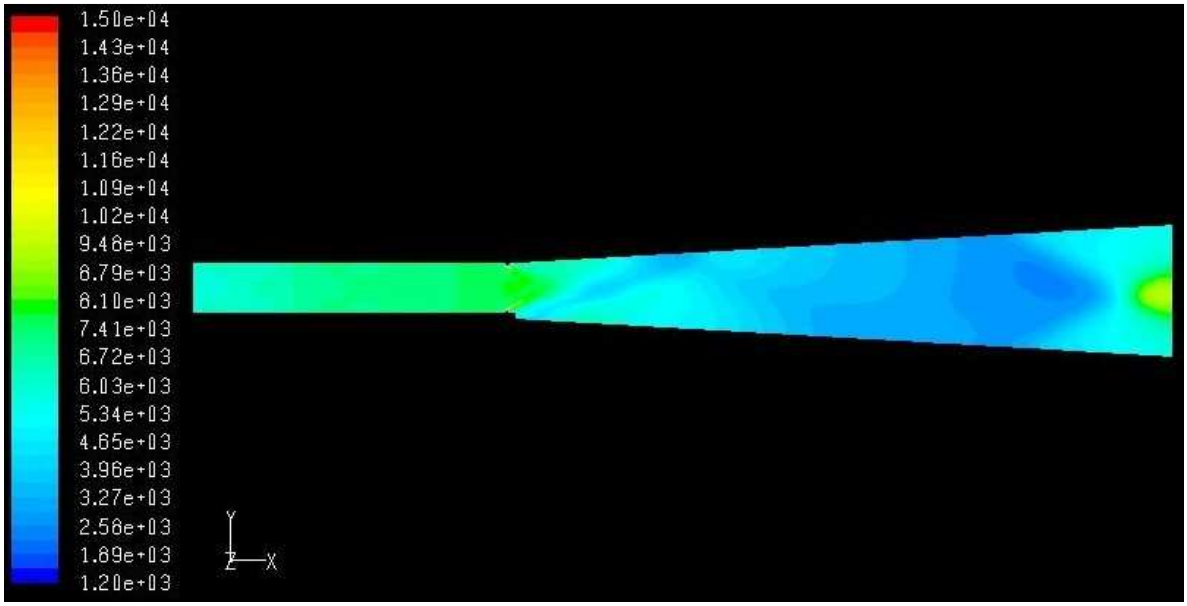

a) scramjet combustor with 2 delta tabs

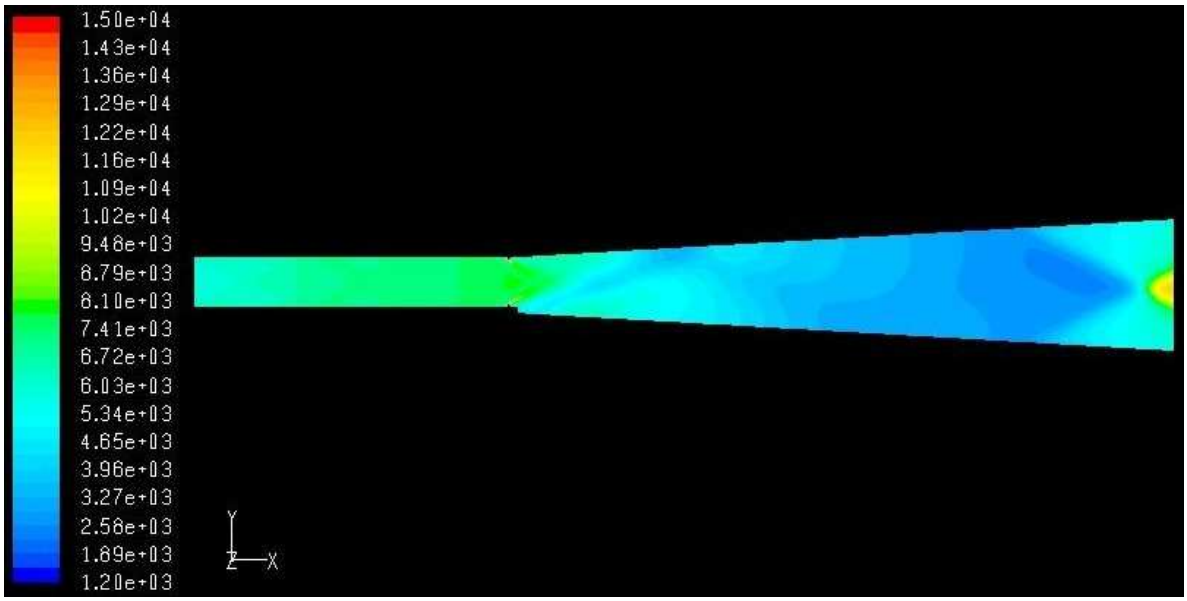

b) scramjet combustor with 4 delta tabs

Fig. 39a Static Pressure (Pa) Contours in the Scramjet in the Plane of Symmetry with Convective Mach Number, M_c = 2.5, T_{oi} = 1500 K and ϕ = 0.45

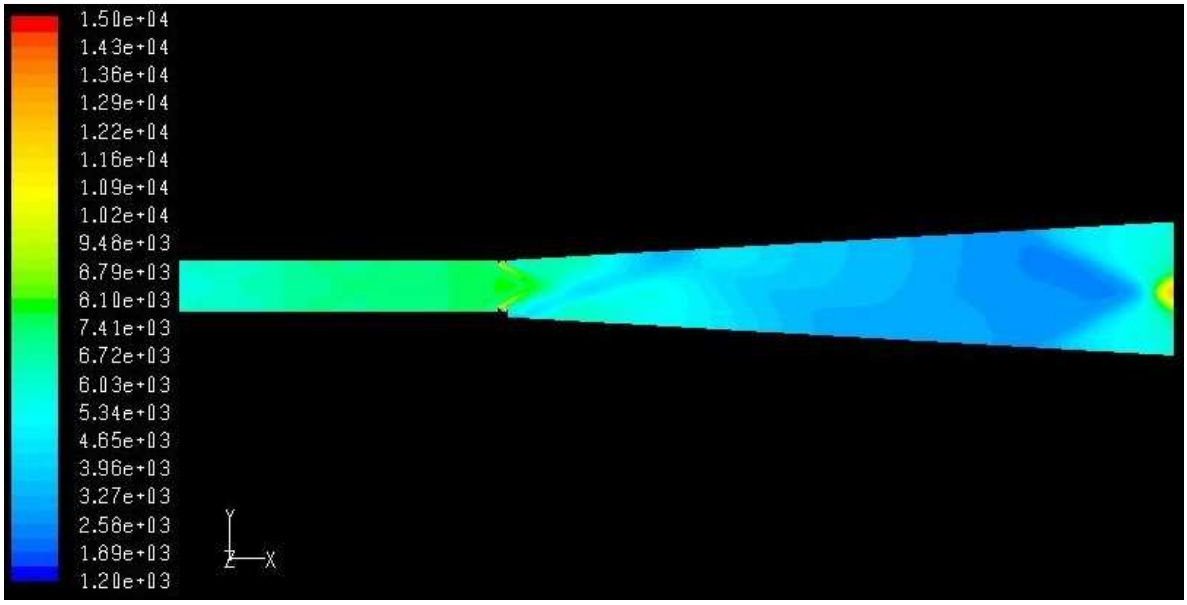

c) scramjet combustor with 8 delta tabs

Fig. 39b Static Pressure (Pa) Contours in the Scramjet in the Plane of Symmetry with Convective Mach Number, M_c = 2.5, T_{oi} = 1500 K and ϕ = 0.45

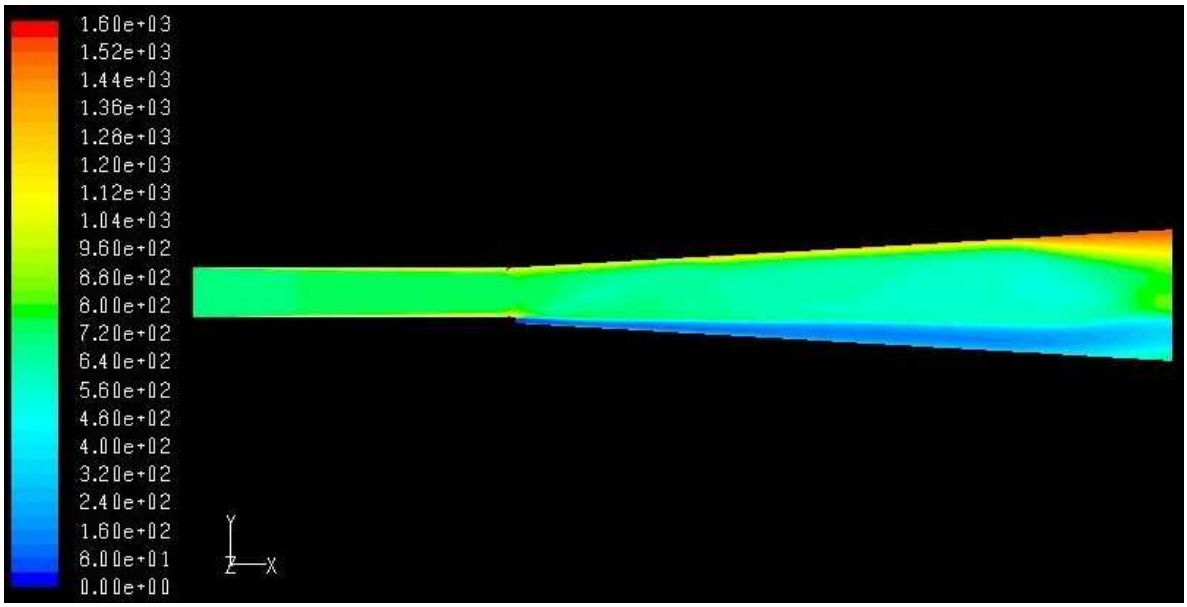

a) scramjet combustor with 2 delta tabs

Fig. 40a Static Temperature (K) Contours in the Scramjet in the Plane of symmetry with Convective Mach Number, M_c = 2.5, T_{oi} = 1500 K and ϕ = 0.45

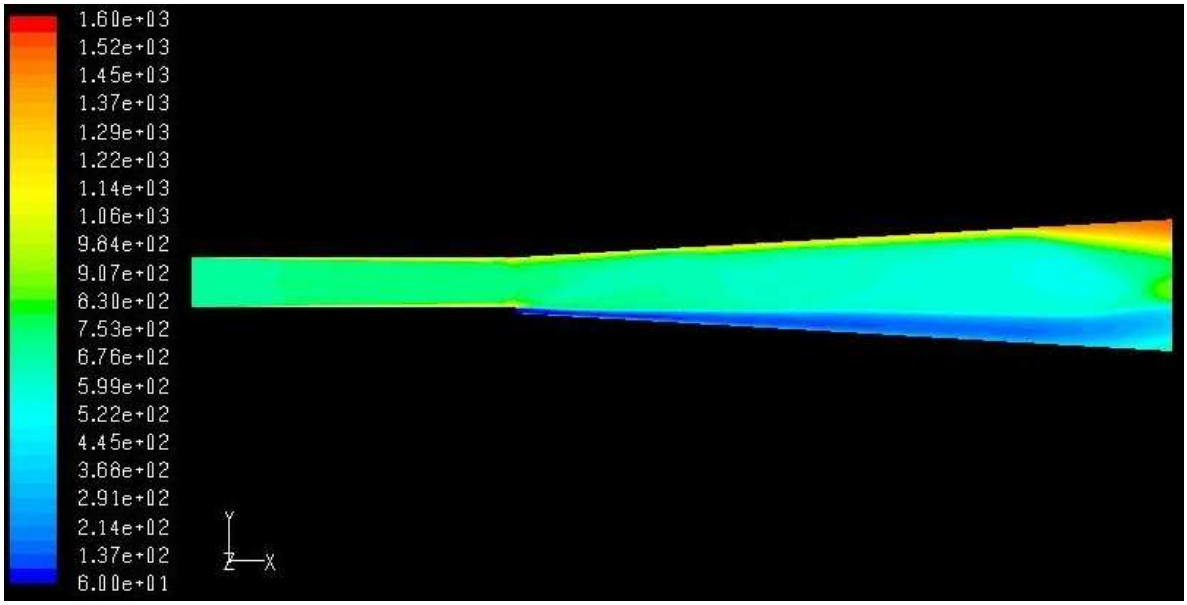

b) scramjet combustor with 4 delta tabs

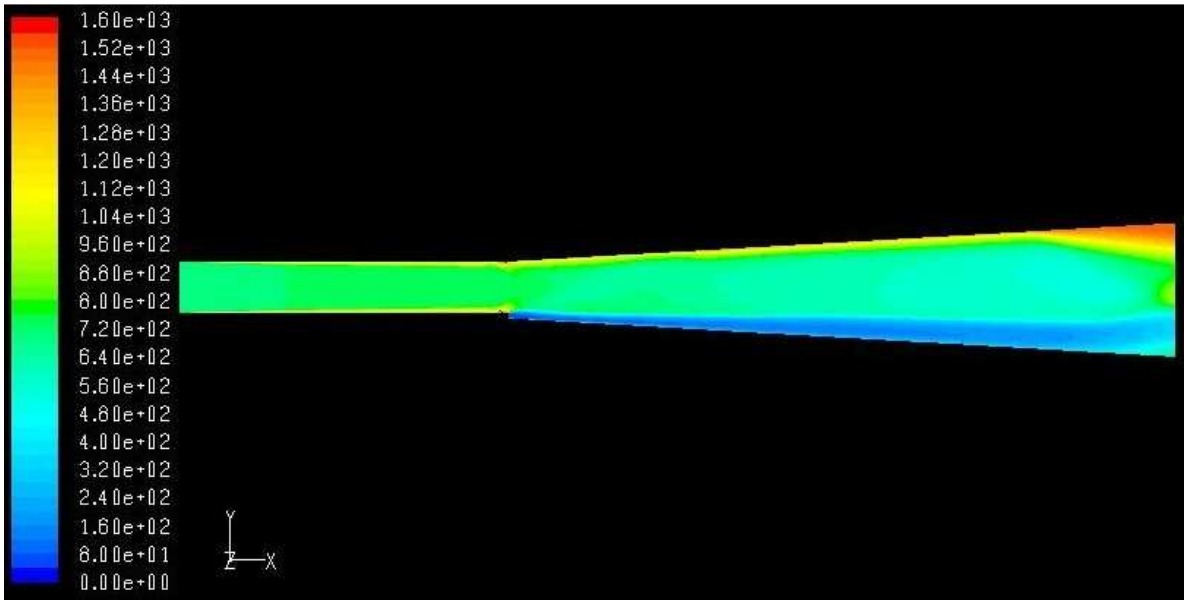

c) scramjet combustor with 8 delta tabs

Fig. 40b Static Temperature (K) Contours in the Scramjet in the Plane of symmetry with Convective Mach Number, M_c = 2.5, T_{oi} = 1500 K and ϕ = 0.45

5.3 Results and Discussions of the Scramjet with Relieved Ramp, Delta Tabs and Suction Collar

The most effective combination of the relieved ramp and delta tabs is numerically established in the previous section. For the rest of the present study this combination, i.e., the ramp+4 tabs, is extended to include the counterflow concept and suction collar. Three different sets of the configurations, ramp+suction collar I, ramp+4 tabs+suction collar I and ramp+4 tabs+suction collar II, are numerically investigated in the present study. The locations of the suction collars are as follows:

1) Suction collar I: 0.91 of the divergent section in the streamwise direction toward the exit and 3.3 % of the divergent surface area in x-y plane.
2) Suction collar II: 0.86 of the divergent section in the streamwise direction toward the exit and 5 % of the divergent surface area in x-y plane.

Detailed geometries of the rectangular suction collars are presented in Fig. 41.

The un-installed thrust developed for the case of the relieved ramp+suction collar I is determined to be 102.49 N with the total pressure loss of 46.1 %. Compared to the ramp+4 tabs, the ramp+4 tabs scheme generates an additional 4.8 % of un-installed thrust, and the total pressure loss is 4.85 % less than the ramp+suction collar I.

The un-installed thrust developed for the cases of the ramp+4 tabs+suction collar I and ramp+4 tabs+suction collar II is 111.08 and 89.29 N, respectively. The total pressure loss is 43.50 and 45.10 %, respectively. The static temperature of the cases is 938.9 and 924.6 K at the exit plane. The ramp+4 tabs+suction collar I is thus a more effective fuel injection method for the scramjet combustor than the ramp+tabs or ramp+4 tabs+suction collar II. The present CFD study demonstrates that the location of the suction collar and the extent of the suction are the major parameters that improve the efficiency of the scramjet combustor. Numerical results and the computed aerodynamic properties are presented in Table 3 and Fig. 42 to 47.

Table 3 Mass-averaged values for the flow properties at the exit plane (ϕ = 0.45)

Test Set	Mach number	Pressure* Static	Pressure* Total	Static Temp *	γ	Thrust increment (%)
		Suction collar I				
1	1.701	0.079	0.539	0.643	1.373	45.8
		Suction collar I + 4 Tabs				
2	1.72	0.08	0.565	0.623	1.374	58.1
		Suction collar II + 4 Tabs				
3	1.78	0.07	0.549	0.616	1.373	27.1

(*non-dimensionalized with T_{0i} = 1500 K and P_{0i} = 101,325 Pa)

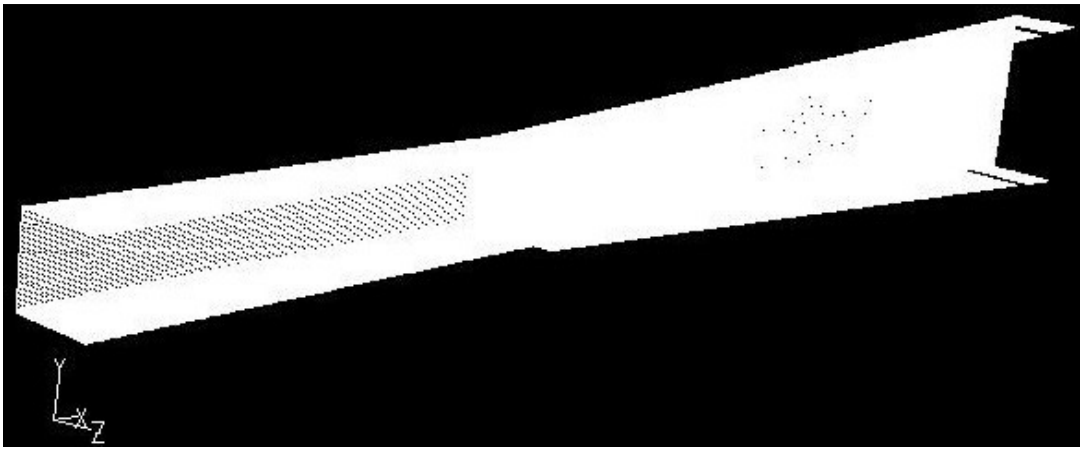

a) Ramp+4 Tabs +Suction Collar

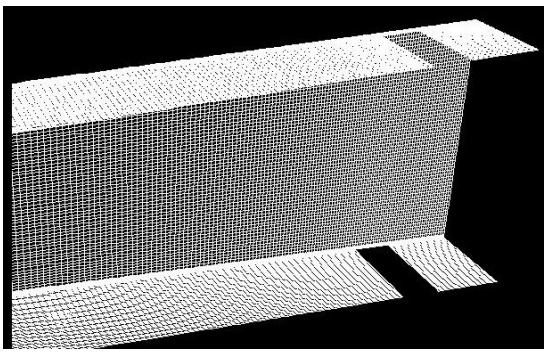

b) Suction Collar I

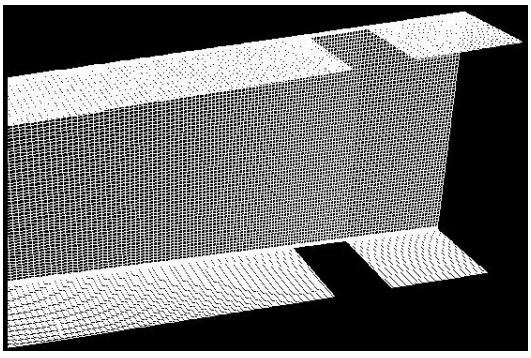

c) Suction Collar II

Fig. 41 Geometries of the Scramjet with Different Suction Collars

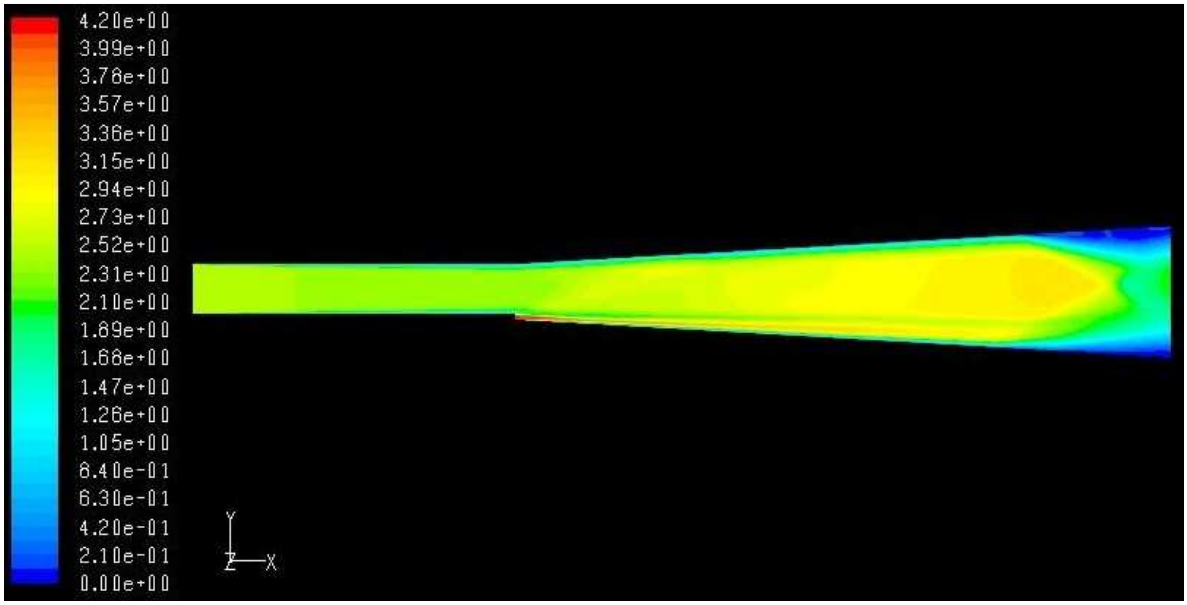

a) Ramp+Suction Collar I

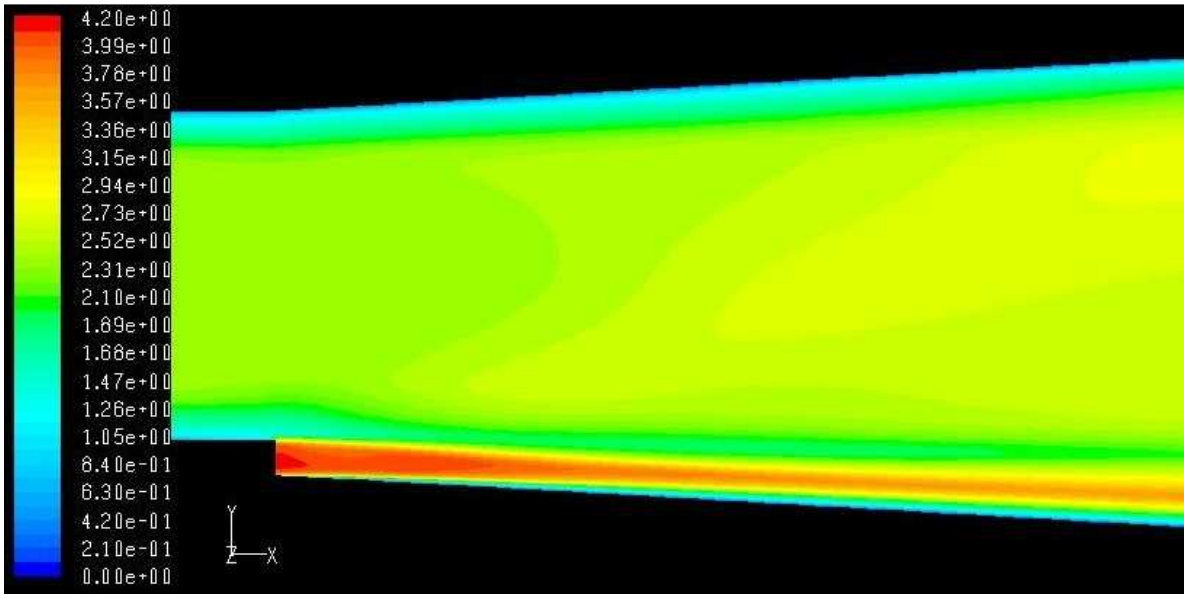

b) detailed Mach number contours around the Ramp

Fig. 42 Mach Number Contours in the Scramjet in the Plane of Symmetry with Convective Mach Number, M_c = 2.5, T_{oi} = 1500 K and ϕ = 0.45

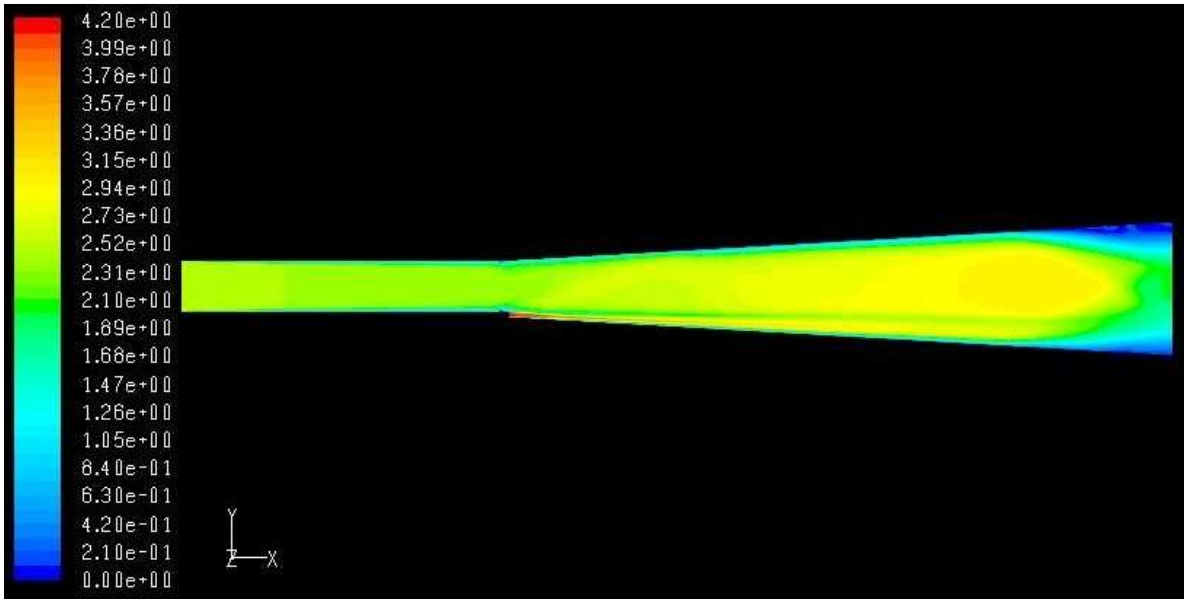

a) Ramp+4 Tabs+Suction Collar I

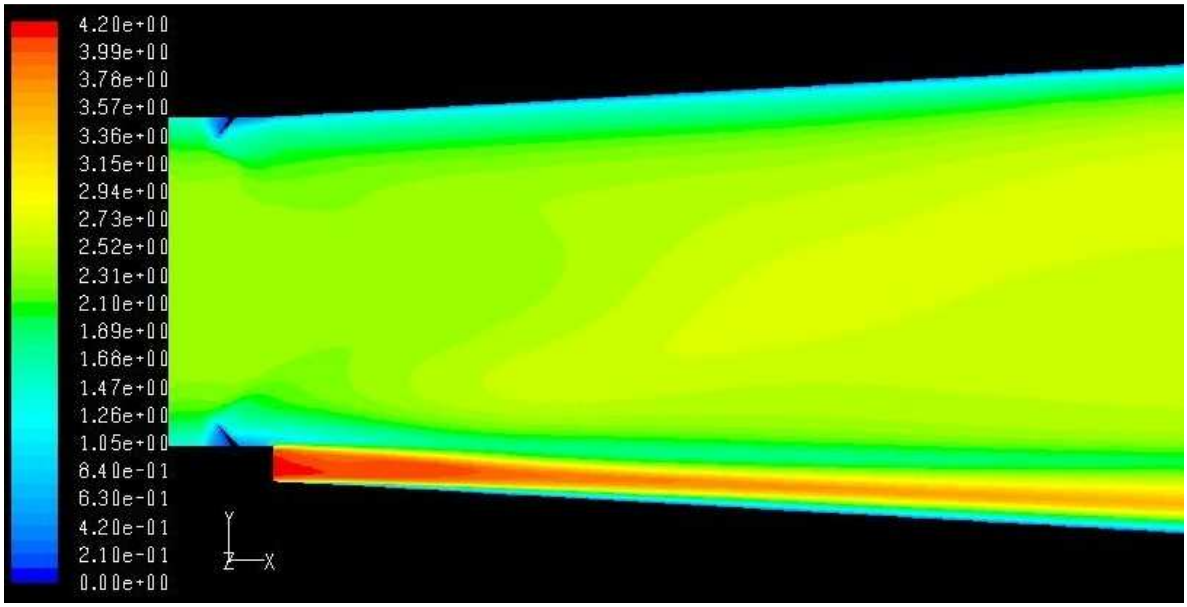

b) detailed Mach number contours around the Ramp

Fig. 43 Mach Number Contours in the Scramjet in the Plane of Symmetry with Convective Mach Number, M_c = 2.5, T_{oi} = 1500 K and ϕ = 0.45

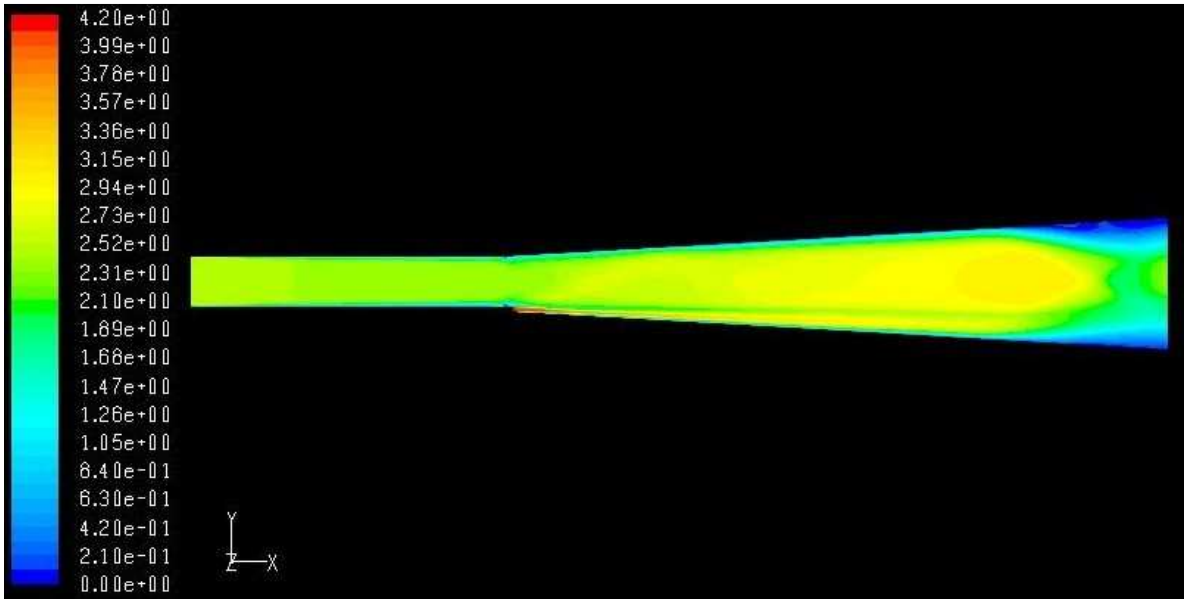

a) Ramp+4 Tabs+Suction Collar II

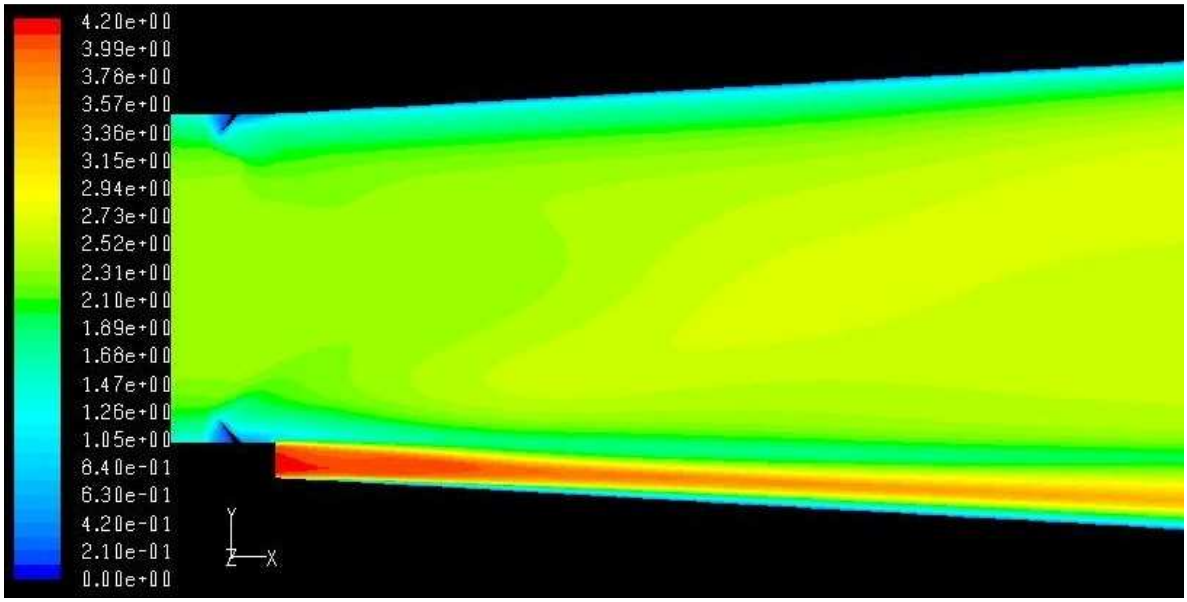

b) detailed Mach number contours around the Ramp

Fig. 44 Mach Number Contours in the Scramjet in the Plane of Symmetry with Convective Mach Number, M_c = 2.5, T_{oi} = 1500 K and ϕ = 0.45

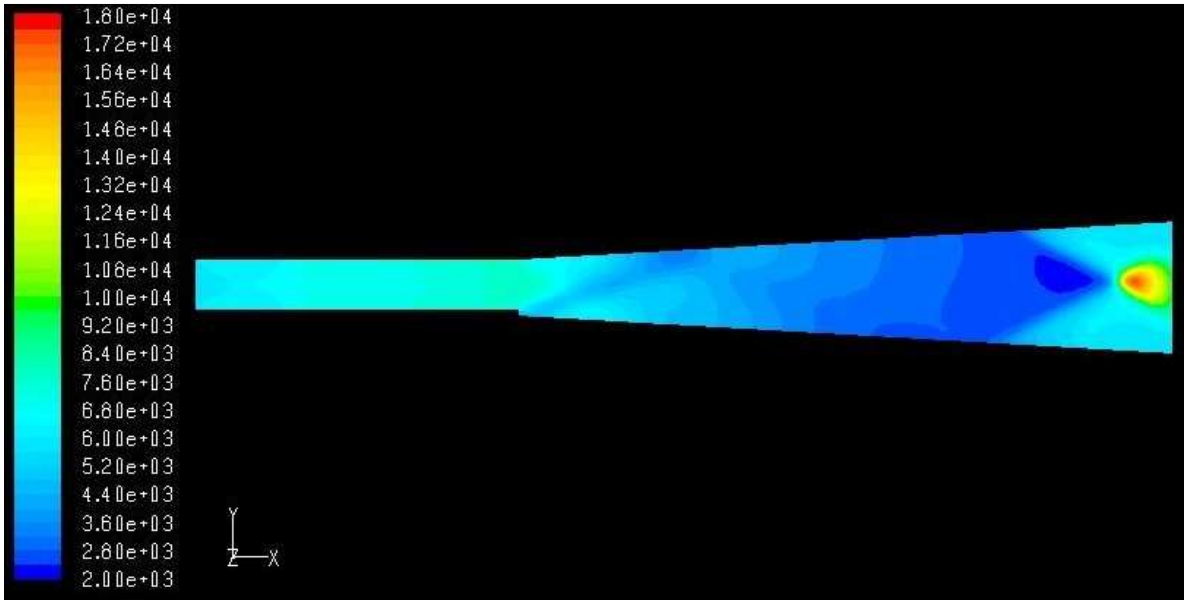

a) Ramp+Suction Collar I

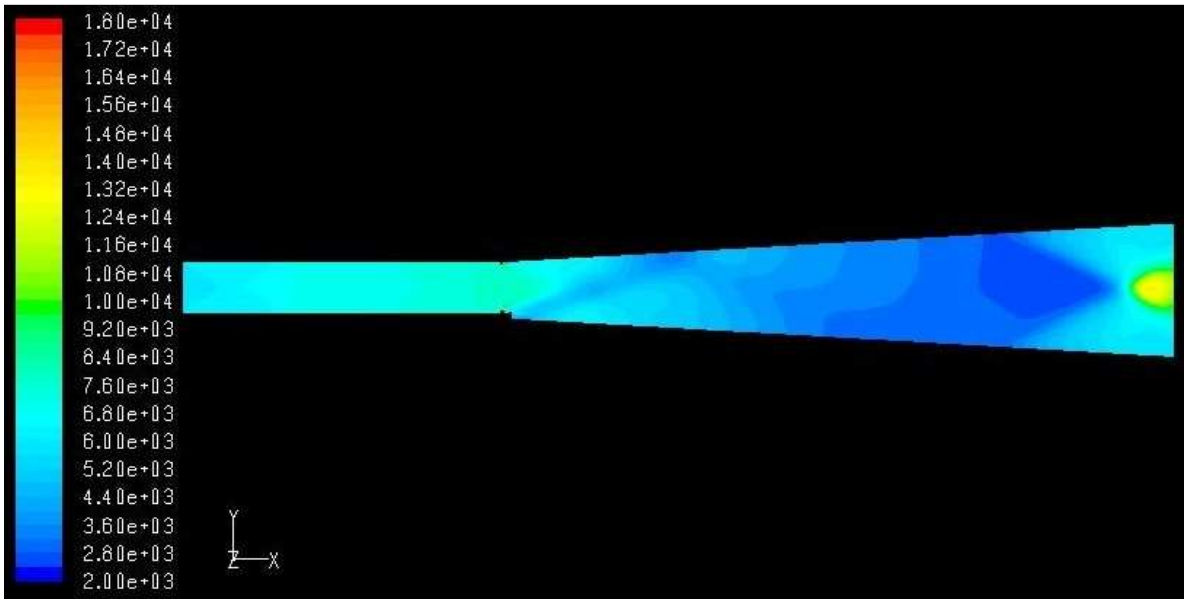

b) Ramp+4 Tabs+Suction Collar I

Fig. 45a Static Pressure (Pa) Contours in the Scramjet in the Plane of Symmetry with Convective Mach Number, M_c = 2.5, T_{oi} = 1500 K and ϕ = 0.45

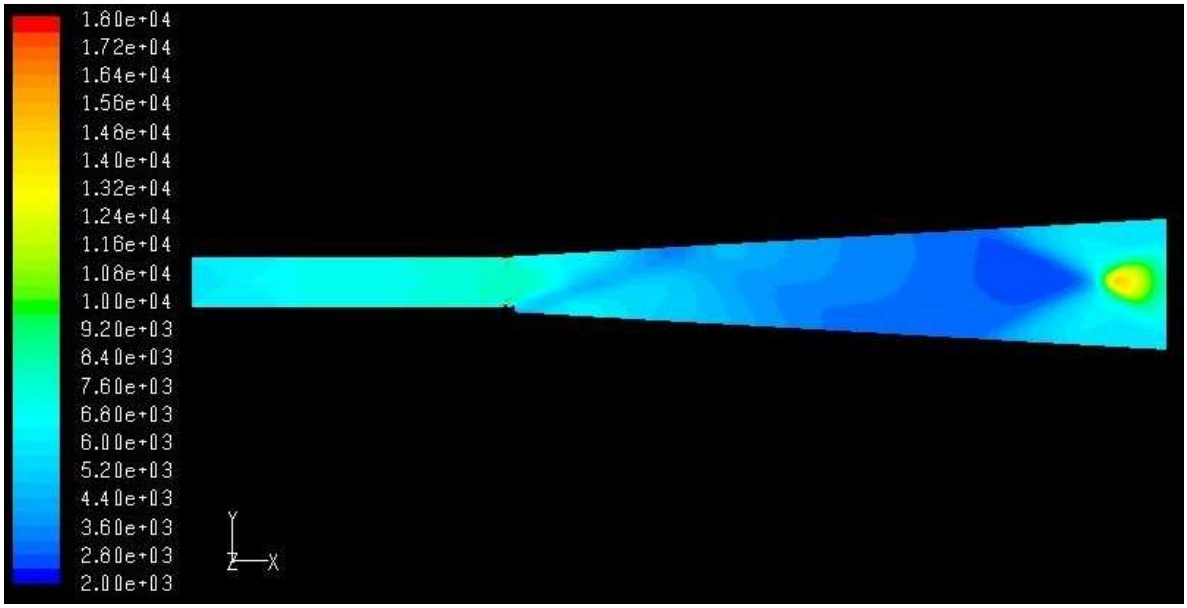

c) Ramp+4 Tabs+Suction Collar II

Fig. 45b Static Pressure (Pa) Contours in the Scramjet in the Plane of Symmetry with Convective Mach Number, M_c = 2.5, T_{oi} = 1500 K and ϕ = 0.45

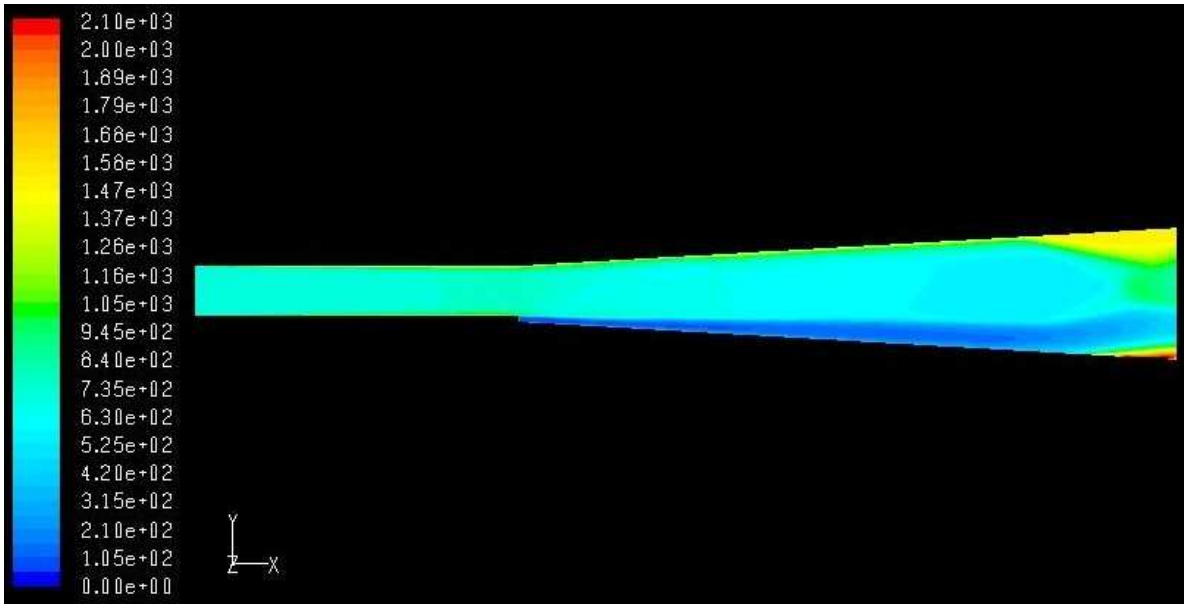

a) Ramp+Suction Collar I

Fig. 46a Static Temperature (K) Contours in the Scramjet in the Plane of Symmetry with Convective Mach Number, M_c = 2.5, T_{oi} = 1500 K and ϕ = 0.45

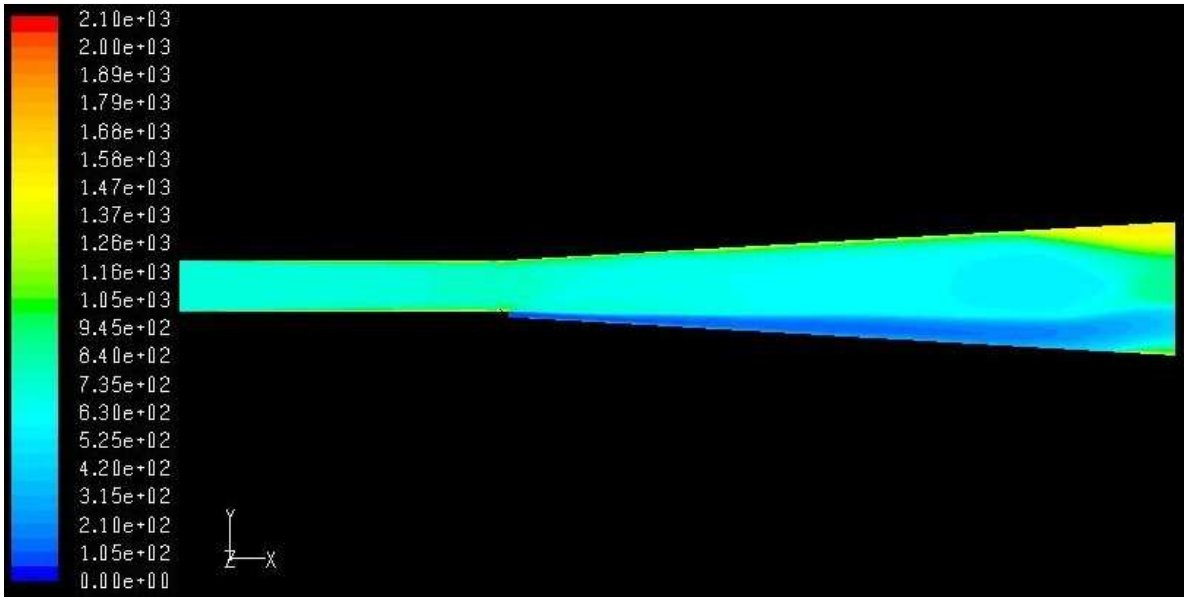

b) Ramp+4 Tabs+Suction Collar I

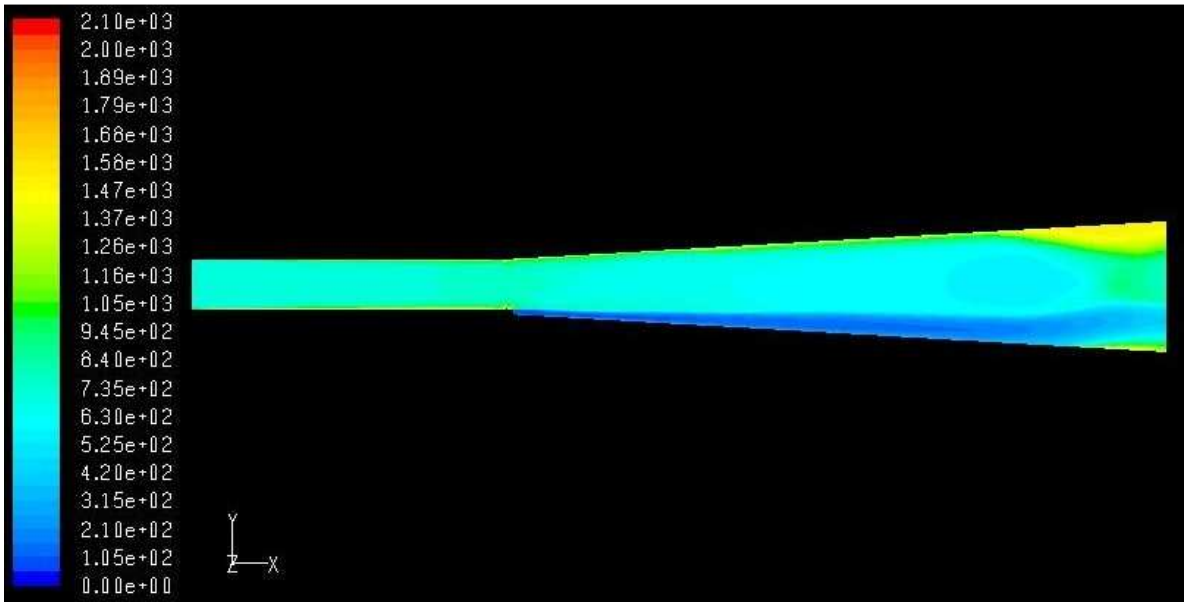

c) Ramp+4 Tabs+Suction Collar II

Fig. 46b Static Temperature (K) Contours in the Scramjet in the Plane of Symmetry with Convective Mach Number, M_c = 2.5, T_{oi} = 1500 K and ϕ = 0.45

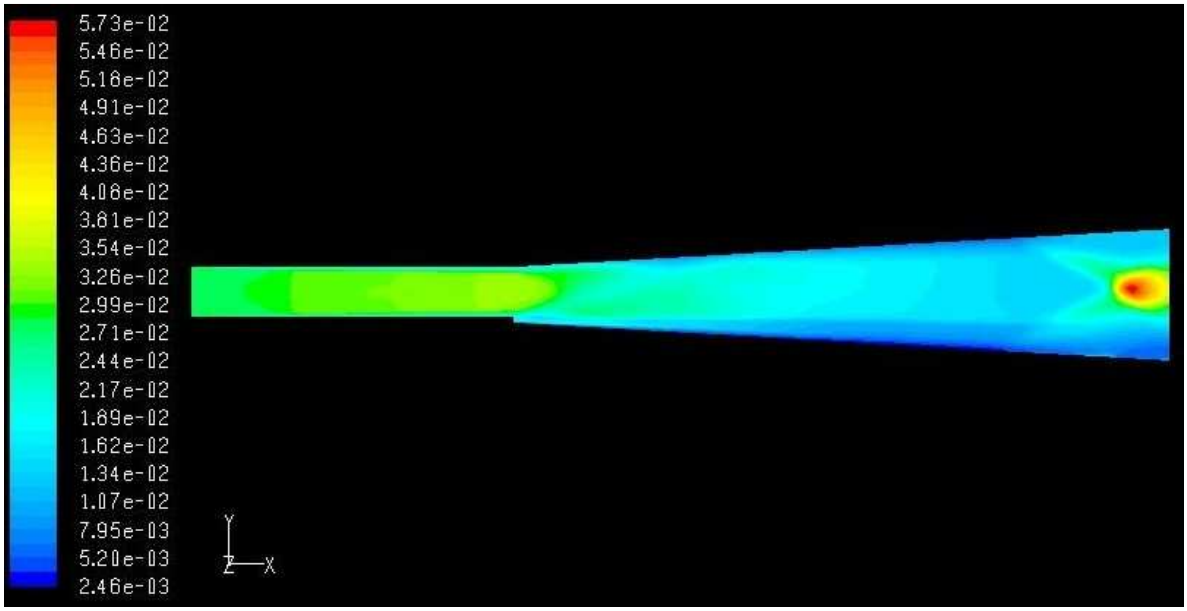

a) Ramp+Suction Collar I

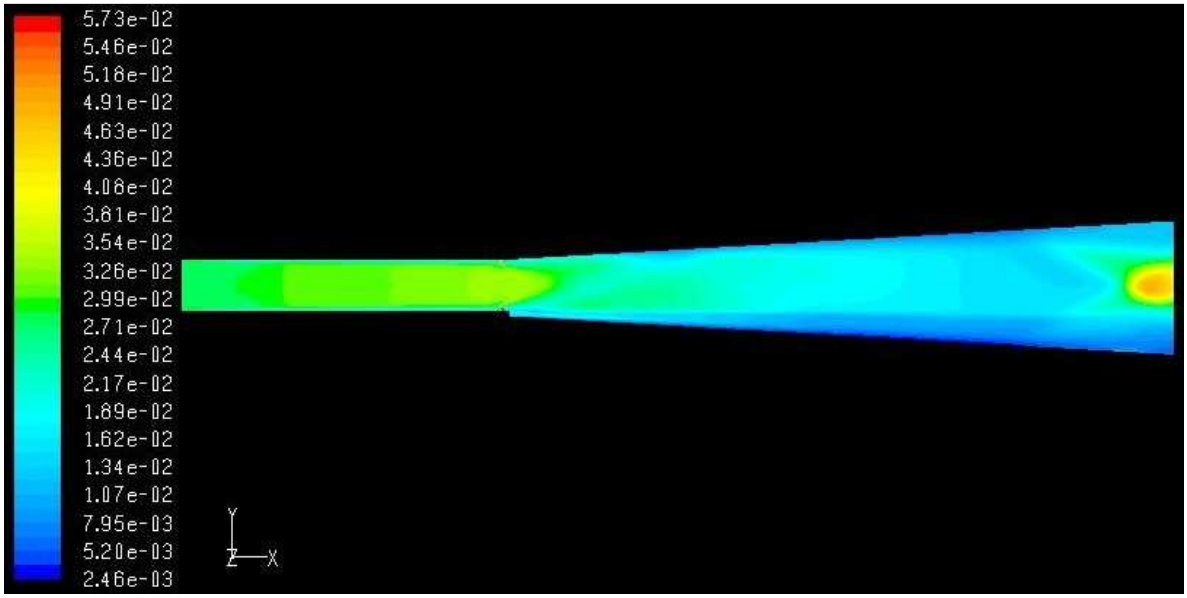

b) Ramp+4 Tabs+Suction Collar I

Fig. 47a Density (kg/m^3) Contours in the Scramjet in the Plane of Symmetry with Convective Mach Number, M_c = 2.5, T_{oi} = 1500 K and ϕ = 0.45

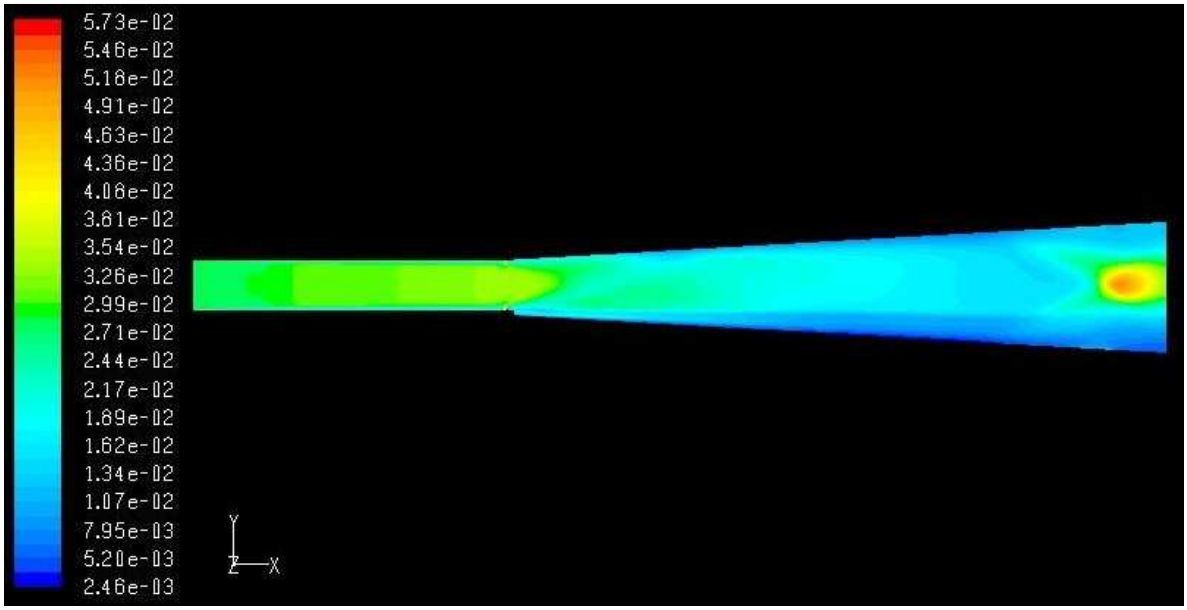

c) Ramp+4 Tabs+Suction Collar II

Fig. 47b Density (kg/m^3) Contours in the Scramjet in the Plane of Symmetry with Convective Mach Number, M_c = 2.5, T_{oi} = 1500 K and ϕ = 0.45

5.4 Results and Discussions of the Scramjet with Relieved Ramp and 4 Tabs at the Fuel Inlet

Four delta tabs are mounted on the fuel inlet normal to the incoming hydrogen fuel jet to enhance shear-layer mixing and reduce the fuel jet potential core length by creating the global instability, weakening the shock-cell strength, of the fuel jet flowfield. Total projected blockage area is 0.67 % of the fuel inlet. The outline drawings of the generated grids are shown in Fig. 48.

Two different sets of the configurations, ramp+4 tabs+4 tabs at the fuel inlet and ramp+4 tabs+suction collar I+4 tabs at the fuel inlet, are numerically investigated in the present study. The thrust developed for the cases of ramp+4 tabs+4 tabs at the fuel inlet and ramp+4 tabs+suction collar I+4 tabs at the fuel inlet is 87.91 N and 121.57 N, respectively. The total pressure loss is 42.42 and 44.29 %, respectively. The static temperature is 908.3 K and 964.9 K at the exit plane, respectively. Numerical results are presented in the Table 4 and Fig. 49 to 52. Compared to the ramp+4 tabs+suction collar I data, which is the previously best fuel injection scheme for the present CFD study, there is an additional 15 % increase of the un-installed thrust, but there is only an additional 0.79 % loss of total pressure caused by the presence of the 4 tabs in the hydrogen fuel inlet with 2.76 % additional increase of the static temperature at the exit plane.

Compared to the experimental[29] and numerical[33] data of the strut and wall injection, Tomioka et al.[29] designed a multi-staged supersonic combustor model with a strut for the first stage and wall-mounted injectors for the second stage, the thrust force for the strut+wall injection scheme is calculated to be 181.86 N where the mass-averaged Mach number is 1.386 at the exit. The total pressure loss is about 75 % with ϕ equals to 1.05, ϕ=0.44 from strut and ϕ=0.61 from wall-mounted injectors. There is an additional 88.1 % increase of the thrust with an additional 5 % loss of the total pressure compared to the strut injection, but the amount of fuel injected is increased from ϕ=0.34 to ϕ=1.05. However, in the present numerical study the thrust force for the ramp+4 tabs+suction

collar I+4 tabs at the fuel inlet scheme is calculated to have an additional 73 % increase in the thrust with an additional 3.37% loss of the total pressure comparing with the ramp injection alone as compared to the baseline case. The equivalence ratio is kept to 0.45, i.e., no additional fuel is injected. This is a clear indication that the mixing and combustion are much more efficient in this injection scheme. Therefore, the ramp+4 tabs+suction collar I+4 tabs at the fuel inlet scheme is a much more effective method for the scramjet combustor than the strut or a multi-staged strut+wall injection scheme.

Table 4 Mass-averaged values for the flow properties at the exit plane (ϕ = 0.45)

Test Set	Mach number	Pressure*		Static Temp*	γ	Thrust increment (%)
		Static	Total			
		4 Tabs+4 Tabs at Fuel Inlet				
1	1.87	0.065	0.576	0.606	1.373	25.2
		4 Tabs+Suction collar I+4 Tabs at Fuel Inlet				
2	1.69	0.087	0.557	0.643	1.374	73

(*non-dimensionalized with T_{0i} = 1500 K and P_{0i} = 101,325 Pa)

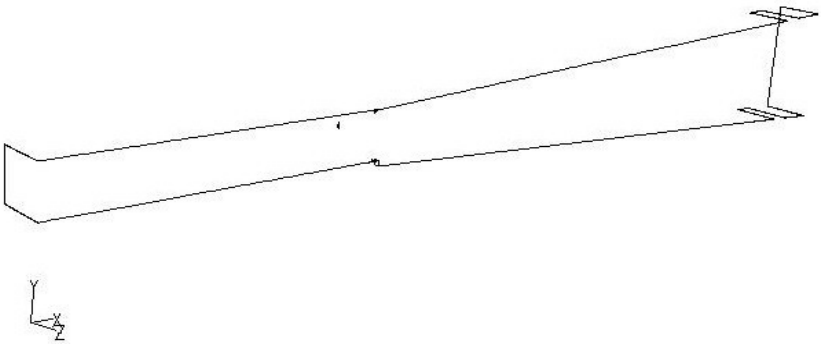

a) Ramp+4 Tabs+Suction Collar I+4 Tabs at Fuel Inlet

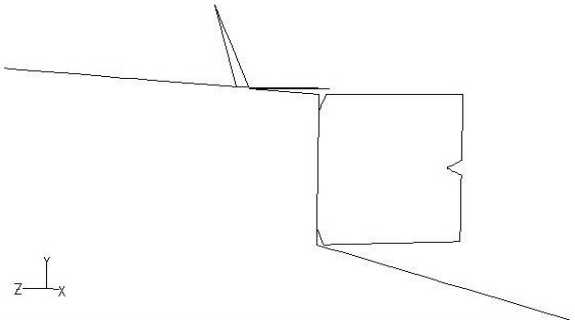

b) Detailed View of 4 delta Tabs at Fuel Inlet

Fig. 48 Outline Drawing of the Scramjet Combustor

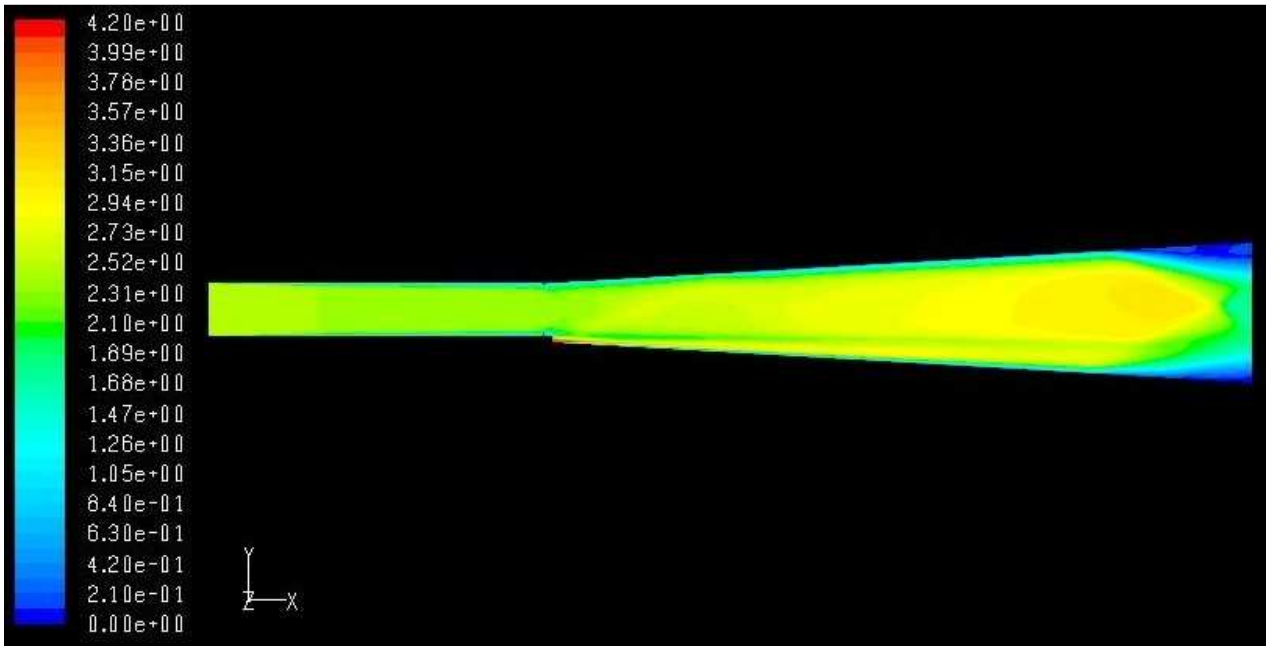

Fig. 49 Mach Number Contours in the Scramjet in the Plane of Symmetry with Convective Mach Number, M_c = 2.5, T_{oi} = 1500 K and ϕ= 0.45 (Ramp+4 Tabs+Suction Collar I+4 Tabs at Fuel Inlet Scheme)

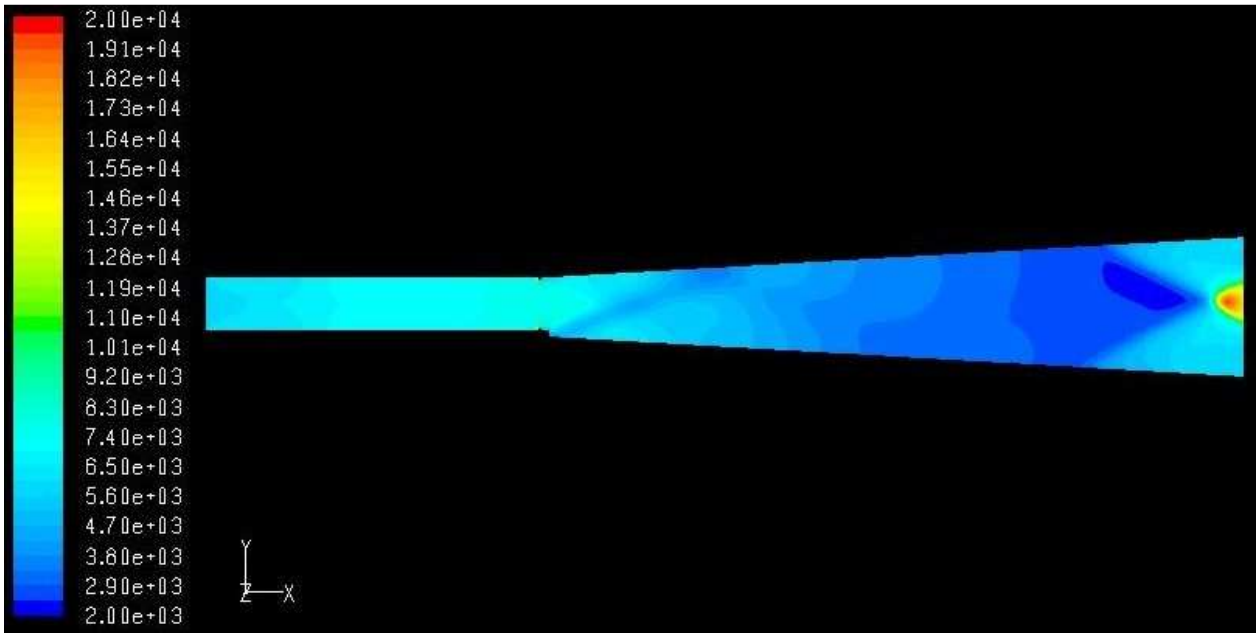

Fig. 50 Static Pressure (Pa) Contours in the Scramjet in the Plane of Symmetry with Convective Mach Number, M_c = 2.5, T_{oi} = 1500 K and ϕ= 0.45 (Ramp+4 Tabs+Suction Collar I+4 Tabs at Fuel Inlet Scheme)

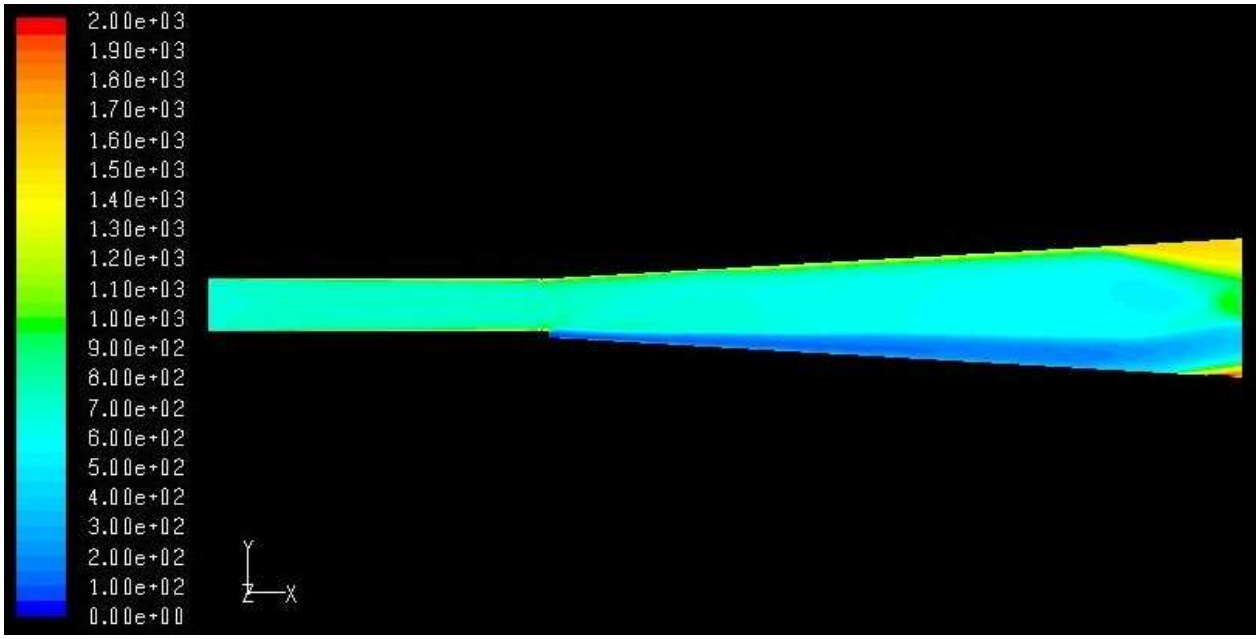

Fig. 51 Static Temperature (K) Contours in the Scramjet in the Plane of Symmetry with Convective Mach Number, M_c = 2.5, T_{oi} = 1500 K and ϕ= 0.45 (Ramp+4 Tabs+Suction Collar I+4 Tabs at Fuel Inlet Scheme)

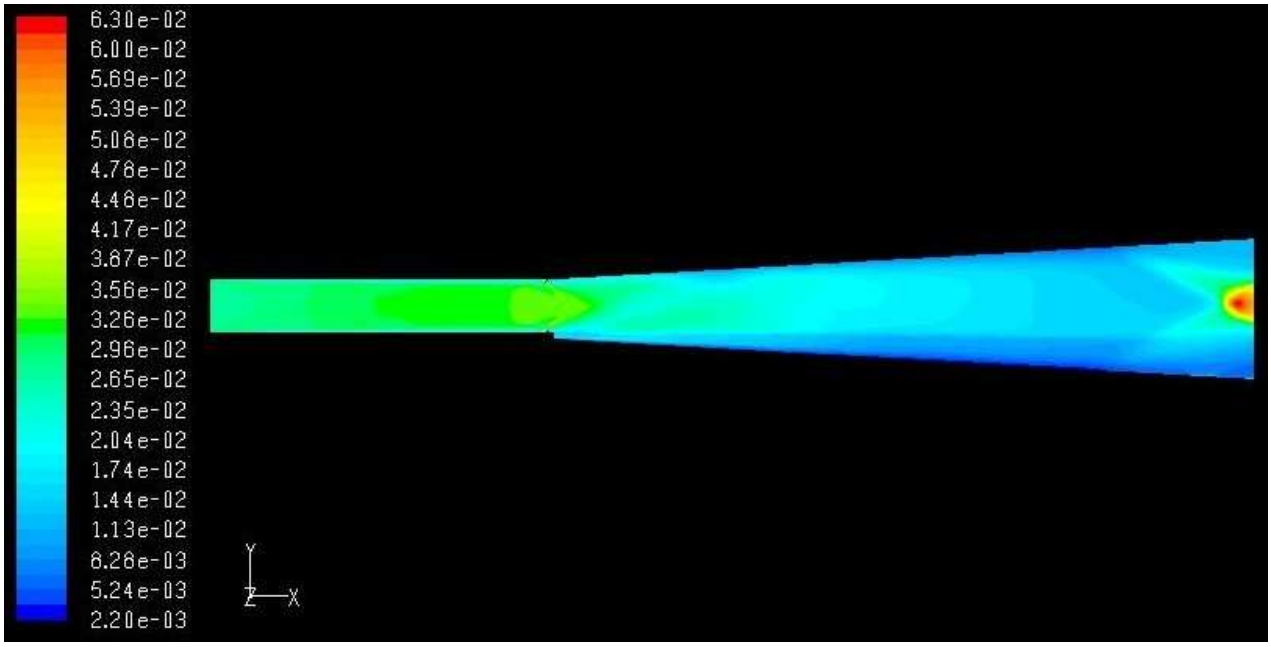

Fig. 52 Density (kg/m^3) Contours in the Scramjet in the Plane of Symmetry with Convective Mach Number, M_c = 2.5, T_{oi} = 1500 K and ϕ= 0.45 (Ramp+4 Tabs+Suction Collar I+4 Tabs at Fuel Inlet Scheme)

5.5 Results and Discussions of the Scramjet with Normal Fuel Injection (Wall Injection)

Three different sets of the configurations, baseline, 4 delta tabs and 4 delta tabs+suction collar I, are numerically investigated in the present study. Dimensions of the tabs and suction collar are all the same as compared to the previous parallel fuel injection schemes and located at the same locations in the scramjet combustor. The thrust force for the baseline case is determined to be 29.98 N. The mass-averaged exit Mach number is 1.83 and the total pressure lose is 70 %. The thrust developed for the cases of the 4 delta tabs and 4 delta tabs+suction collar I is 36.03 N and 49.28 N, respectively. The total pressure loss is 71.9 and 74.7 %, respectively. Numerical results are presented in the Table 5 and Fig. 53 to 56. Even though combustion is achieved in very short distances from the wall mounted injector, the separation zone caused by a detached normal shock upstream of the jet acts as a flameholder, with significant losses in total pressure, which are the major problems with these injection schemes. This is a clear indication that mixing and combustion are poor in these injection schemes, resulting in poor scramjet cycle efficiency as compared to the parallel fuel injection scheme.

Table 5 Mass-averaged values for the flow properties at the exit plane (ϕ=0.45)

Test Set	Mach number	Pressure*		Static Temp*	γ	Thrust increment (%)
		Static	Total			
		Baseline (fuel)				
1	1.83	0.055	0.304	0.577	1.377	0
		4 Tabs				
2	1.78	0.058	0.281	0.591	1.377	20
		4 Tabs+Suction I				
3	1.74	0.064	0.253	0.621	1.376	63.3

(*non-dimensionalized with T_{0i} = 1500 K and P_{0i} = 101,325 Pa)

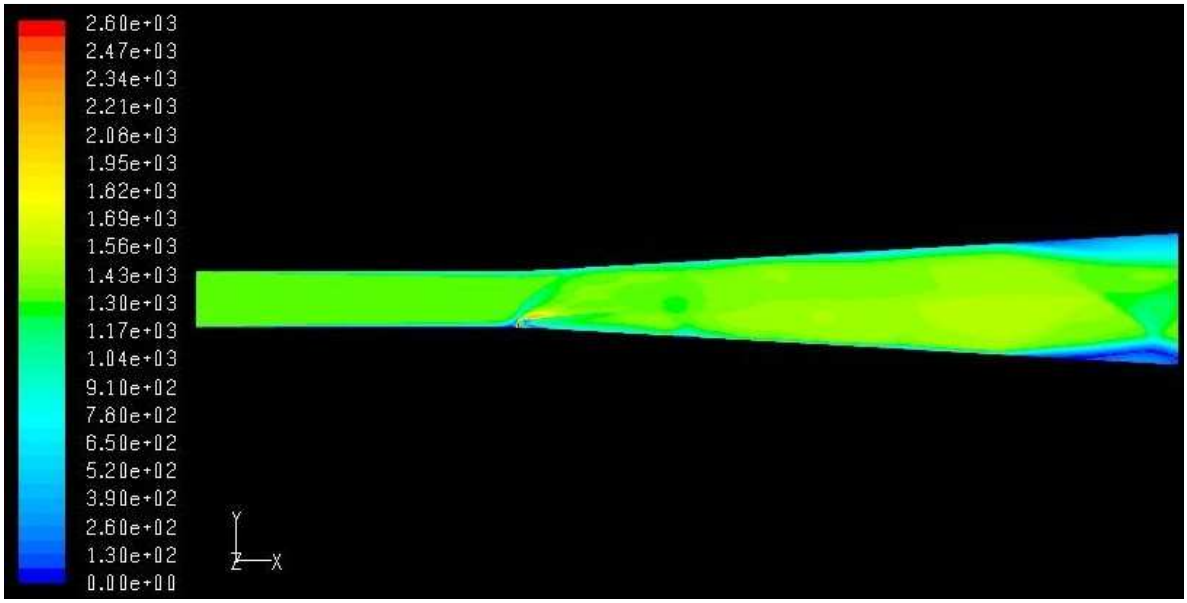

a) normal fuel injection at the wall

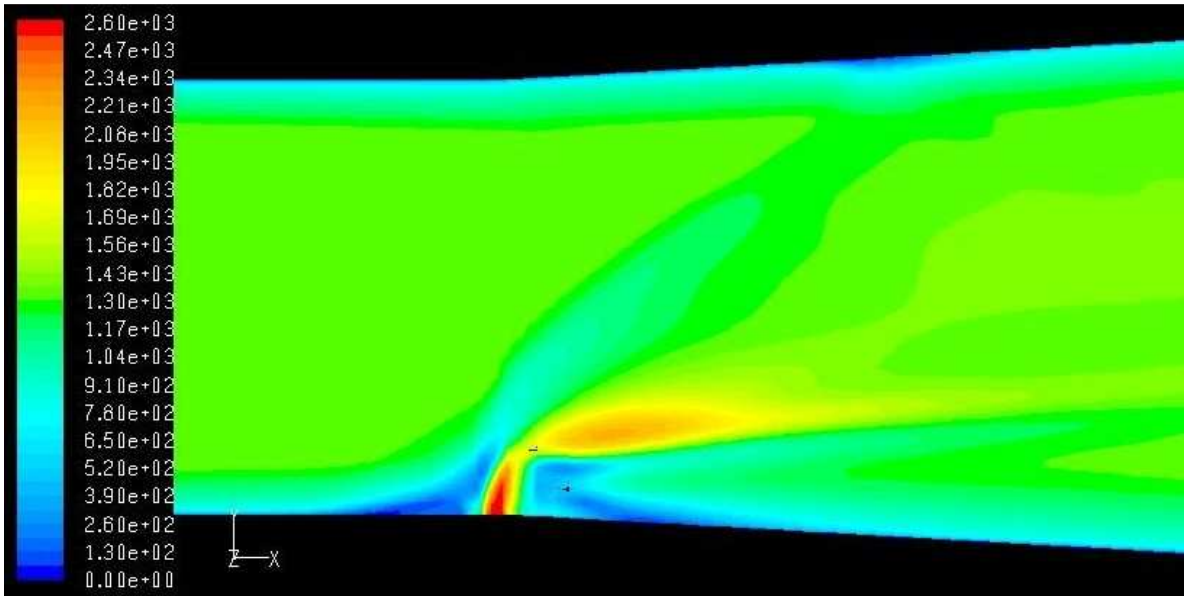

b) at the wall injection (detailed view)

Fig. 53 Velocity (m/sec) Contours in the Scramjet in the Plane of Symmetry with Convective Mach Number, M_c = 2.5, T_{oi} = 1500 K and ϕ= 0.45 (Normal Injection)

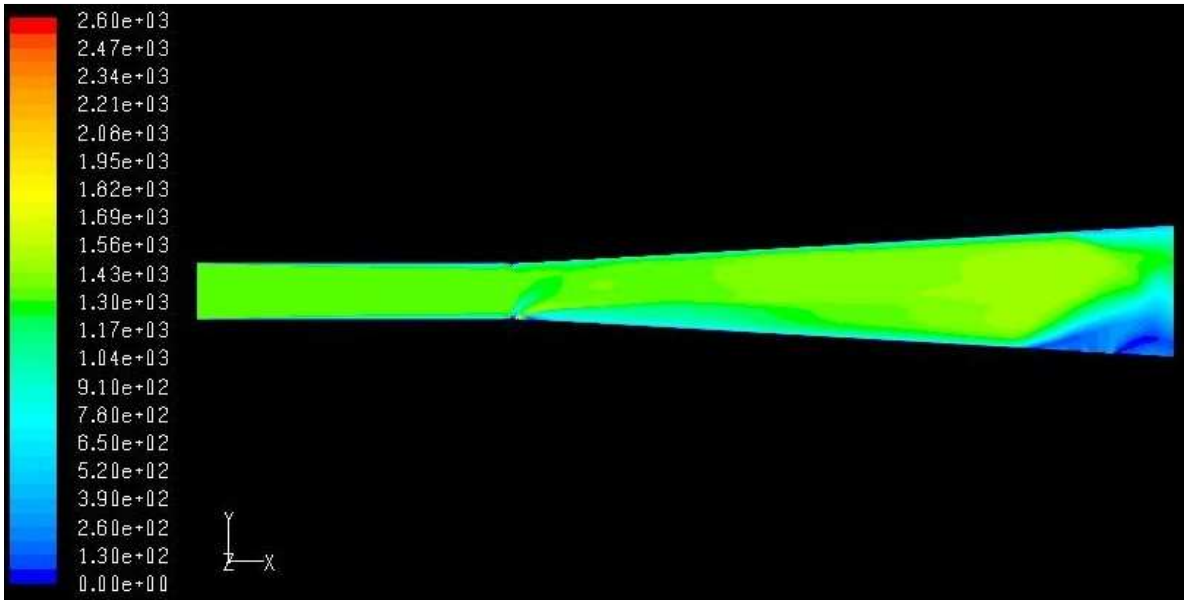

Fig. 54 Velocity (m/sec) Contours in the Scramjet in the Plane of Symmetry with Convective Mach Number, M_c = 2.5, T_{oi} = 1500 K and ϕ= 0.45 (4 Tabs+Suction collar I)

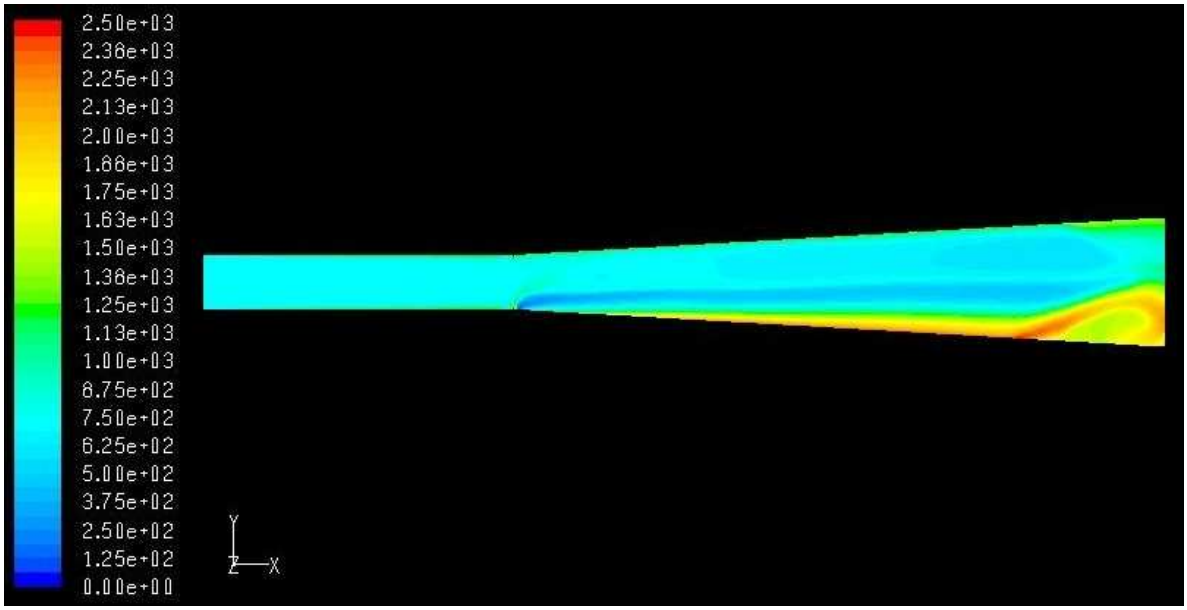

Fig. 55 Static Temperature (K) Contours in the Scramjet in the Plane of Symmetry with Convective Mach Number, M_c = 2.5, T_{oi} = 1500 K and ϕ= 0.45 (4 Tabs+Suction collar I)

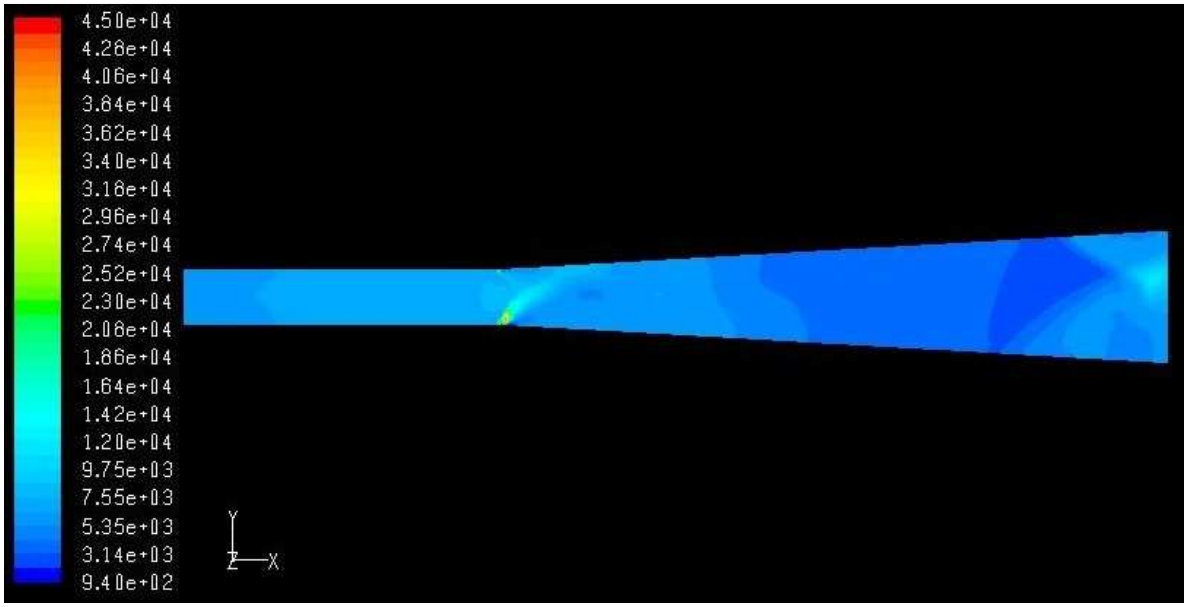

a) normal fuel injection at the wall

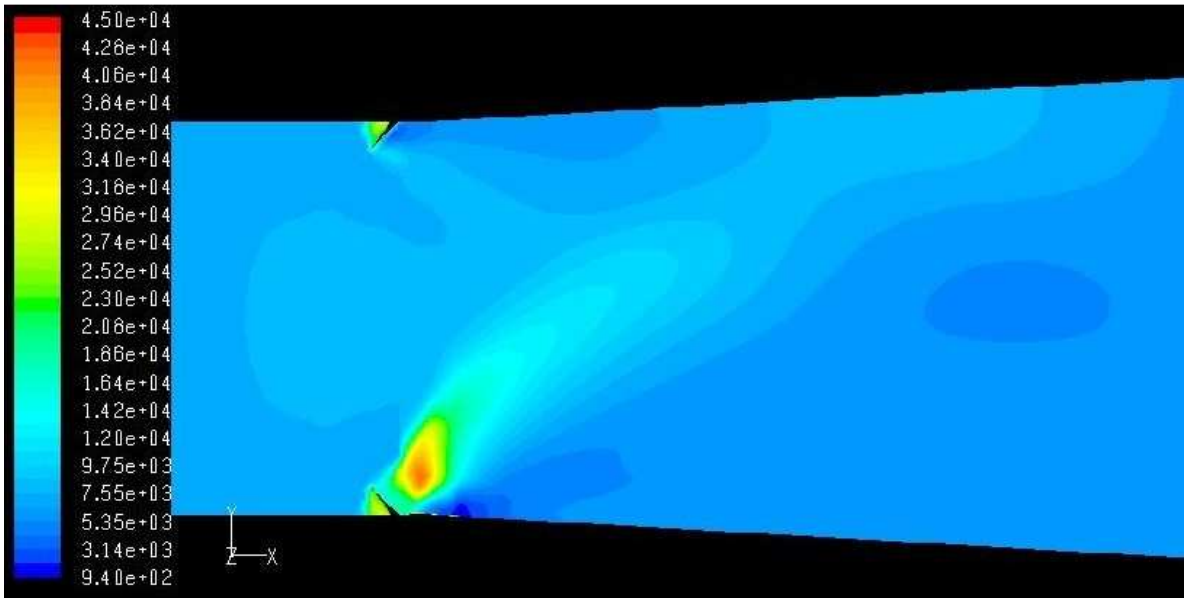

b) at the wall injection (detailed view)

Fig. 56 Static Pressure (Pa) Contours in the Scramjet in the Plane of Symmetry with Convective Mach Number, M_c = 2.5, T_{oi} = 1500 K and ϕ= 0.45 (4 Tabs+Suction collar I)

6 Conclusions and Recommendations

Detailed numerical simulations of the scramjet combustor have been performed for the reacting flows with the parallel fuel injection (ramp injection) and normal fuel injection (wall injection) schemes. Incorporated in the scramjet combustors are tabs and suction collars as means of mixing enhancement. The main mechanism for mixing enhancement is the generation of streamwise vorticity along with the induced global instability of the shear layer. All of the numerical results for the fuel injection schemes are summarized in the Table 6. Mixing and combustion of the relieved ramp configuration produce inferior results as compared to the strut and multi-staged strut+wall injection schemes. However, the relieved ramp+tabs+suction collar schemes, combined with delta tabs and counterflow concept, generate the most favorable improvement in the mixing and combustion in the scramjet combustor at the combustion chamber entry Mach number of 2.5 and the stagnation temperature and pressure of 1500 K and 101,325 Pa, respectively. These results clearly indicate that the injection schemes used in the present study are superior to the Tomioka et al.[29] multi-staged supersonic combustor model with a strut for the first stage and wall-mounted injectors for the second stage. The relieved ramp+tabs+suction collar schemes are also very sensitive to the location and size of the suction collars on the divergent section of the scramjet combustor. In the present CFD study, only two different suction collars are investigated. For the future studies, the optimization of the size, shape and location of the suction collars is recommended. The optimization of the size of the tabs is also recommended.

Table 6 Mass-averaged values for the flow properties at the exit plane (ϕ=0.45)

Test set	Mach number	Pressure* Static	Pressure* Total	Static Temp*	γ	Thrust increment (%)
	Parallel Fuel Injection					
		Baseline (Ramp, Thrust= 70.28 N)				
	1.969	0.057	0.591	0.576	1.374	0
		Ramp+tabs				
2 Tabs	1.815	0.069	0.563	0.606	1.374	29.1
4 Tabs	1.815	0.073	0.588	0.602	1.374	50.6
8 Tabs	1.819	0.071	0.574	0.603	1.374	40.9
		Ramp+suction collar				
I	1.701	0.079	0.539	0.643	1.373	45.8
		Ramp+4 tabs+suction collar				
I	1.724	0.08	0.565	0.623	1.374	58.1
II	1.782	0.07	0.549	0.616	1.373	27.1
		4 Tabs+4 tabs at fuel inlet				
1	1.866	0.065	0.576	0.606	1.373	25.2
		4 tabs+suction collar I+4 tabs at fuel inlet				
2	1.686	0.087	0.557	0.643	1.374	73
	Normal Fuel Injection					
		Baseline (fuel, Thrust=29.98N)				
1	1.831	0.055	0.304	0.577	1.377	0
		4 Tabs				
2	1.782	0.058	0.281	0.591	1.377	20
		4 Tabs+suction collar I				
3	1.743	0.064	0.253	0.621	1.376	63.3

(*non-dimensionalized with T_{0i} = 1500 K and P_{0i} = 101,325 Pa)

7 References

1. Strykowski, P.J., Krothapali, A., and Wishart, D., “The Enhancement of Mixing in High-Speed Heated Jets Using a Counterflowing Nozzle,” AIAA Paper 92-3262, July 1996.
2. Strykowski, P.J., and Niccum, D.L., “The Stability of Countercurrent Mixing Layers in Circular Jets,” Journal of Fluid Mechanics, Vol. 227, 1991, pp. 309-343.
3. Seiner J. M., Dash S. M., and Kenzakowski D.C., “Historical survey on enhanced mixing in scramjet engines,” AIAA Journal of Propulsion and Power, Vol. 17, pp 1273-1286, 2001.
4. Morris, P.J., Giridharan, G., and Lilley, G.M., “On the Turbulent Mixing of Compressible Free Shear Layers,” Proceedings Royal Society London, Series A: Mathematical and Physical Sciences, Vol 431, 1990, pp. 219-243.
5. Lu, G., and Lele, S.K., “Spatial Growth of Disturbances in a Skewed Compressible Mixing Layer,” AIAA Paper 93-0214, Jan. 1993.
6. Lele, S. K., “Direct Numerical Simulation of Compressible Free Shear Layer Flows,” AIAA Paper 89-0374, Jan. 1989.
7. Childs, R., Nixion, D., Keefe, L. R., and Rodman, L. C., “A Study of Compressible Turbulence,” AIAA Paper 93-0659, Jan. 1993
8. Birch, S. F., and Eggers, J.M., “A Critical Review of the Experimental Data for Developed Turbulent free Shear Layers,” Free Turbulent Shear Flows, SP-321, NASA, Vol. 1, 1972, pp. 11-37.
9. Brown, G. L., and Roshko, A., “On Density Effects and Large Structure in Turbulent Mixing Layers,” Journal of Fluid Mechanics, Vol. 64, Pt. 4, 1974, pp. 775-816.
10. Papamouschou, D., and Roshko, A., “The Compressible Turbulent Shear Layer: An Experimental Study,” Journal of Fluid Mechanics, Vol. 197, 1988, pp. 453-477.

11. Gobel, S. G., and Dutton, J. C., “Experimental Study of Compressible Turbulent Mixing Layers,” AIAA Journal, Vol. 29, No. 4, 1991, pp. 538-546.
12. Bird, R. B., Stewart, W. E., and Lightfoot, E. N., “Transport Phenomena,” John Wiley, New York, 1960.
13. Heiser William H. and Pratt David T., “Hypersonic Airbreathing Propulsion,” AIAA Education Series, 1994.
14. Gropengiesser, H., “Study of the Stability of Boundary Layers in Compressible Fluids,” NASA TT-F-12, 1970, pp. 786.
15. Sarkar, S., and Balakrishnan, L., “Application of a Reynolds Stress Turbulence Model to the Compressible Shear Layer,” NASA, Inst. for Computer Applications in Science and Engineering, ICASE Rept. 90-18, 1990.
16. Seiner, J. M., and Grosch, C. E., “Effect of Tabs on Mixing on Round Jets,” AIAA/CEAS Aeroacoustics Meeting Proceedings, Paper 98-2326, Toulouse, France, June 1998.
17. Grosch, C. E., Seiner, J. M., Hussaini, M. Y., and Jackson, T. L., “ Numerical Simulation of Mixing Enhancement in a Hot Supersonic Jet,” Physics of Fluids, Vol. 9, No. 4, 1997, pp. 1125-1143.
18. Zaman K.B.M.Q., Reeder M.F., and Samimy M., “Supersonic jet mixing enhancement by delta-tabs,” AIAA 92-3548, 1992.
19. Samimy M., Zaman K.B.M.Q., and Reeder M.F., “Effect of tabs on the flow and noise field of an axisymmetric jet,” AIAA Journal, Vol. 31, pp609-615, 1993.
20. Reddy D.R., Steffen C.J., and Zaman K.B.M.Q., “Computation of 3D compressible flow from a rectangular nozzle with delta tabs,” ASME Paper 97-GT-257, 1997.
21. Behrouzi Parviz and McGuirk James J., “Jet Mixing Enhancement Using Fluid Tabs,” AIAA Paper 2004-2401, July 2004.

22. Huerre, P., and Monkewitz, P.A., “Absolute and Convective Instabilities in Free Shear Layers,” Journal of Fluid Mechanics, Vol. 159, 1985, pp.151-168.
23. Shih, C., Alvi, F. S., and Washington, D.M., “Effect of Counterflow on the Aeroacoustic Properties of a Supersonic Jet,” Journal of Aircraft, Vol. 36, No. 2, March-April 1999.
24. Lee, M.P., McMillin, B.K., Palmer, J.L., and Hanson, R.K., “Two Dimensional Imaging of Combustion Phenomena in a Shock Tube Using Planner Laser-Induced Fluorescence,” AIAA Paper 91-0460, 1991.
25. Dimotakis, P.E., “Turbulent Free Shear Layer Mixing and Combustion,” High Speed Flight Propulsion Systems, edited by S.N.B. Murthy and E.T. Curran, Vol. 137, Progress in Astronautics and Aeronautics, AIAA, Washington, DC, 1991, pp. 265-340.
26. Drummond, J.P., Carpenter, M.H., Riggins, D.W., and Adams, M.S., “Mixing Enhancement in a Supersonic Combustor,” AIAA Paper 89-2794, July 1989.
27. Donohue, J.M., McDaniel, J.C., Jr., and Haj-Hariri, H., “Experimental and Numerical Study of Swept Ramp Injection into a Supersonic Flowfield,” AIAA Journal, Vol. 32, No. 9, 1994, pp. 1860-1867.
28. Tomioka, S., et al., “Testing of a Scramjet Engine with a Strut at M8 Flight Condition,” AIAA paper 98-3134, 1998.
29. Tomioka, S., Murakami, A., Kudo, K., and Mitani, T., “Combustion Tests of a staged Supersonic Combustor with a Strut,” Journal of Propulsion and Power, Vol. 17, No. 2, 2001, pp. 293-300.
30. Abdel-Salam, T.M., Tiwari, S.N., Chaturvedi, S.K., and Mohieldin, T.O., “Mixing and Combustion in Scramjet Combustor with Raised and Relieved Ramp,” AIAA paper 2000-3709, July 2000.
31. Rodriguez, C.G., and Cutler, A.D., “Numerical Analysis of the SCHOLAR Supersonic Combustor,” NASA-CR-2003-212689, Dec. 2003.
32. Deep, M., Gokhale, S.S., and Jayaraj, S., “Numerical Modeling of Scramjet Combustor,” Defense Science Journal, Vol. 57, No. 4, July 2007, pp. 513-525.

33. Rajasekaran, A., and Babu, V., “Numerical Simulation of Three-Dimensional Reacting Flow in a Model Supersonic Combustor,” Journal of Propulsion and Power, Vol. 22, No. 4, July-August 2006.

34. Pellett, G.L., Bruno, C., and Chinitz, W., "Review of Air Vitiation Effects on Scramjet Ignition and Flameholding Combustion Processes," AIAA Paper 2002-3880, July 2002

35. Fluent Version 6 User's Guide, Fluent Inc, Lebanon, New Hampshire, 2005

36. Kirchhartz, R.M., Mee, D.J., Stalker, R.J., Jacobs, P.A, and Smart, M.K, "Supersonic Boundary-Layer Combustion: Effects of Upstream Entropy and Shear-Layer Thickness," Journal of Propulsion and Power, Vol. 26, No. 1, January-February 2010.

37. Kumaran, K. and Babu, V., "A Comparison of Numerical Predictions of Supersonic Combustion of Hydrogen using Different Chemistry Models in a Model Combustor," AIAA Paper 2009-716, January 2009

38. Tetlow, M.R., and Doolan, C.J., “Comparison of Hydrogen and Hydrocarbon-Fueled Scramjet Engines for Orbital Insertion,” Journal of Spacecraft and Rockets, Vol. 44, No. 2, March-April 2007.

39. Keistler, P.G., and Hassan, H.A., “Simulation of Supersonic Combustion Involving H_2/Air and C_2H_4/Air,” AIAA Journal, Vol. 48, No. 1, January 2010.